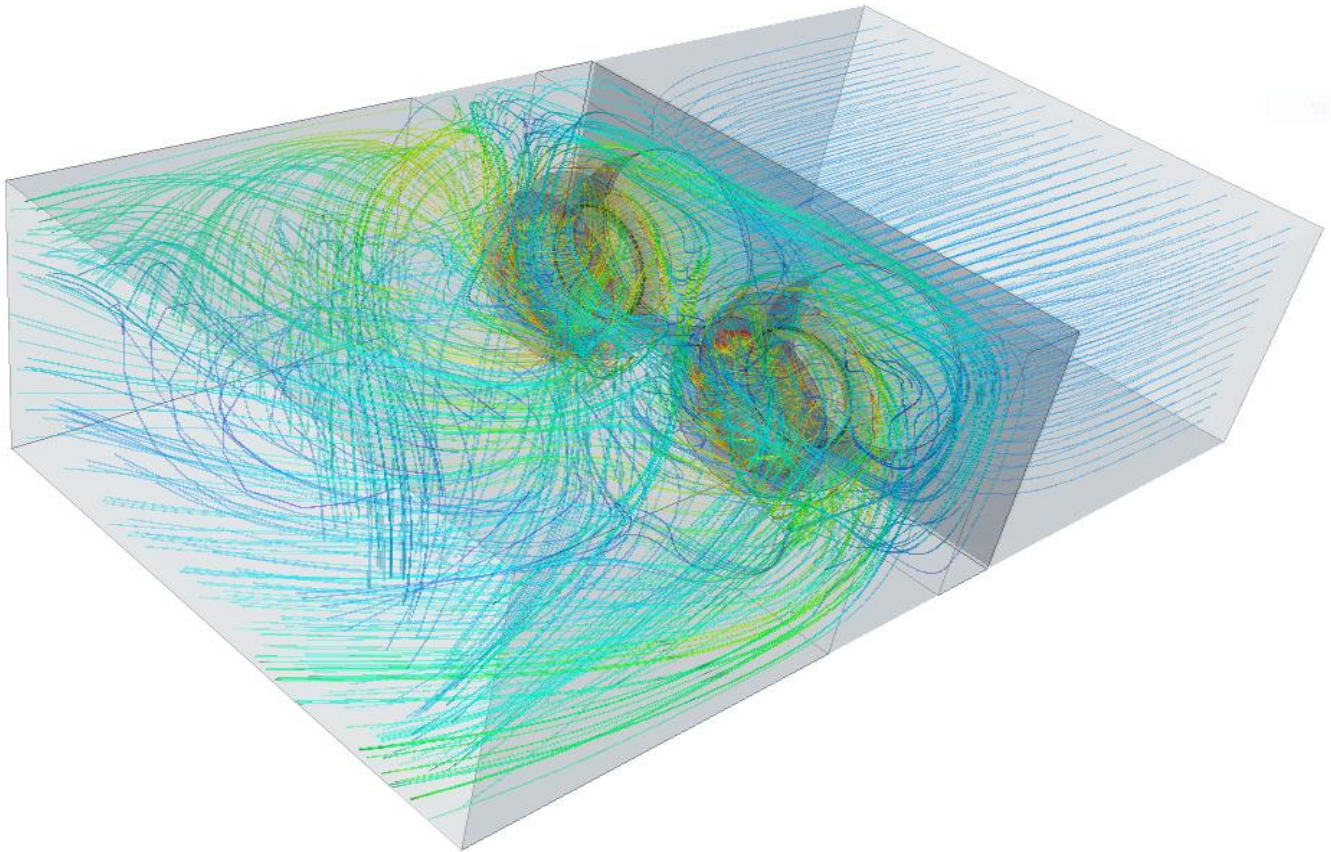




CHALMERS
UNIVERSITY OF TECHNOLOGY



Investigation of the Effect of Multiple Centrifugal Fans Close to Each Other in Operation

A Numerical Study to Improve Fan Efficiency in an Air Handling Unit

Master's thesis in Sustainable Energy Systems

SYLVESTER ȘERBAN STANKIĆ
RADU-CRISTIĂN PLOEȘTEANU

MASTER'S THESIS IN SUSTAINABLE ENERGY SYSTEMS

Investigation of the Effect of Multiple Centrifugal Fans Close to Each Other in Operation

A Numerical Study to Improve Fan Efficiency in an Air Handling Unit

SYLVESTER ȘERBAN STANKIĆ
PLOEȘTEANU RADU-CRISTIAN

Department of Mechanics and Maritime Sciences
Division of Fluid Dynamics
CHALMERS UNIVERSITY OF TECHNOLOGY
Göteborg, Sweden 2019.

Investigation of the Effect of Multiple Centrifugal Fans Close to Each Other in
Operation

A Numerical Study to Improve Fan Efficiency in an Air Handling Unit

SYLVESTER ȘERBAN STANKIĆ

PLOEȘTEANU RADU-CRISTIAN

© SYLVESTER ȘERBAN STANKIĆ & PLOEȘTEANU RADU-CRISTIAN, 2019.

Supervisor: Martin Ottersten, Swegon

Examiner: Professor Lars Davidsson, Mechanics and Maritime Sciences

Master's Thesis 2019:17

Department of Mechanics and Maritime Sciences

Division of Fluid Dynamics

Chalmers University of Technology

SE-412 96 Göteborg

Sweden

Telephone: + 46 (0)31-772 1000

Cover: Geometric scene depicting the streamlines inside an Air Handling Unit with two centrifugal fans operating next to each other, for a supplied airflow rate, Q_s , of 2,1 [m³/s]. The streamlines are colored based on the velocity magnitude for a range of 1-20 [m/s].

Department of Mechanics and Maritime Sciences
Göteborg, Sweden 2019.

Investigation of the Effect of Multiple Centrifugal Fans Close to Each Other in Operation

A Numerical Study to Improve Fan Efficiency in an Air Handling Unit

Master's thesis in Master's programme Sustainable Energy Systems

SYLVESTER ȘERBAN STANKIĆ

PLOEȘTEANU RADU-CRISTIAN

Department of Mechanics and Maritime Sciences

Division of Fluid Dynamics

Chalmers University of Technology

Abstract

Centrifugal fans are commonly utilized in applications for treatment and ventilation of air, given their excellent ability to induce pressure and drive this flow medium. In manufacturing of compact Air Handling Units (AHU), where lower areal footprints are a necessity, several centrifugal fans (in parallel) are often used for each flow direction. It has been shown that there is a risk of decreased individual fan efficiency when multiple fans are introduced next to each other in operation. This is problematic in cases where single, larger fans cannot be used due to mentioned space constraints. The aims of this study were therefore to investigate the reasons as to why this happens and what potential measurements that could be implemented in order to improve fan performance.

Numerical simulations using the commercial Computational Fluid Dynamics (CFD) software STAR CCM+ have been performed on a scaled down version of the supply side down in an AHU, consisting of two centrifugal fans positioned next to each other. Steady state conditions and turbulence modelling (k-epsilon realizable) have been applied for simulating four different airflow rates. Modifications to the initial design of the AHU have also been tested in order to evaluate impact on fan efficiency for the same conditions. The attempted modifications were based on the principle of adding additional geometry in between the centrifugal fans like a wall or guiding vanes (and combination of those). Another principally different design that was investigated was by offsetting one of the fans further downstream from its original position.

By evaluating obtained results it could be concluded that the poor fan performance in the initial design happens due to the open interaction area in between the centrifugal fans, where airstreams from each of the fans will collide and interfere with each other (which adds an extra resistance to the system). Fan performance could be improved by implementing most of above mentioned modifications, and the most promising results were accomplished through the separation of the two centrifugal fans with a straight wall, that covers half of the distance of the outlet chamber, in which the two fans are located. That would theoretically increase the averaged fan efficiency with 3.8-7.3%, relative to that observed in the initial design. The collected data has to be validated in experimental settings, and this lack of comparison at this stage can be seen as one of the main drawbacks with the study.

Key words: Centrifugal fan, Parallel Operation, Fan Efficiency, Air Handling Unit (AHU), Computational Fluid Dynamics (CFD), STAR-CCM+.

Preface

This study was realized during the spring of 2019 and completes the Master's programme Sustainable Energy Systems at Chalmers University of Technology. The study has been proposed by, and carried out for the Swedish ventilation manufacturer Swegon. This project was realized at Chalmers's Department of Mechanics and Maritime Sciences, Gothenburg.

The industrial and academic supervisor of this thesis was Martin Ottersten from Swegon who provided assistance for the use of the program Star-CCM+, as well as numerous discussions and meetings regarding the project. The examiner has been Professor Lars Davidson, the Head of the Fluid Dynamics Division at the department of Mechanics and Maritime Sciences.

Göteborg June 2019.

SYLVESTER ŞERBAN STANKIĆ
PLOEŞTEANU RADU-CRISTIAN

Acknowledgements

First of all, we would like to offer our special thanks to Swegon for the opportunity of being part of such an exciting project with clear connections to reality and concrete engineering problems. We would also like to show our gratitude for being granted with the required advanced engineering tools in the area of Ventilation Systems and for the presentation of the production process at the research centre in Kvänum. Many thanks to Martin Ottersten at Swegon, for the constant aid and various discussions, provided through the process of delivering the master's thesis, for his knowledge and patience with all our questions, from the simplest to the more difficult and important. Big thanks to Erik Sjödin for his support in all the administrative matters concerning the project. Last but not least, we wish to thank Professor Lars Davidson for professionally taking the role of examiner and for accepting the related responsibility, while offering us understanding and support on every occasion.

Nomenclature

Greek Symbols

ΔP	Pressure Difference
ε	Turbulent Dissipation Rate
η_{AHU}	Static Air Handling Unit Efficiency
η_s	Static Fan Efficiency
η_t	Total Fan Efficiency
κ	Von Kármán Constant
λ	Thermal Conductivity
μ	Dynamic Viscosity
ρ	Density
τ	Normal/Shear Stress
Φ	Viscous-Dissipation Function
ω	Rotational Speed

Other Symbols

a	Acceleration
C_p	Specific Heat
d	Distance Between Fans
D	Fan Size
D_{fan}	Fan Diameter
E	Logarithmic Law Offset
F	Force
g	Gravitational Acceleration
H_{case}	Height of Case
k	Turbulent Kinetic Energy
L_{case}	Length of Case
m	Mass
M_f	Fan Moment
P_s	Static Pressure
P_t	Total Pressure
$P_{\text{inlet},s}$	Static Pressure at the Inlet of the AHU
$P_{\text{outlet},s}$	Static Pressure at the Outlet of the AHU
P_{tf}	
Q	Volume Flow Rate
Q_{AHU}	Volume flow through the AHU
Q_s	Supplied Volume Flow
Q_f	Volume Flow Through a Fan
t	Time
T	Temperature

Nomenclature

U	Velocity
\hat{u}	Internal Energy
\mathbf{V}	Velocity Vector
W	Power
W_{case}	Width of case
x	Distance

Abbreviations

AHU	Air Handling Unit
BEP	Best Efficiency Point
CAD	Computer-Aided Design
CAV	Constant Air Volume
CFD	Computational Fluid Dynamics
HVAC	Heating, Ventilation and Air-Conditioning

Contents

Nomenclature.....	ix
1 Introduction.....	1
1.1 Background.....	1
1.2 Goal.....	1
1.3 Limitations.....	2
2 Theory.....	3
2.1 Centrifugal Fan Theory.....	3
2.1.1 Operating Principles and Components.....	3
2.1.2 Blade Types.....	5
2.1.3 Fan and System Curves.....	6
2.1.4 Efficiency and Power Curves (Performance Curves).....	8
2.1.5 Fan Laws.....	9
2.1.6 System Effects.....	10
2.1.7 Parallel Operation.....	11
2.2 Computational Fluid Dynamics.....	13
2.2.1 Governing equations.....	13
2.2.2 Turbulence model - $k-\epsilon$	14
3 Methodology.....	15
3.1 Reference.....	15
3.1.1 Geometry.....	15
3.1.2 Regions.....	17
3.1.3 Meshing.....	19
3.1.4 Boundary Conditions.....	21
3.1.5 Continua.....	22
3.1.6 Simulations and Post Processing.....	23
3.1.7 Efficiency Calculations.....	23
3.2 Modifications of Reference.....	24
3.2.1 Modification 1a: Full Distance Wall.....	24
3.2.2 Modification 1b: Half Distance Wall.....	25
3.2.3 Modification 2: Fan 2 Offset.....	25
3.2.4 Modification 3a: 3 Guiding Vanes.....	26
3.2.5 Modification 3b: 1 Guiding Vane.....	27

Contents

3.2.6	Modification 4: 1 Guiding Vane with Wall	28
4	Results.....	30
4.1	Reference	30
4.1.1	Fan Efficiency and Pressure Rise.....	30
4.1.2	AHU Efficiency and Pressure Rise.....	31
4.1.3	Scalar and Vector Plots.....	31
4.1.4	Notation about Operating Point 1 and its stability	35
4.2	Comparison between Reference and Modifications.....	35
4.2.1	Average Fan Efficiency	35
4.2.2	AHU Efficiency	36
4.2.3	Range of Efficiency Improvement.....	37
4.2.4	Vector Flows of the Modifications	38
5	Discussion	40
5.1	Reference	40
5.2	Modifications.....	42
5.3	Methods	43
6	Conclusion.....	45
7	Future Work.....	46
	References.....	47
	Appendix.....	I
A.1	Mesh Settings	I
A.2	Mesh Quality.....	VI
A.3	Cell Count and Iterations.....	XII
A.4	Residuals	XIII

1 Introduction

1.1 Background

Air handling units (AHU) are important devices that ensure proper quality and temperature of supplied air, for various industrial and commercial applications, by mechanically providing it through different duct systems. In operation, the units normally consist of several centrifugal fans, that pressurize the flows in both supply and exhaust directions. It has been shown that there is a risk of decreased individual fan efficiency when multiple fans are introduced next to each other in operation, as a result of factors such as uneven loading and instability [1, 2]. This is problematic in cases where such configurations are required to ensure larger air flows. Having single larger fans, to meet the required flows, may not always be possible due to geometrical constraints within the AHU. Several smaller centrifugal fans are then utilized (in parallel), enabling space efficient solutions, with lower areal footprints.

Swegon, the company whose goal is to provide an optimal indoor climate, has initiated an investigation into this matter. Potential benefits, such as decreased operational costs from lowered energy consumption, and reduced environmental impacts, are lucrative and point out the importance to why the thesis should be performed.

1.2 Goal

The goal of the project is to determine the reasons as to why the efficiency losses occur when AHUs are equipped with multiple centrifugal fans on the supply and return pathways. This should be done by modelling the fans in an AHU with the help of the commercial Computational Fluid Dynamics (CFD) software Star-CCM+. Once these issues have been identified, potential solutions should be investigated and implemented in order to improve the current operating conditions.

Since the problem refers to an efficiency loss of the system, a connection between such drawbacks and the energy use could be established. As such, possible impacts on the energy savings from potential improvements would be important aspects to take into consideration.

Furthermore, there are some analytical questions that should be taken into account after performing the various simulations. The questions are as follows:

- What is the physical explanation to why the individual fan efficiency decreases when multiple fans are introduced next to each other in operation? What are some of the main phenomena that can be observed in the flow field?
- In case of finding alternative designs that can increase the individual fan efficiency, by how much is it possible (in %) and what would that mean for energy saving purposes?
- What difficulties could be encountered for the application of the potentially viable designs and how could they be overcome?

1.3 Limitations

Linked to the project work of modelling and investigating centrifugal fans in an AHU, the main limitations are as follow:

- Only the supply side is to be modelled in the CFD-software. The initial CAD-geometry of the fans in the AHU is provided by Swegon.
- The amount of fans to be modelled in operation next to each other is two and not more. This is done to decrease complexity and time requirements of the study.
- Validation of the simulations (experimental tests in wind tunnels) is not a direct part of this thesis, as it will be performed by Swegon.

2 Theory

In the second chapter, the paper presents the theory related to the work in order to aid the reader to have a comprehensive view of the concepts and application of different techniques. This chapter consists of the technology behind the used fans, fundamental equations which illustrate the physics behind the simulations, and the interaction between the fluid and the structure of the system.

2.1 Centrifugal Fan Theory

In the following section, the basic principles of how centrifugal fans work are presented. More specifically, this chapter introduces the individual parts that constitute the centrifugal fan and important process parameters linked to its operation. This theory, as a whole, is made with the context of the centrifugal fan being a vital part of the AHU.

2.1.1 Operating Principles and Components

A centrifugal fan (or blower) is a rotating device that mechanically sets the surrounding fluid in motion. The main objective is to pressurize the flow for various applications, where pressure losses occur upstream and/or downstream of the fan. In the case of having an AHU for example, several of these losses are present along the inlet and outlet directions, originating from effects due to frictional losses of the surrounding walls but also as a consequence of the different components that the flow has to pass through on its way. Dampers, filters, heat exchangers and diffusers are a few common examples of such components that lead to pressure drops. The centrifugal fan must compensate for all the pressure losses that occur along the way and ensure that the proper pressure conditions are met to drive the flow in the desired direction. Centrifugal fans are frequently applied in airstreams with high particulate content, moisture and temperatures [2].

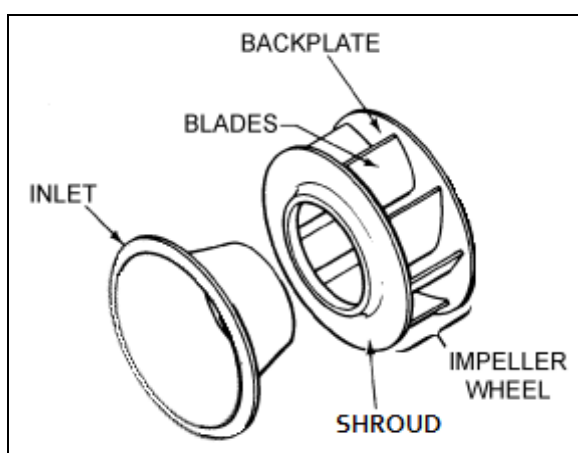


Figure 1: Overview of the individual components present in a centrifugal fan [1].

Theory

The main components of a centrifugal fan are shown in *Figure 1*. The impeller wheel, consisting of a set number of identical blades that are placed in between a shroud and a backplate, is rotating with a constant angular velocity. This results in a centrifugal force imparting mechanical work leading to increased static and kinetic energy of the flowing airstream [1]. An inlet is positioned before the shroud and leads the flow towards the centre of the rotating impeller. A small gap has to be present between the shroud and the collar, as one part is fixated (the inlet collar) while the other one is moving (the shroud with its connected parts). When the fluid is passing through the impeller and is caught up in the spacing between the blades, the components of the velocity vectors undergo a change in radial and tangential directions [1, 3]. Both velocity components increase in magnitude which leads to a larger total velocity at the outlet of the impeller. The flow also gains some static pressure while passing through the impeller, mainly due to the centrifugal force imparting work on the columns of air trapped in between the blades. The collected flow in the wheel exits perpendicular to the axis of rotation. In other words, the air gains kinetic energy through its movement from the impeller hub to the blade tips, which is later converted into an increase of the static pressure as the air velocity decreases before discharge [2].

The impeller is by practice driven by an electrical motor. It can be mounted directly on the backplate, like shown in *Figure 2*. This configuration is called a direct drive, where the motor is in direct, physical contact with the fan and is suitable for Constant Air Volume (CAV) applications. In most modern AHU applications, where high efficiency is required, this type of setup is predominant [4]. By observing *Figure 2* and comparing it with *Figure 1*, one noticeable difference can be seen, and that is that the fans in *Figure 2* have some additional surrounding frameworks intended for structural integrity. These types of fans are called plenum fans, and are most commonly applied in ducted outlet systems. A plenum is a pressurized chamber where the flow is accumulated. The plenum section is connected to an outlet duct and on the inlet side, there is usually an inlet duct. This type of configuration is very common in Heating, Ventilating and Air-Conditioning (HVAC) applications [1].

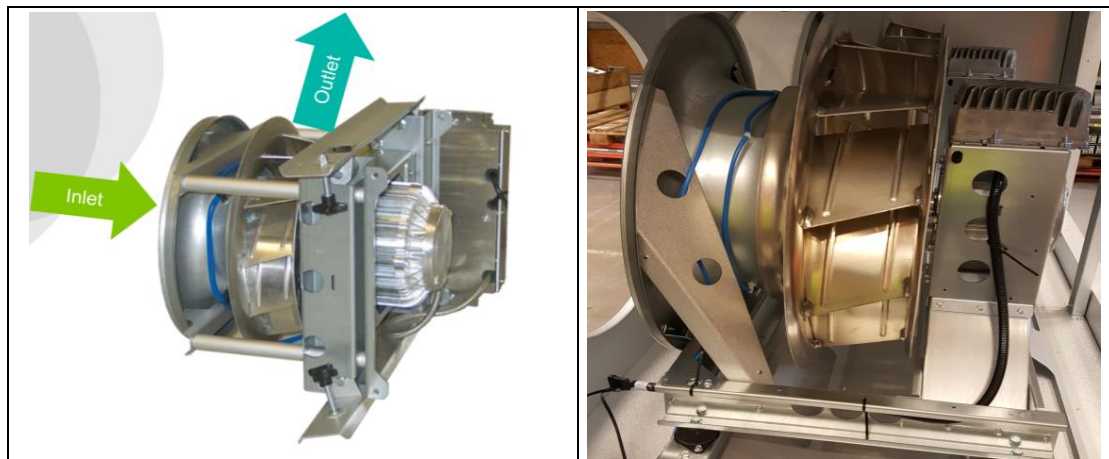


Figure 2: Centrifugal fans commonly used in AHU applications, also known as a plenum-fans (Courtesy of Swegon).

2.1.2 Blade Types

For centrifugal fans, there are three distinctive types of blades that are commonly applied in operation; those are forward inclined blades, backward inclined blades and radial blades [5]. A typical centrifugal fan mounted with forward inclined blades is illustrated in *Figure 3*. These types of blades are curved and face in the same direction as the speed of rotation. Compared to other configurations the blades are shorter and more numerous. The forward inclined blades have the advantage that they can deliver a relatively large amount of air volume at the downside of lower velocity and pressure [5].

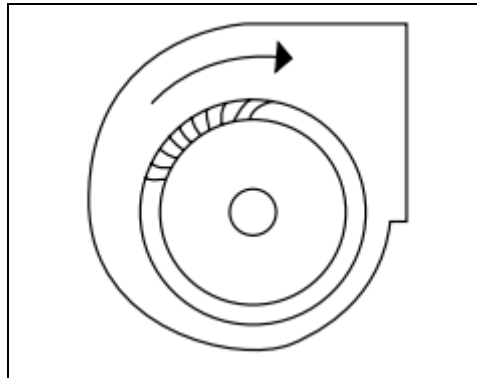


Figure 3: Schematic of a typical centrifugal fan with forward inclined blades [5].

Backward inclined blades come in three variants which can be seen in *Figure 4*. They are named Flat Single Thickness, Curved Single thickness and Curved Airfoil. A distinguishing feature is the position and geometry of the blades, which tilt away from the direction of fan rotation. As fans with backward inclined blades can deliver medium to high airflows at high pressures, they are suitable for AHU applications [5]. Among the three mentioned types, Curved Airfoil blades are the most efficient, with efficiencies exceeding 85 %, partially due to their low rotating mass. However, this fan type is highly susceptible to unstable operation due to stall and erosion because of the thin blade walls, which could eventually lead to cavity formation on the blades [3]. These fan types are designed in a manner in which the impeller itself provides most of the fan's total pressure gain. The abruptly declining fan characteristic underlines an insensitivity towards pressure changes in the system, a characteristic which accepts small additions to the flow resistance of the system, such as dirty filters, without affecting the volume airflow [6].

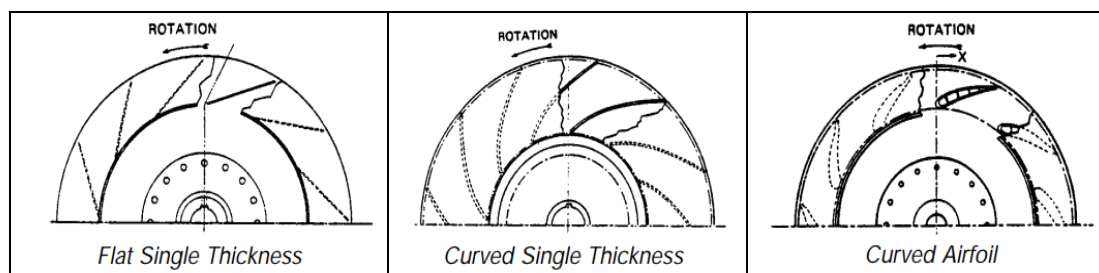


Figure 4: Variations of backward inclined fan blades in a centrifugal fan [5].

Last, but not least, there are a set of radial bladed fans, that can be seen in *Figure 5*. Depending on position and shape of the blades, they are classified as Radial Blade, Air Wheel or Radial Tip. Characteristic features are deeper, heavier and more narrow blades in comparison to forward- and backward inclined-blades. Radial bladed fans are used in cases where medium to high pressures are required, at low volumes of air, and are suitable in harsh environments with high levels of dust and particulate matter [5].

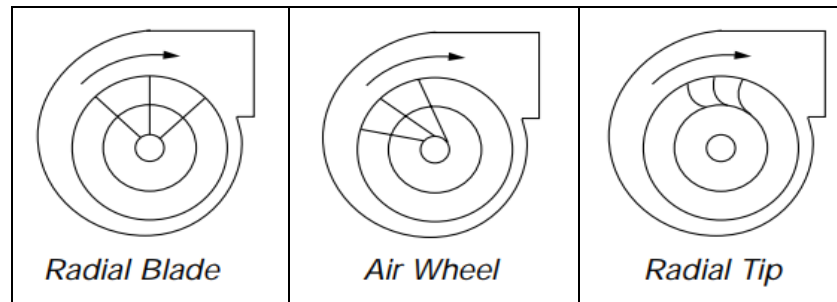


Figure 5: Different radial bladed centrifugal fans commonly used [5].

2.1.3 Fan and System Curves

A fan and system curve is plotted in *Figure 6*. When combined together, these two types of curves describe the interaction between fan and surrounding system, for a variable range of pressures and volumetric airflows. The fan curve describes the performance of a fan in terms of what pressure that can be delivered at a certain airflow. In general, there is a peak in pressure that is obtained at a defined volumetric flow rate. Thereafter, the pressure will decrease steadily at increasing airflows until a minimum pressure is established at the far end of the defined spectrum. The shape of the fan curve varies based on parameters such as fan type, size and rotational speed. It is obtained for individual fans by testing and rating in controlled environments. These procedures are performed by the fan manufacturers, that publish the fan performance data afterwards, enabling proper fan selection [1]. When it comes to the rotational speed, which is constant across the entire fan curve, a larger value will translate the curve upwards, while a smaller value leads to the reversed effect. That is, that the fan curve will be shifted downwards.

The system curve, which has a parabolic shape, describes the characteristics of the system resistance and the losses that occur upstream and downstream of the operating fan. In other words, the system curve gives information about the total pressure drop caused by whole system for a given flow rate. Hence, the system curve depends on factors like duct type, their orientation but also the many system components that are utilized within the system [2]. It is important to notice that the shape of the system curve should be established beforehand selecting a fan, and this is done by the engineer at hand. The intersection between the system curve and the fan curve is called the operational point. It is the one set condition, at which the fan will operate. It can be interpreted as: for a certain amount of total pressure drop caused by the system, there is an exact equal amount of pressure increase that can be delivered by the fan, to offset the loss and drive the flow.

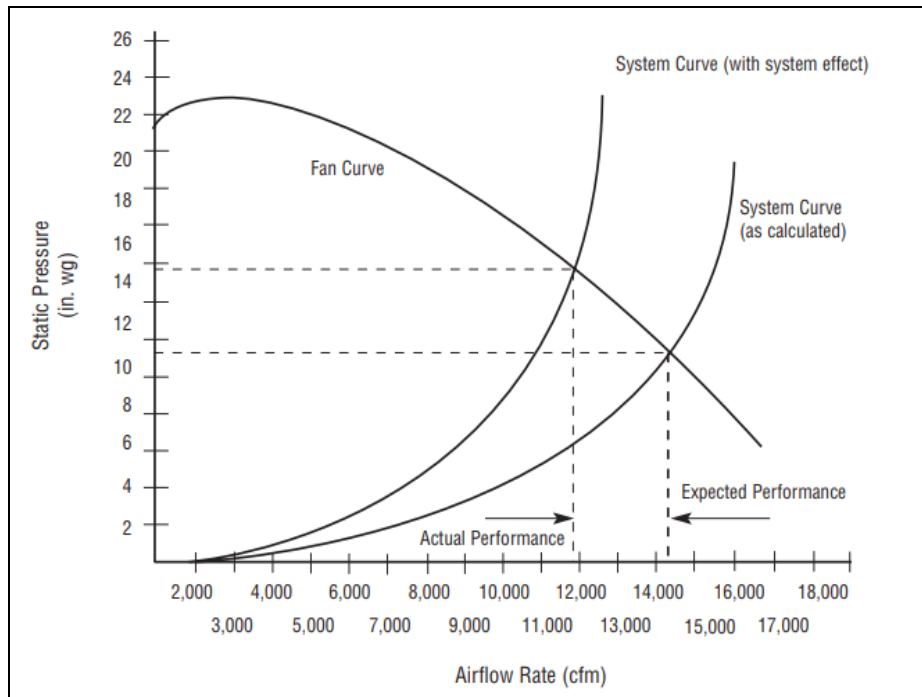


Figure 6: Fan and system curve plotted for a range of pressures and volumetric flows [2].

The expected operating point and its performance based on the intersection between the calculated system curve and the given fan curve may be shifted to the left on the fan curve when accounting for system effects. It is the degradation in performance (higher pressure loss for the same flow) due to unfavourable flow conditions at the inlet or outlet of the fan and as a result of interactivity between components in the system [2, 7]. System effects (which is described more clearly in Section 2.1.6) is therefore very important to account for when establishing the operational point.

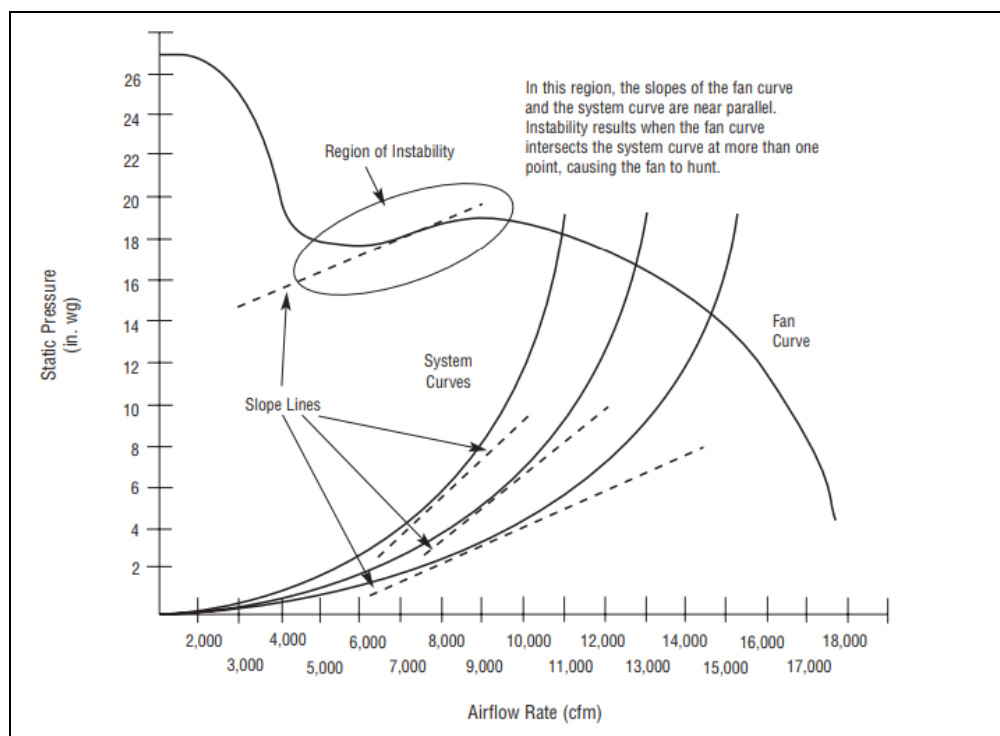


Figure 7: Region of instability shown for a fan curve with multiple system curves [2].

Theory

As shown in *Figure 7*, illustrating another principal fan curve, there is a region to the left of the peak pressure, where there is an increased risk of induced fan instability. Three different system curves are shown, that all have the same slope directions as the instability region. In case of having a system curve with even greater inherent resistance (shifted even further to the left), and directly intersecting with the fan curve in this region of instability, drastically reduced performance can be expected. It is a result of the interaction between the fan and the system [2]. For the bigger part of the fan curve, there is a general relation between flow and pressure, and that is that an increase in airflow is related to a decrease in pressure. In the region of instability however, the fan works to increase the airflow, and that results in the pressure being temporarily increased as well. As a response to the increased pressure, the airflow will start to decrease and thus a lowered pressure is obtained. To combat this, the fan will try to increase the airflow again like in the initial state, and so the cycle repeats itself. This constant and rapid alternation between different states leads to a lowered fan efficiency, with excessive noise generation and promotes wear and tear on the different components of the fan [2].

2.1.4 Efficiency and Power Curves (Performance Curves)

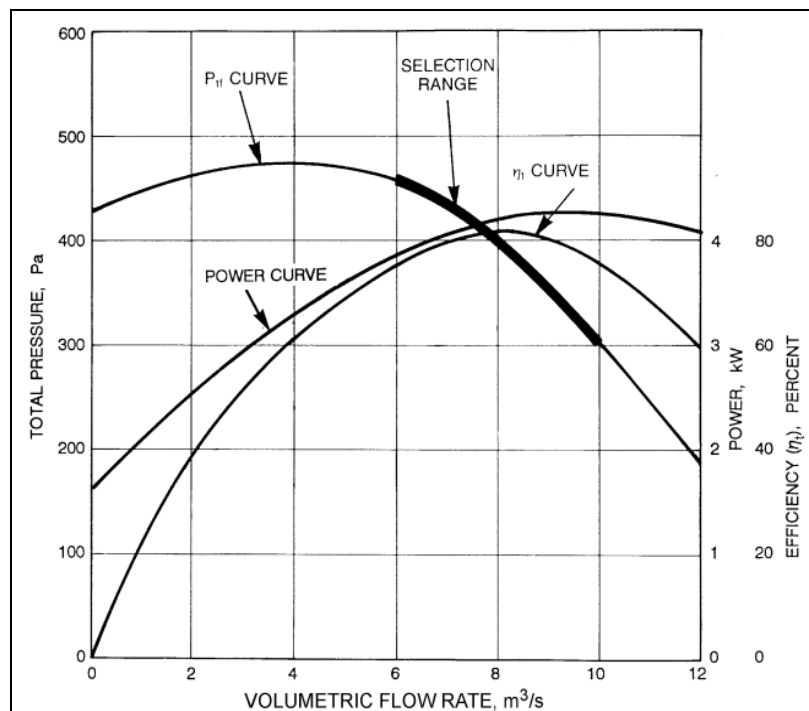


Figure 8: Fan curve with selection range based on an efficiency and power curve [1].

In addition to the fan curve (labeled here as a P_{tf} curve, where P_{tf} stands for fan total pressure), an efficiency and power curve is displayed in *Figure 8* (η_t is total efficiency). These curves together are also known as performance curves [1]. As can be seen, the efficiency peaks somewhere to the right of the peak pressure on the fan curve. The power curve, which gives the input power to the shaft that is connected to the fan, has a shape according to the figure. Increased volumetric flow rates will tend to lead to increased required power levels, up until a point where the power reaches its maximum value. The power levels will start to self-limit and become lower afterwards. This behaviour, often called “non-overloading”, is a desirable feature that can be achieved by backward inclined fans [5].

Based on the efficiency curve a selection range is presented. The operational point should be positioned within this range to obtain a high fan efficiency. Preferably it should be located at the fan peak efficiency, as it provides the most cost-effective operation of the fan in terms of efficiency and maintenance. It is called the Best Efficiency Point (BEP) [2]. All the curves that are shown in *Figure 8* are based on the total pressure, as indicated by the subscripts. The fan- and efficiency curves will look slightly different when being based on the static pressure. This is demonstrated in *Figure 9*, where the performance curves are given for both static- and total pressure conditions. Subscript t stands for total while s equals static. It is of high importance to differentiate between these two counterparts; as the static pressure and efficiency always will be lower than the total one. This is something that some fan manufacturers take advantage of when displaying performance data to the general public (publishing the total efficiency instead of the static efficiency).

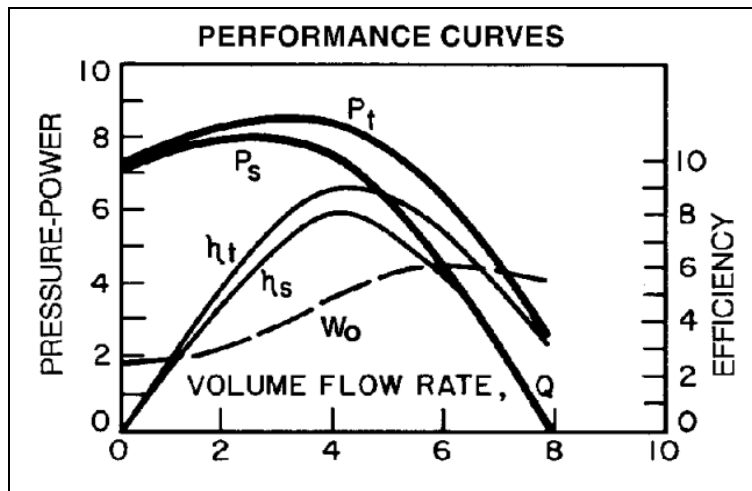


Figure 9: Fan, efficiency and power curves for total and static pressure [1].

2.1.5 Fan Laws

The Affinity Laws, also known as Fan or Pump Laws, based on the application, are a series of relationships between flow, rotational speed, static pressure and power [8]. These laws are presented in the following table (*Table 1*):

Table 1: Fan Laws

Law Number	Dependent Variables	Independent Variables
A1	$Q_1 = Q_2 \times$	$(D_1/D_2)^3 (\omega_1/\omega_2)$
A2	$p_1 = p_2 \times$	$(D_1/D_2)^2 (\omega_1/\omega_2)^2 (\rho_1/\rho_2)$
A3	$W_1 = W_2 \times$	$(D_1/D_2)^5 (\omega_1/\omega_2)^3 (\rho_1/\rho_2)$
B1	$Q_1 = Q_2 \times$	$(D_1/D_2)^2 (p_1/p_2)^{1/2} (\rho_2/\rho_1)^{1/2}$
B2	$\omega_1 = \omega_2 \times$	$(D_2/D_1) (p_1/p_2)^{1/2} (\rho_2/\rho_1)^{1/2}$
B3	$W_1 = W_2 \times$	$(D_1/D_2)^2 (p_1/p_2)^{3/2} (\rho_2/\rho_1)^{1/2}$
C1	$\omega_1 = \omega_2 \times$	$(D_2/D_1)^3 (Q_1/Q_2)$
C2	$p_1 = p_2 \times$	$(D_2/D_1)^4 (Q_1/Q_2)^2 (\rho_1/\rho_2)$
C3	$W_1 = W_2 \times$	$(D_2/D_1)^4 (Q_1/Q_2)^3 (\rho_1/\rho_2)$

Note: Subscript 1 indicates the variable of the fan under consideration, while subscript 2 represents the variable for the tested fan.

where:

Q - Volume flow rate [m³/s];

ω - Rotational speed [rpm];

p - Static pressure [kPa];

ρ - Gas density [kg/m³];

D - Fan size [mm];

W - Power [kW].

Rotational speed must be considered concurrently with other issues, such as variation in the fan load, airstream temperature, ambient noise and mechanical strength of the fan. Variations and uncertainties in system requirements are critical to fan type and fan rotational speed selection. Fans that generate high airflow at relatively low speeds (for example, forward-curved blade centrifugal fans) require a relatively accurate estimate of the system airflow and pressure demand. If, for some reason, system requirements are uncertain, then an improper guess at fan rotational speed can cause under-performance or excessive airflow and pressure. Airstream temperature has an important impact on fan-speed limits because of the effect of heat on the mechanical strength of most materials. At high temperatures, all materials exhibit lower yield strengths. Because the forces on shafts, blades, and bearings are proportional to the square of the rotational speed, high-temperature applications are often served by fans that operate at relatively low speeds.

2.1.6 System Effects

System effect is the deterioration in system performance (increased resistance) caused by unfavourable flow conditions in close proximity to the operating fan. Each component in a system has a loss coefficient that describes its pressure drop [2]. As these coefficients are based on ideal conditions, with uniform flow profiles at inlet and outlet, and disturbances within the system easily can create swirls and vortices, there is a risk of inducing system effects with deviations from mentioned ideal loss coefficients [2]. That leads to detrimental effects like poor fan performance in combination with excessive vibration and noise generation [9].

Figure 10 shows how the system effect impacts the position of the operational point on a fan curve at the outlet of a system. A shift from point (1) to (2) leads to a deficiency in airflow as a result of an increased design resistance. There are different suggestions of how one could try to decrease or eliminate the system effects downstream and/or upstream of a fan. For example, through introduction of guiding or turning vanes, splitters and altering size, shape and orientation of the ducts [2, 7]. The overall goal is to get a more uniform flow closer to the ideal testing conditions.

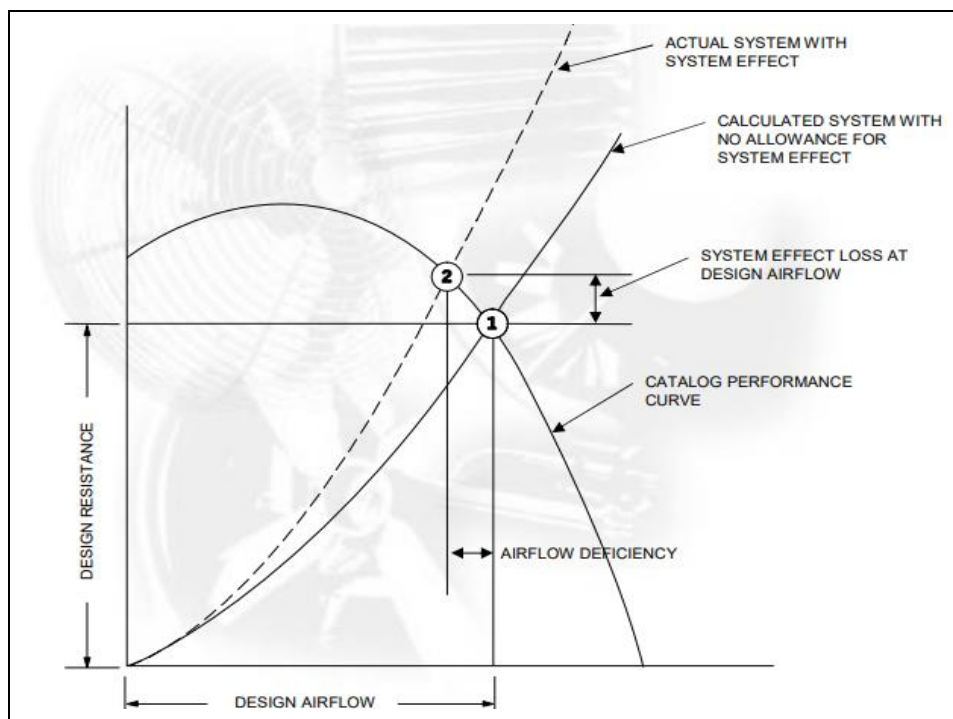


Figure 10: Outlet system effect and its impact on the operational point [10].

2.1.7 Parallel Operation

Introduction of more than one centrifugal fan, in parallel operation, can be advantageous from many points of view. As mentioned before, having several smaller fans, instead of a larger one, is a flexible solution in case of space constraints. It may not always be possible to fit a larger fan that can meet the desired flow. Other mentioned pros of parallel configurations are higher efficiencies for a wide range of air volumes, redundancy (back-up fan is available in case one of the fans stops working) and lower noise generation [2].

When running multiple fans, there are some instability risks, that have to be considered. *Figure 11* displays a combined fan curve (two fans in parallel) and a single fan curve. As can be seen by the shaded regions in black, instability can occur, in case the system curve intersects with the combined fan curve through this area. It is explained by the fact that the fans will have unequal loading, where one of the fans takes the bigger load and requires more electrical power compared to the other one, which is severely underloaded and performs at low efficiency. The fans can start to alternate in this behaviour. At one point in time one fan may be underloaded, to suddenly at another point in time be overloaded. This fan behaviour is known as “hunting”, a cyclic behaviour in which the fans try to find a stable operating point [1] [2], and can induce annoying noise patterns. Therefore, when operating with multiple fans, it is important to ensure that the operating point is to the right of point A on the curve.

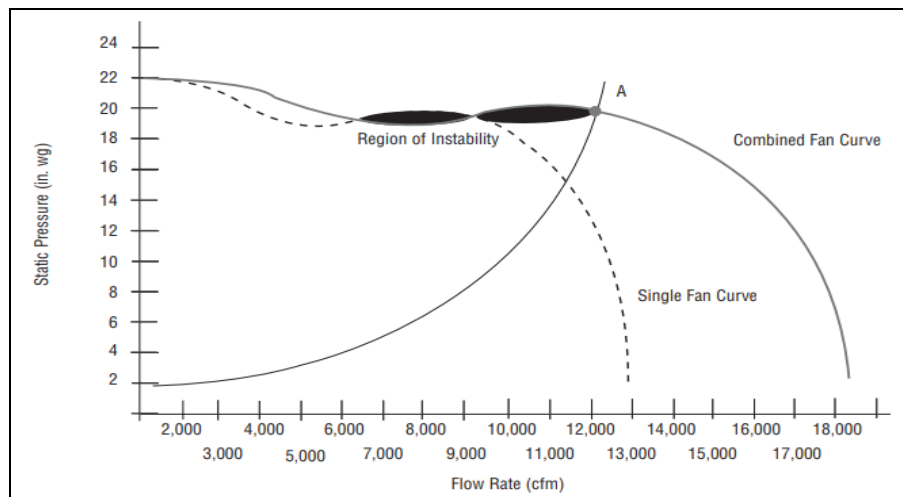


Figure 11: Illustration of difference between single and combined (parallel operation) fan curves [3].

The display of a parallel centrifugal fan setup under manufacturing stages can be seen in *Figure 12* and *Figure 13* below. The pictures, that have been taken at Swegon’s manufacturing site in Kvänum, show different views of one of the larger setups that are being sold currently.



Figure 12: Front view of a parallel centrifugal fan setup (Swegon, Kvänum, 2019).



Figure 13: Back view of a parallel centrifugal fan setup (Swegon, Kvänum, 2019).

2.2 Computational Fluid Dynamics

2.2.1 Governing equations

The fundamental equations (for continuity, momentum and energy) which describe the fluid motion are presented here. These equations are the cornerstones of fluid dynamics, and have to be solved by the CFD-software. This theory gives a brief overview of these important physical correlations.

2.2.1.1 Continuity

The principle of continuity states that the mass of a fluid has to be conserved within a system, meaning that the mass flowing into the system is equal to the mass flowing out from the system [11]. It can be written as [12]:

$$\frac{\partial \rho}{\partial t} + \frac{\partial \rho U_1}{\partial x_1} + \frac{\partial \rho U_2}{\partial x_2} + \frac{\partial \rho U_3}{\partial x_3} = 0 \quad (2.1)$$

where ρ is the density and U_1 , U_2 , and U_3 represent the different velocities in a three dimensional cartesian coordinate system. With tensor notation, which is commonly applied, the same equation can be formulated on compact form as:

$$\frac{\partial \rho}{\partial t} + \frac{\partial \rho U_i}{\partial x_i} = 0, \text{ simplified to } \frac{\partial U_i}{\partial x_i} = 0 \text{ if incompressible flow is assumed} \quad (2.2)$$

2.2.1.2 Momentum

The equations that describe the balance of momentum, or motion, are based on Newton's second law ($F=ma$). The source of the experienced forces on the fluid elements in each direction arise from body forces, like the gravitational force, and surface forces due to shear and normal stresses in the flow field [13]. That will lead to local accelerations according to Newton's second law. The equations of momentum, also known as the Navier-Stokes equations, are a different way of expressing this and can be formulated as follows [12]:

$$\frac{\partial U_i}{\partial t} + U_j \frac{\partial U_i}{\partial x_j} = -\frac{1}{\rho} \frac{\partial P}{\partial x_i} + \frac{1}{\rho} \frac{\partial \tau_{ji}}{\partial x_j} + g_i \quad (2.3)$$

where U is the velocity, ρ is the density, P is the pressure, τ is the tensor stress and g is the gravitational acceleration. For turbulent flow using an eddy-viscosity model, the equation reads as [14]:

$$\frac{\partial \rho U_i}{\partial t} + \frac{\partial}{\partial x_j} (\rho U_i U_j) = -\frac{\partial P}{\partial x_i} + \frac{\partial}{\partial x_j} \left[(\mu + \mu_t) \left(\frac{\partial U_i}{\partial x_j} + \frac{\partial U_j}{\partial x_i} \right) \right] \quad (2.4)$$

2.2.1.3 Energy

Equations related to the energy of fluid elements are based on the first law of thermodynamics, describing the principle of energy conservation. The law states that: for an enclosed system, the difference in internal energy between two states must be equal to the amount of heat added to the system minus the work that the system has performed on its surroundings [15]. The energy equation, in differential form, can be written as [3]:

$$\rho \frac{d\hat{u}}{dt} + \rho(\nabla \cdot \mathbf{V}) = \nabla \cdot (\lambda \nabla T) + \Phi \quad (2.5)$$

where \hat{u} is the internal energy, ρ the density, \mathbf{V} the velocity vector, λ the thermal conductivity, T the temperature and Φ the viscous-dissipation function (see reference [3] for more information about this function). This equation is valid for general conditions of flows that are compressible, conduct heat and are viscous in nature. For an incompressible flow with a constant density, viscosity and thermal conductivity, the equation can be reduced to [3]:

$$\rho C_p \frac{dT}{dt} = \lambda \nabla^2 T + \Phi \quad (2.6)$$

containing the specific heat C_p at constant pressure. Given the assumptions stated above this equation is a more simplified, hence more preferable version. In turbulent form, the energy equation reads:

$$\rho C_p \frac{dT}{dt} = \nabla \cdot [(\lambda + \lambda_t) \nabla T] + \Phi \quad (2.7)$$

2.2.2 Turbulence model - k-ε

With flows that are highly turbulent, like the ones observed in this study, some kind of turbulence model needs to be used. This in order to account for, and resolve critical regions, in close proximity to solid surfaces (walls). As k-ε turbulence modelling is used throughout the different simulations, the theory behind it is briefly described here.

The k-ε turbulence model is a model that requires solving of two additional transport equations for the turbulent kinetic energy k , and the turbulent dissipation rate ε , why it is called a two equation model. It is a model where the turbulent viscosity can be determined from these additional equations [16] [17]. This type of turbulence model is very common in industrial engineering applications.

There is an improved version of the model, called the realizable k-ε model, that satisfies certain mathematical constraints known as the Reynolds stresses. This is done by introducing a new equation of transport for ε , and defining a critical constant C that can vary, being a function of turbulence properties and the mean flow [18].

3 Methodology

The third chapter contains explanations of the general workflow and setup of the different models that were simulated in the CFD-software Star-CCM+. It is a simulation tool developed and created by Siemens, with a user-friendly interface. All preparations, simulations and post-processing can be performed at the same place, with possibilities of handling a wide array of physical flow phenomena.

3.1 Reference

The first step that was taken was to establish and set up the reference case for the supply side of an AHU in which two centrifugal fans operating next to each other are positioned. The set up consisted of the creation and simulation of a model based on a current geometry of the fans in an AHU, for a different model within Swegon’s catalogue. This reference model was to be used to analyse and determine the causes of the fan efficiency drop and to provide the building blocks upon which different solutions were to be tested. The most vital steps in this process are described in the subsections below.

3.1.1 Geometry

Swegon provided the CAD-geometry for the supply side of the AHU, consisting of a rectangular casing with two centrifugal fans positioned next to each other (see *Figure 14* and *Figure 15*). As this geometry had been created in an external CAD-software (Solidworks), it had to be imported into STAR-CCM. The model is scaled down, to decrease the mesh size of the AHU. Thus, reasonable time requirements can be achieved when performing the different simulations. The distances of the different edges in the casing (in the scaled down version) are displayed in *Figure 16* and a summary of some of the most important geometrical parameters are given in *Table 1*.

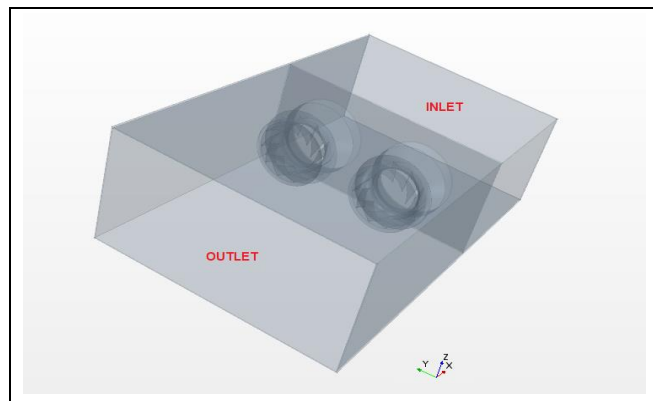


Figure 14: Transparent view of the CAD-model consisting of centrifugal fans and casing for inlet- and outlet.

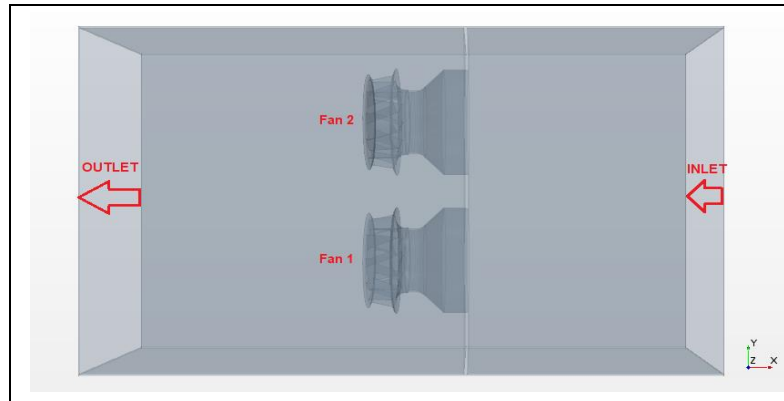


Figure 15: Transparent top view of the CAD-model, illustrating the centrifugal fans and the flow direction.

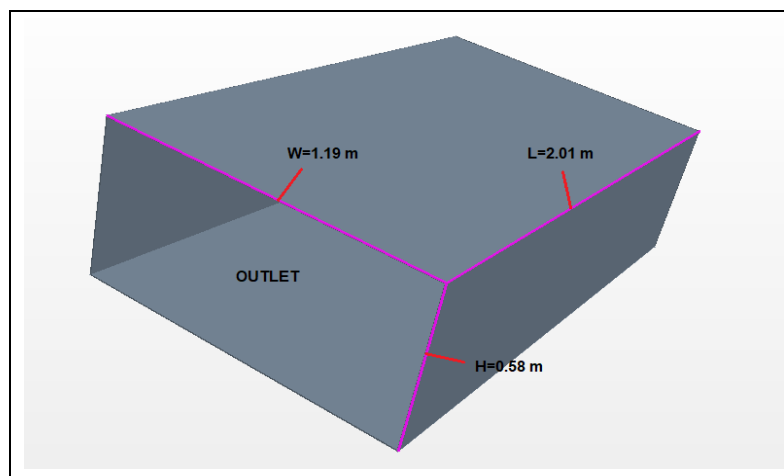


Figure 16: Non-transparent view in perspective showing the height, width and length of the casing.

Table 2: Important geometrical parameters in the AHU

Parameter	Value
Length of case (L_{case})	2.01 [m]
Height of case (H_{case})	0.58 [m]
Width of case (W_{case})	1.19 [m]
Diameter fan (D_{fan})	0.4 [m]
Distance between fans (d)	0.12 [m]

Some of the physical parts that in reality exist in the casing, like motors, control equipment and additional frameworks for the fans have been omitted and are not part of the geometry. This is a simplified model that mainly focuses on the interaction between the fans.

The inlet, outlet, fan 1 and fan 2 each had to have its own geometry part in Star-CCM+. These four parts were created based on the given CAD-model. A geometry part is an object with a collection of surfaces and curves that describe the geometry, and is used in later operations of the modelling process. The goal was to obtain all the enclosing surfaces of the fluid domains. In the end, these surfaces could be separated and organized under their respective geometry part nodes in the programme.

3.1.2 Regions

Each geometry part had to be assigned to a corresponding region, where the volume domain with its surrounding boundaries are specified. While the parts describe the simulation in terms of geometry, the actual meshing and solving of physics is based on the regions. As multiple regions are present they needed to be joined together which was done by performing an imprint operation. Another important aspect was to have in-place interfaces between the boundaries of the connecting regions. That ensures that the computational information can be transferred accurately from one region to another during simulation.

3.1.2.1 Inlet Region

This region represents a static part of the model and was built upon all the inner surfaces of the inlet volume of the casing and the two cones that are connected to the fans. The boundaries that can be found in this region is the inlet-boundary for the whole assembly (see *Figure 17*), the outlet boundaries from the cones, (the same as the inlet surfaces to the fans (see *Figure 18*) and the rest of the volume enclosing wall-boundaries.

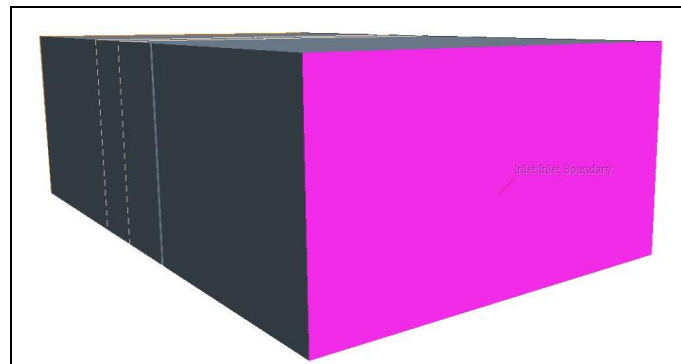


Figure 17: Inlet-boundary of the AHU.

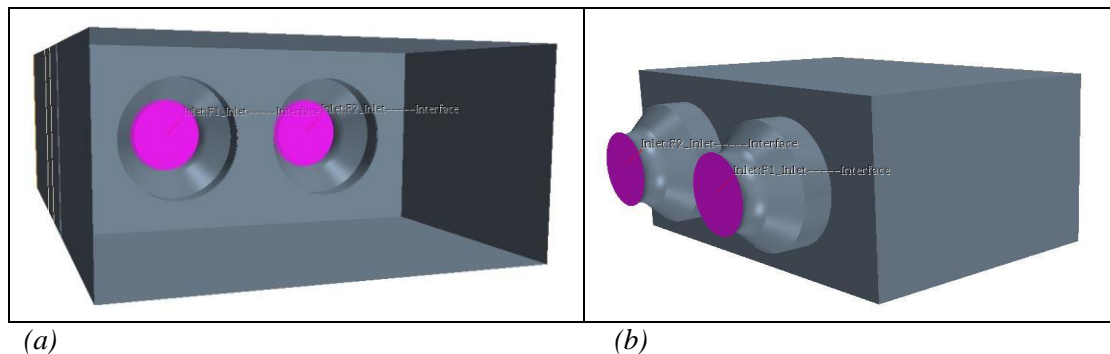


Figure 18: Outlet boundaries of the inlet region (inlet surfaces to the fans): (a) Inlet view (b) Outlet view.

3.1.2.2 Outlet Region

As with the inlet region, the outlet region also represents a static section of the AHU and was constructed from the inner surfaces of the outlet volume, where the chamber with the two fans are located. These surfaces represent the inner walls of the outlet and the external, rotating surfaces of the fans. The boundaries of this region are represented by the walls and cones of the casing, the so called “wall-boundaries”, the outlet boundary of the AHU (see *Figure 19*), the exhaust boundaries of the fans (see *Figure 20*) and a small gap present between each fan and the casing (see *Figure 21*). The last two mentioned boundaries are the interfaces found between the fan- and outlet regions.

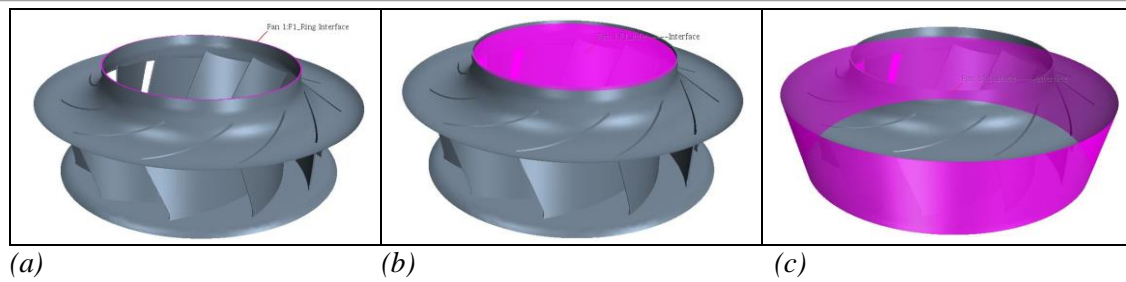


Figure 23: The interfaces for one fan. (a) Gap (b) Inlet (c) Exhaust

3.1.3 Meshing

Meshing was performed individually for the different regions within the operations node of Star-CCM+. A mesh-plane cutting through the supply side of the AHU can be seen in *Figure 24* and shows the differences in terms of mesh size across the connected regions. A finer mesh, with more cells, has been created in areas of high importance. That is, inside the fans, in between them and at segments of walls that are in close proximity. As the interaction of the fans is the primary interest of this study, it is important to have a denser mesh in these areas, to try and capture the flow behaviour as accurately as possible. A coarser mesh could be created closer to the inlet and outlet, to decrease the total amount of cells to be simulated. In the end, the whole simulation domain would consist of approximately 6.8 million cells.

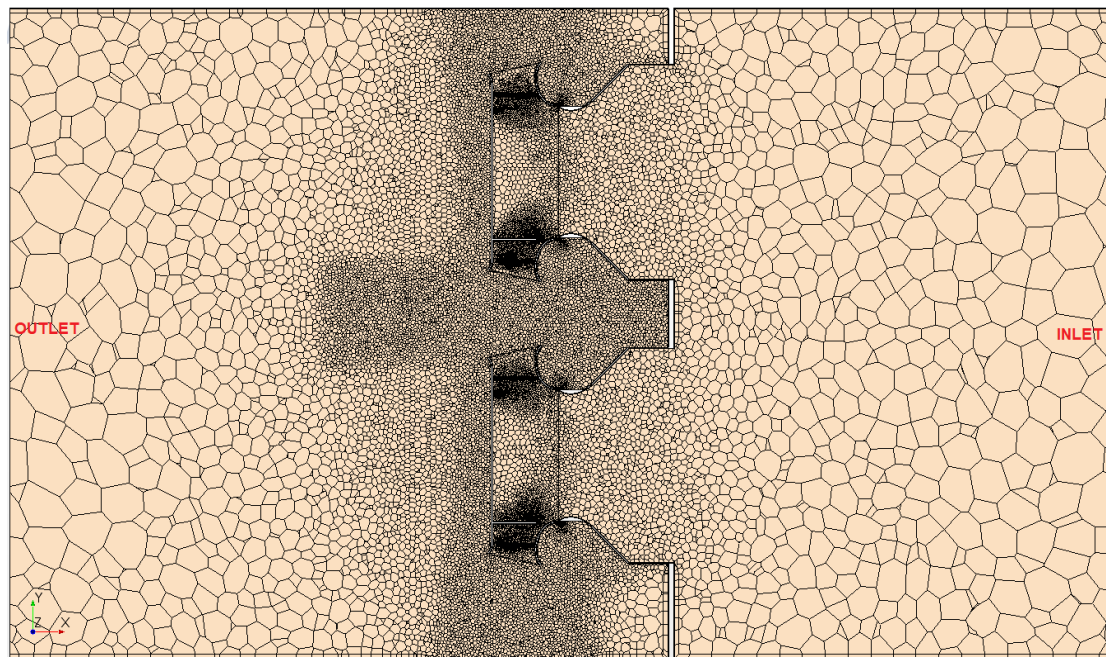


Figure 24: Volume mesh of the different regions shown in a plane section cutting through the AHU.

Another mesh-plane, normal to the axis of rotation, and cutting through both fans is shown in *Figure 25*. As can be seen, the mesh around the blade curvature is the finest, with a target surface size of 2 mm, while the surrounding cells in the plane have a target surface size of 5 mm. The largest cells in the model are located close to the inlet and outlet (see *Figure 26*) and have a target surface size of 10 cm. Most of the meshing in the refined regions has been done with custom controls of the individual surfaces (based on meshing instructions from Swegon) instead of using the standard inbuilt default controls. This was made in order to facilitate the controllability of the meshing process. In addition, several wake refinements have been applied to create an anisotropic mesh. For example, the refined area downstream and in between the

Methodology

fans is based on such a wake refinement in negative x-direction. A more detailed specification of the different mesh settings for the fans is given in Appendix (see A1).

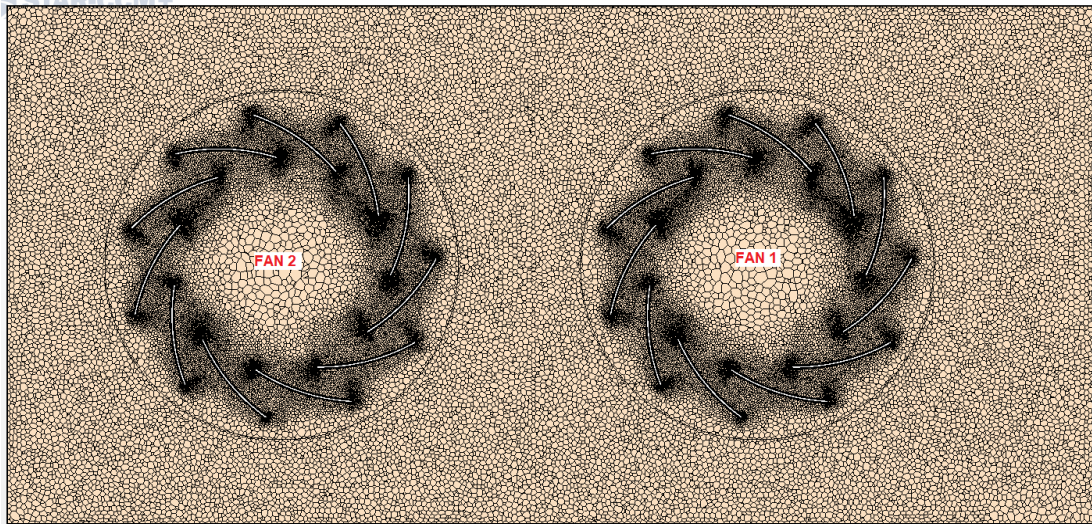


Figure 25: Volume mesh in a plane normal to the rotation axis in the outlet region.

A list of mesher types that have been applied in the model is given in *Table 3*. Initial meshing of the different boundary surfaces has been made with a surface remesher. When it comes to the core volume mesh treatment, a polyhedral mesher has been chosen, which gives the generated cells a polyhedral shape. Lastly, close to the walls, a prism layer mesher has been utilized. Thin prism layers are then generated to accurately account for turbulent boundary layers and steep velocity profiles in the flow field. The prism layers have been controlled in terms of first layer thickness and total height. For the refined regions, 5 prism layers are present next to the walls, while 3 prism layers have been used at walls in the coarser regions.

Table 3: Mesher applications and types used in the modelling.

Mesher Application	Type used
Surface Mesher	Surface Remesher
Core Volume Mesher	Polyhedral Mesher
Boundary Layer Mesher	Prism Layer Mesher

Mesh quality had to be considered during the meshing process and the main metrics that were examined were cell quality, skewness angle and volume change. The distributions of these quality parameters across the volume mesh are shown in histogram plots, see Appendix (A2). The user manual from Star-CCM+ provides guidelines for what the upper or lower limit of these criteria should be in order to have an acceptable mesh quality. For the cell quality, the worst value obtained was 0.02 for 1204 cells. Unsatisfying cells, also known as bad cells, are considered to be those with a value lower than $1.0e-05$ [19]. Furthermore, the largest skewness angle was 87.7° and that applied for 5364 cells. A skewness angle of 90° or more can cause convergence issues [19]. Finally, the lowest volume change attained was 0.023 for a frequency of 14679 cells, in relation to the limit of bad cells that occur at values lower than 0.01 [19].

3.1.4 Boundary Conditions

Boundary conditions have been provided from Swegon based on the previous centrifugal fan simulations that have been conducted from the company's side. The inlet boundary conditions are displayed in *Table 4a*. The specification in terms of type was set to mass flow inlet, normal to the boundary surface. Four different simulations, labelled as Operating Points, were conducted with increasing mass flow rates. This was done, as AHU-applications usually require a span of mass flows that need to be delivered throughout operation, and therefore this variability had to be taken into account. The method for turbulence specification was set to intensity and length scale.

Table 4a: Inlet boundary conditions.

Parameter	Physics Value
Mass Flow Rate	Operating Point 1: 1.23 [kg/s] Operating Point 2: 1.87 [kg/s] Operating Point 3: 2.57 [kg/s] Operating Point 4: 3.19 [kg/s]
Turbulence Intensity	4.5 [%] used for simulation 1-4
Turbulent Length Scale	0.054 [m] used for simulation 1-4

The boundary conditions that are valid for all walls throughout the model are shown in *Table 4b*. A blended wall-function is used where the log law offset (E) and Von Karman constant (κ) are defined. The default values for these two parameters were applied. All walls are set to the no-slip condition.

Table 4b: Wall boundary conditions.

Parameter	Physics Value
E (log law offset)	9.0 [-] used for Operating Point 1-4
κ (The Von Karman constant)	0.42 [-] used for Operating Point 1-4

When it comes to the outlet boundary conditions, that can be seen in *Table 4c*, the type was defined as a pressure outlet. Once again, intensity and length scale were used in the turbulence specification.

Table 4c: Outlet boundary conditions.

Parameter	Physics Value
Pressure	1.0 [atm] used for Operating Point 1-4
Turbulence Intensity	4.0 [%] used for Operating Point 1-4
Turbulent Length Scale	0.087 [m] used for Operating Point 1-4

3.1.5 Continua

The physics continuum in terms of models and initial conditions are given in *Table 5a* and *Table 5b* and are based on settings provided from Swegon. Enabled models are valid for all Operating Points. For the initial conditions, turbulent velocity scale and velocity was altered between the different simulation points.

Table 5a: Physics continuum in terms of chosen models for the simulations.

Condition	Enabled Models
Flow	Coupled
Space	Three Dimensional
Time	Steady
Material	Gas (Air)
Equation of state	Constant Density
Viscous Regime	Turbulent
Reynolds-Averaged Turbulence	Realizable k- ϵ Two Layer
Wall Treatment	Two-Layer All y^+ Wall Treatment
Wall Distance	Exact Wall Distance
Gradients	Hybrid Gauss-LSQ

Table 5b: Physics continuum in terms of initial conditions for the simulations.

Parameter	Value
Pressure	0 [Pa] used for Operating Point 1-4
Turbulence Intensity	4 [%] used for Operating Point 1-4
Turbulent Length Scale	0.265 [m] used for Operating Point 1-4
Turbulent Velocity Scale	1.5 [m/s] used for Operating Point 1 2.2 [m/s] used for Operating Point 2 3.0 [m/s] used for Operating Point 3 3.7 [m/s] used for Operating Point 4
Velocity	[-1.5, 0, 0] [m/s] used for Operating Point 1 [-2.2, 0, 0] [m/s] used for Operating Point 2 [-3.0, 0, 0] [m/s] used for Operating Point 3 [-3.7, 0, 0] [m/s] used for Operating Point 4

3.1.6 Simulations and Post Processing

As could be seen from *Table 5a*, all simulations were performed in a steady-state condition. To study convergence during the simulations, several plots had been set up for process sensitive variables at different surfaces of the model. Example of such variables were static pressure (area averaged) and mass flow; monitored at the defined interface boundaries and over the inlet and outlet of the total unit. Momentum is another parameter that was set up for the fans and was based on all the individual fan surfaces. The residuals needed to be examined alongside, to study the change in error from one iteration to the next one. In case of severe residual oscillations, lower values were used for the under relaxation factors, in order to introduce some stability (at the cost of calculation speed). For an arbitrary simulation, it would be stopped when all convergence monitors had reached steady values, in combination with the residuals of that simulation reaching low enough values and not fluctuating too heavily. Some general data for the conducted simulations in terms of cell count, iterations and residual behaviour is presented in Appendix (see A3 and A4).

The solutions could be studied more in detail by setting up scalar- and vector scenes of the flow field. A few of the parameters that would be of interest to look into were the pressure distribution around the blades and across the domains, the velocity in the direction of flow (x-direction), the total velocity magnitude and the wall shear stresses. Reports that were generated beforehand could be used to get a scalar value for each of the monitored variables at the last iteration, and that data collection would form the basis for performing efficiency calculations (see Section 3.1.7) and creating graphs in an external software (Excel).

3.1.7 Efficiency Calculations

In order to evaluate fan performance for the studied system, Swegon provided a formula which was used to determine the static efficiency of the fans for the conducted simulations:

$$\eta_s = \frac{(P_{inlet,s} - P_{outlet,s}) \cdot Q_{f,i}}{M_{f,i} \cdot \omega} \quad (3.1.1)$$

where:

η_s - Static Fan Efficiency [-];	$Q_{f,i}$ - Volume Flow through fan i [m^3/s];
$P_{inlet,s}$ - Static Pressure at Inlet of AHU [Pa];	$M_{f,i}$ - Moment of fan i [Nm];
$P_{outlet,s}$ - Static Pressure at Outlet of AHU [Pa];	ω - Rotational speed [rad/s].

Similarly, a formula was used to determine the static efficiency of the AHU as a whole, and that was made according to:

$$\eta_{AHU} = \frac{(P_{inlet,s} - P_{outlet,s}) \cdot Q_{AHU}}{(M_{Fan1} + M_{Fan2}) \cdot \omega} \quad (3.1.2)$$

where:

η_{AHU} - Static AHU Efficiency [-]	Q_{AHU} - Volume Flow through AHU [m^3/s];
$P_{inlet,s}$ - Static Pressure at Inlet of AHU [Pa];	$M_{Fan1} + M_{Fan2}$ - Moment for both fans [Nm];
$P_{outlet,s}$ - Static Pressure at Outlet of AHU [Pa];	ω - Rotational speed [rad/s].

3.2 Modifications of Reference

Substitute designs of the reference case, that are briefly described in the following subsections, were investigated in order to study the impact on fan efficiency and overall performance of the AHU. Additional surfaces could be added to the reference model, granted that the initial geometry of the casing and fans was maintained. The conditions of the four Operating Points described previously have been applied to these modifications. Obtained mesh quality parameters for these designs are given in Appendix (see A2).

3.2.1 Modification 1a: Full Distance Wall

In modification 1a, seen in *Figure 26* and *27*, the implementation of a wall between the two fans was studied. This is a full distance wall that covers the whole outlet region, and splits the outlet chamber in two separate pathways. The wall is centered between the fans and has the same thickness (5 mm) as all the other walls of the casing.

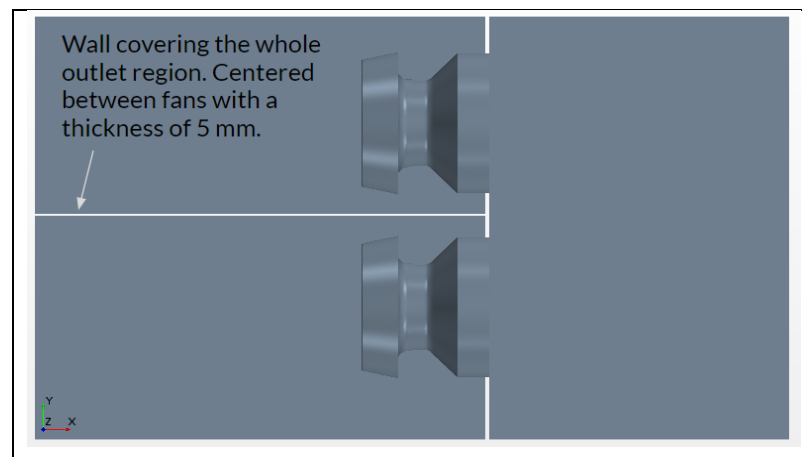


Figure 26: Modification 1a where a full distance wall, covering the whole outlet region, has been added.

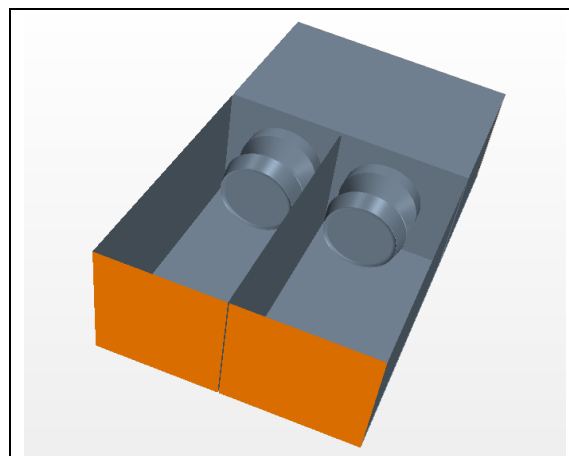


Figure 27: Modification 1a seen from a perspective view.

3.2.2 Modification 1b: Half Distance Wall

Modification 1b is based on the same principle as modification 1a, where a wall has been added between the fans. The major difference is the length of the applied wall that covers half of the outlet region. See *Figure 28* and *Figure 29*. Hence, this is a half distance wall, that partially separates the outlet region.

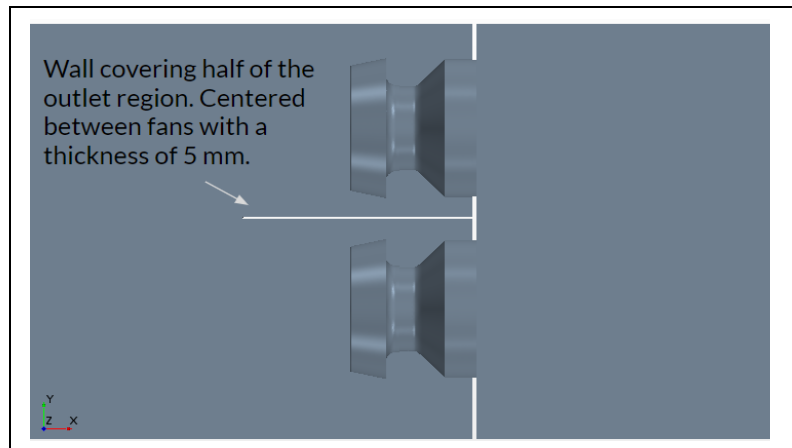


Figure 28: 1b, where a half distance wall, covering half of the outlet region, has been added.

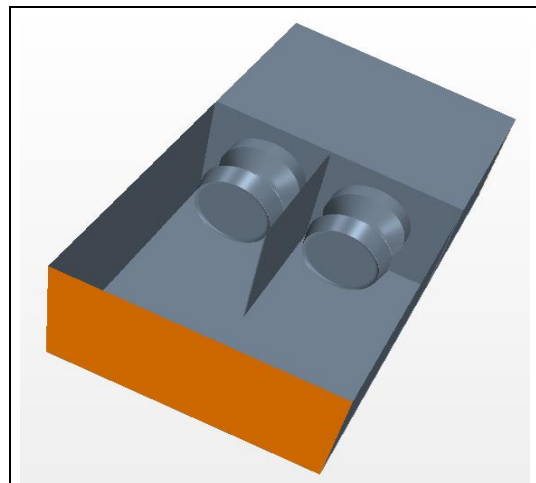


Figure 29: Modification 1b seen from a perspective view

3.2.3 Modification 2: Fan 2 Offset

As a result of their spatial position, there is a region between the fans in which pressurised air coming from the exhaust of both fans meets, leading to a pressure front that affects the fan operation. In order to avoid such an influence, one of the modifications that was brought to the model, was to offset one of the fans.

Initially, a decision had to be taken with respect to the fan that required a relocation. In the geometry of the initial case, the first fan (Fan 1) had more free space at its exhaust as a result of the control system's space requirement. The additional space led to an increased distance between the first fan and one of the walls of the outlet region (represented below in *Figure 30*). By offsetting the second fan, more space was created for its exhaust and the negative influence that affected both fans due to their proximity was reduced.

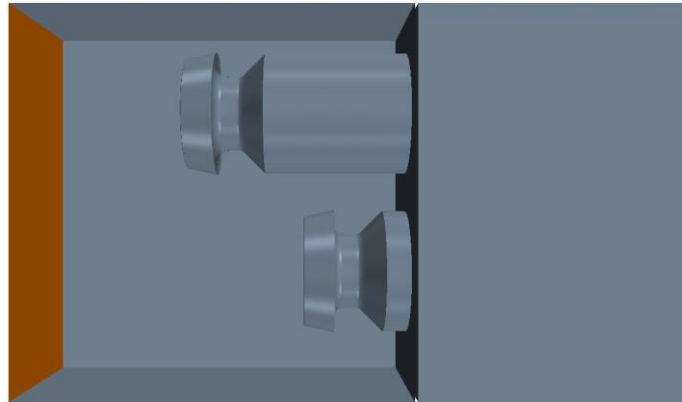


Figure 30: Modification 2, relocation of the second fan, downstream in the outlet region.

Figure 30 shows the new position of the second fan. The fan was moved 0,4 [m] downstream from the first fan in order to avoid the interference of the two fans upon each other as much as possible. The relocation took place by extending a part of the casing (the straight cone) that is connected to the impeller inlet. This decision was taken due to the fact that the change of any other part from the geometry would have had a large impact on the fan operation.

Since the modification only affected the geometry of the AHU system, all of the initial settings were unchanged. The redesigned casing that allowed for the offset of the second fan was included in the same regions as it was before the change.

3.2.4 Modification 3a: 3 Guiding Vanes

A different set of simulations was realized for a system which consisted of three guiding vanes placed in between the two fans, in close proximity to their outlet (see *Figure 31* and *Figure 32*). The role of the added guiding vanes was similar to the wall model, that is to separate the exhausted flows from the fans, while providing a new role of guiding the flow towards the outlet with less overall resistance.

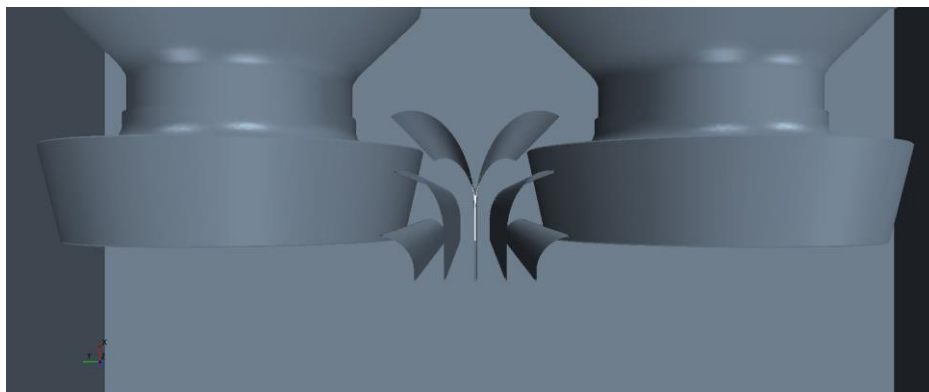


Figure 31: Modification 3a, where 3 Guiding Vanes have been added next to each fan's outlet, in the interaction area of the outlet region.

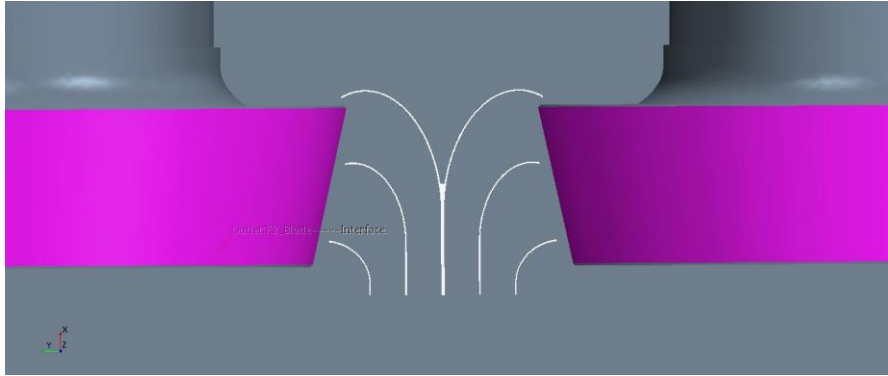


Figure 32: Top view of Modification 3a in the outlet region.

The Guiding Vanes consist of two mirrored sets of three fins that meet at the half distance between the two fans. These vanes cover the whole height of the chamber and are anchored on two opposing walls of the casing, with fins that have a thickness of 1 [mm].

3.2.5 Modification 3b: 1 Guiding Vane

This modification of the Guiding Vanes was realised in order to observe the difference in performance and efficiency of the system when there is only one guiding vane placed in between the fans. See *Figures 33* and *34*. The goal of this modification was to investigate the effect of a simplified model that could be a more economically viable solution, both in terms of material requirements, design complexity and implementation restraints.

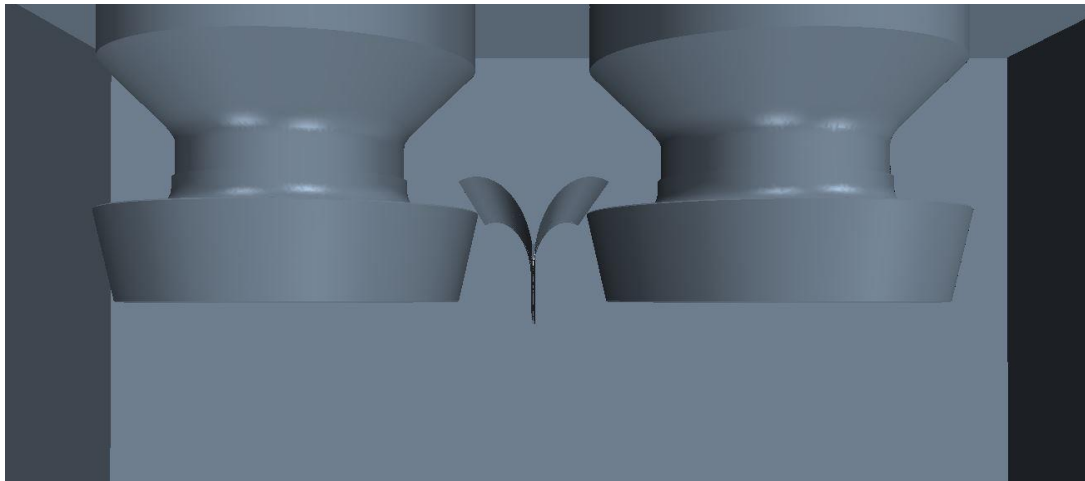


Figure 33: Modification 3b, where 1 Guiding Vane has been added next to each fan's outlet, in the interaction area of the outlet region.

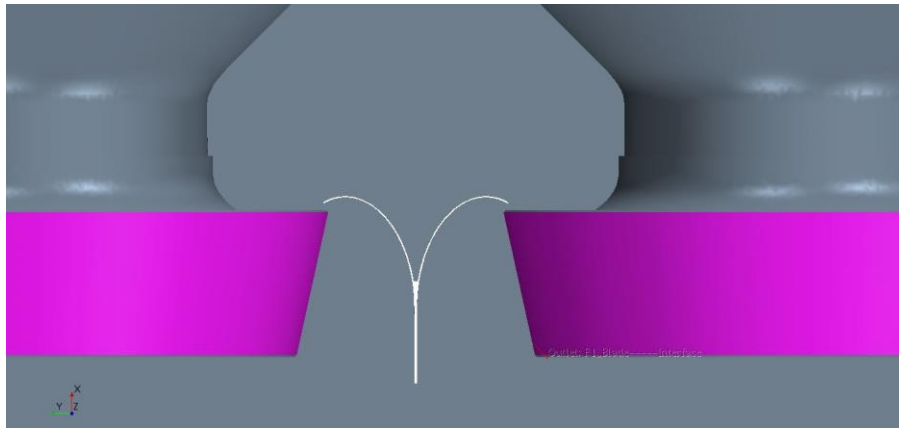


Figure 34: Top view of Modification 3b in the outlet region.

3.2.6 Modification 4: 1 Guiding Vane with Wall

A second and final modification of the Guiding Vanes case combines two previous designs: Modification 1b: Half Distance Wall and Modification 3b:1 Guiding Vane (see Figures 35 and 36). This design contains the previously described guiding vane placed in between the two fans and an extension towards the outlet of the chamber. The aim of this investigation was to determine if such a change in the geometry would provide a more efficient design than the designs it was based upon.

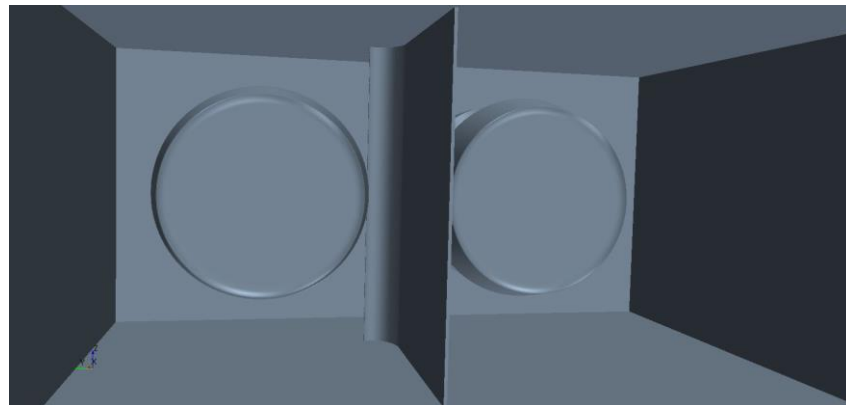


Figure 35: Modification 4, where 1 Guiding Vane with an extended wall has been added in the outlet region.

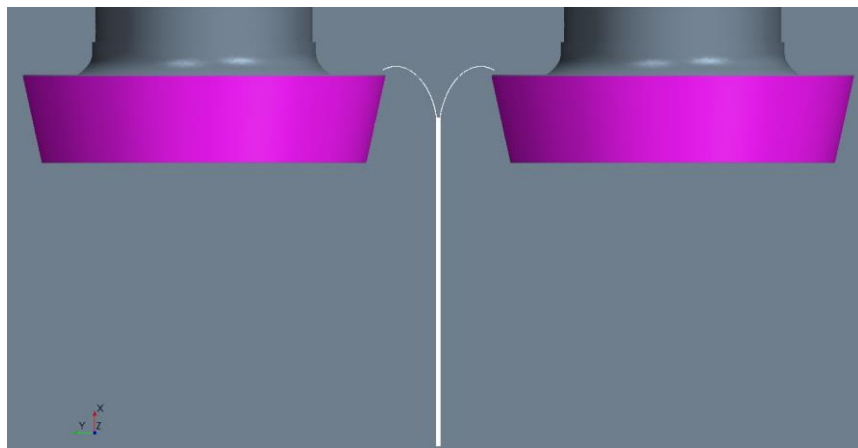


Figure 36: Top view of Modification 4 in the outlet region.

Methodology

The Guiding Vane is located in the same position as in the previous model, with its fins of 1 [mm] thickness. The difference between the cases lies with the 5 [mm] thick wall which is placed between the fans. Its position begins from the intersection of the two vanes and ends at 0.4 [m] downstream, at the midpoint of the outlet region.

4 Results

The fourth chapter presents the most important results from the conducted simulations of the reference case and the modified designs. All efficiencies and pressures are given in terms of static conditions. Comparisons are shown and the best performing solutions are presented in more detail.

4.1 Reference

4.1.1 Fan Efficiency and Pressure Rise

A first set of results indicate the fan efficiency and pressure rise values for the reference case. As presented in *Figure 37*, the pressure rise curve for each fan tends to follow the same trajectory, with small deviations in achieved pressure rise at the first and second Operating Points. Peak pressure rise for both fans occur at Operating Point 2, at a flow rate of 1.54 m³/s. In regards to fan efficiency, there are apparent differences between the two fans at low supplied air flows, represented by Operating Points 1 and 2. The largest discrepancy can be observed at Operating Point 1, where a difference of approximately 8% between the fan efficiencies can be seen (see *Table 6*). Based on the average fan efficiency curve, the best performance will occur somewhere between Operating Points 2 and 3.

Table 6: Overall data for Reference in terms of efficiency and pressure rise for each Operating Point.

	Efficiency points Fan1	Efficiency points Fan2	Average Efficiency	Pressure rise Fan1	Pressure rise Fan2	Pressure rise AHU	AHU Efficiency
Representation	----- ● -----	----- ▲ -----	- - - + - - -	--- x ---	--- x ---	--- ■ ---	- - + - -
Notation	η_s [%]	η_s [%]	η_{Avg} [%]	ΔP [Pa]	ΔP [Pa]	ΔP [Pa]	η_{AHU} [%]
Operating point 1	53,5	45,8	49,6	1020	950	914	50,0
Operating point 2	60,4	64,2	62,3	1087	1116	902	62,9
Operating point 3	61,5	61,9	61,7	1030	1029	638	61,8
Operating point 4	38,6	39,0	38,8	868	863	251	38,8

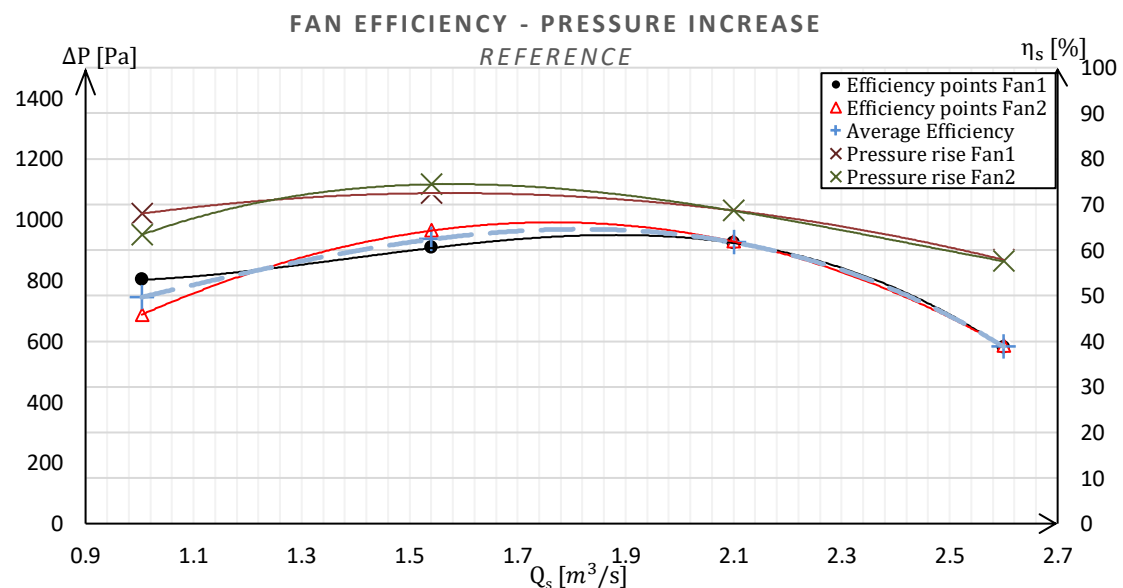


Figure 37: Fan efficiency and pressure increase curves for Operating Points 1-4.

4.1.2 AHU Efficiency and Pressure Rise

The efficiency and pressurisation of the system for the reference case is displayed in *Figure 38*. The pressure rise over the AHU, which is obtained as the difference between inlet and outlet of the system, is almost identical at Operating Points 1 and 2 and thus, the peak pressure rise is obtained somewhere in between these two points. With larger volumetric flows, the pressure rise over the unit will decrease rapidly. The overall shape of the AHU efficiency curve is identical to the average fan efficiency curve seen in *Figure 37*. Consequently, the best AHU performance is produced somewhere between the conditions defining Operating Points 2 and 3.

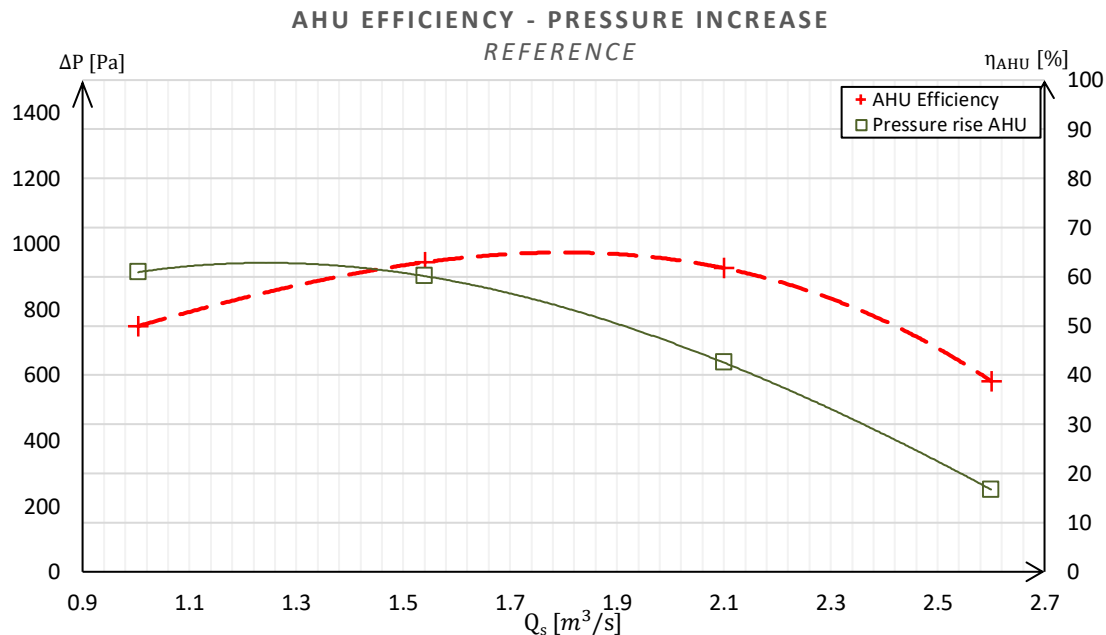


Figure 38: AHU efficiency and pressure rise curves for Operating Points 1-4.

4.1.3 Scalar and Vector Plots

4.1.3.1 Static Pressure

The static pressure across the different regions for the reference case (seen from above) and its development across the four Operating Points is shown in *Figure 39*. As can be seen, the static pressure is higher in the outlet region compared to the inlet region, which is expected, as the fans are supposed to pressurize the flow. The pressure buildup is especially significant in between the fans and at the surrounding walls in close proximity to the fans. This is illustrated more clearly in *Figure 40*, where plane sections across both fans are presented (normal to the axis of rotation). When studying the different plots from this view, it can be seen that the pressure distribution fluctuates across these planes. In all of the cases, there is a larger circumferential section around the fans with lower pressure, compared to what is procured outwards, at the corners of the casing. This can be seen as an undesirable feature, as a more even pressure distribution is a characteristic of a better performing system.

Results

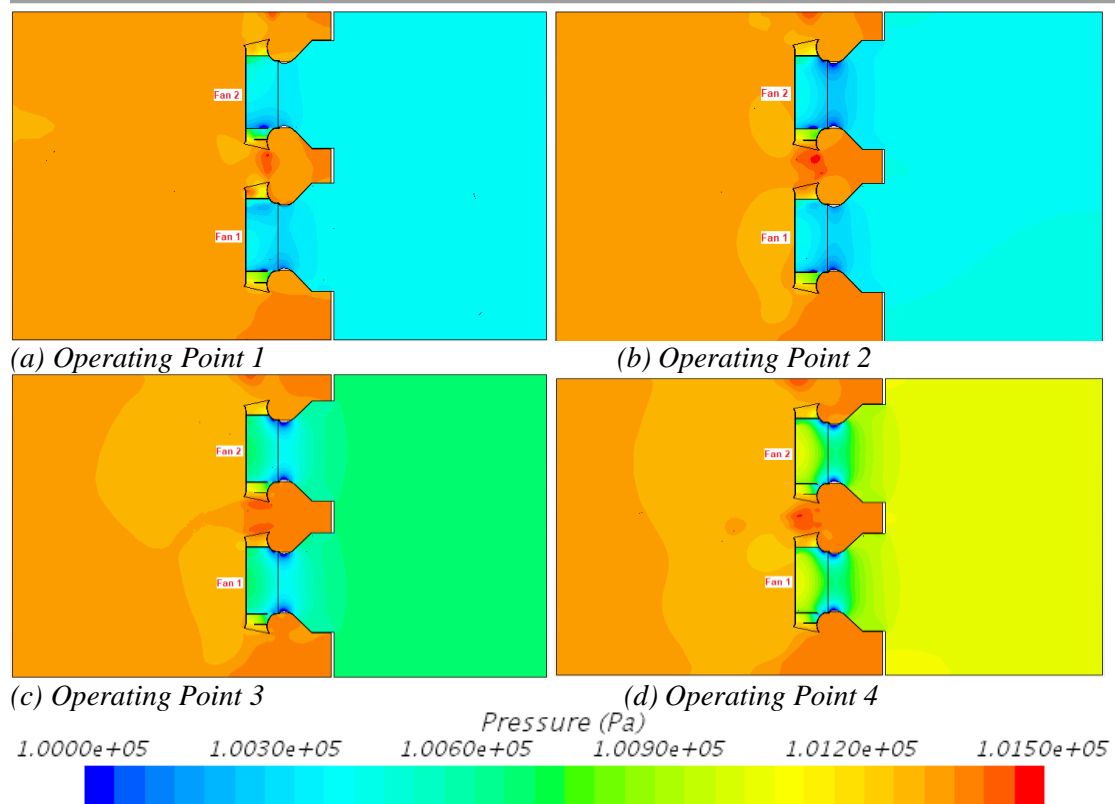


Figure 39: Static pressure for the different regions shown in a plane section cutting through the AHU, valid for Operating Points 1-4.

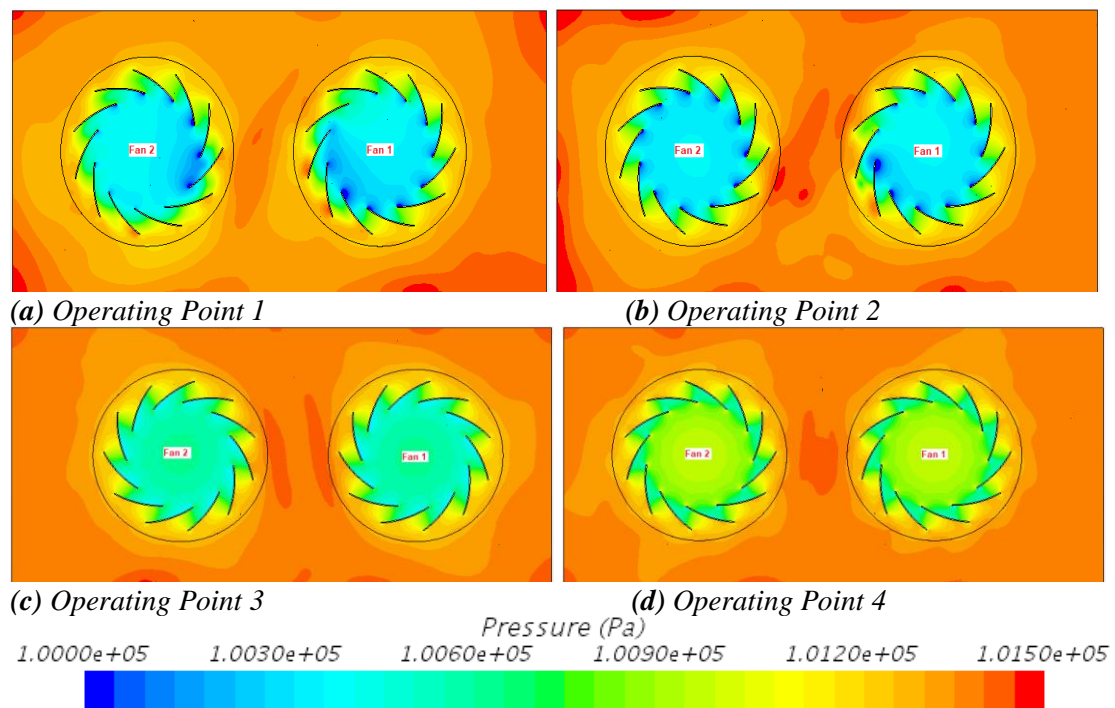


Figure 40: Static pressure in the outlet region shown for a plane normal to the rotation axis, valid for Operating Points 1-4.

4.1.3.2 Velocity Magnitude

Presented in *Figure 41* is the velocity magnitude across both fans for Operating Points 1-4 in the reference case. One of the common denominators is the fact that higher velocity magnitudes are obtained around the outlets of the fans. As the flow gets closer to the surrounding walls, the velocity magnitude tends to drop to zero. Another observation is that the velocity magnitude appears to be reduced in the region between the fans (dark blue colour), indicating a loss of the kinetic energy in the medium. By looking at the different plots this flow behaviour seems to become more apparent when transitioning from lower to higher airflow rates.

A secondary effect that can be observed is related to the velocity magnitude spikes that can be found around the blades of both fans in Operating Point 1 and some small tendencies of this occurrence happening for Fan 1 in Operating Point 2. These increased velocity magnitudes are highly undesirable and lead to poor fan performance. This is reflected in and backed up by the the individual fan efficiency data (*Table 6*). By taking Operating Point 2 as an example, Fan 1 operates with 3.8% less efficiency compared to Fan 2. When it comes to Operating Point 1, the second fan has far more blades with elevated levels in velocity magnitude than its counterpart, and naturally this would mean that one would expect a reduced performance for this specific fan. That is true, as the results show that Fan 2 operates with 7.7% less efficiency compared to Fan 1. For the cases of Operating Points 3 and 4, where the velocity magnitude distribution is almost completely even for both fans, results show they work at practically the same efficiency (see *Table 6*), which is highly desirable in this type of application.

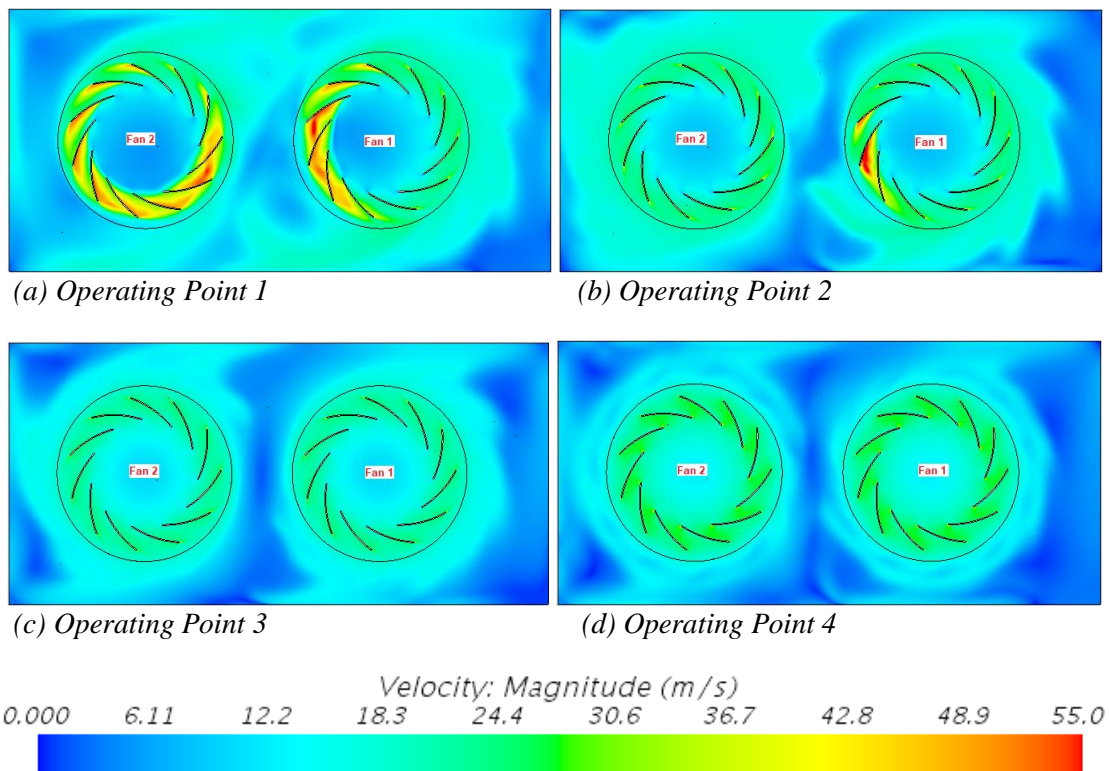


Figure 41: Velocity magnitude in the outlet region shown for a plane normal to the rotation axis, valid for Operating Points 1-4.

4.1.3.3 Vector Flow

The vector flow based upon velocity for the reference case, for Operating Point 1-4, seen from above and across the different regions, is illustrated in *Figure 42*. A flow visualization tool named “*Line Integral Convolution*” has been applied to these vector plots, to aid with understanding of the overall direction and magnitude of the flow fields. As can be seen, the velocity of the air flow will increase in the neck sections of the fans before discharging radially from said rotating devices. Most of the outgoing flow from the fans will hit the surrounding walls and then align with them in a parallel direction, before leaving the ducted outlet.

As for the interaction area in between the fans, the streams from each fan will hit and interfere with each other, which introduces a major problem in terms of achievable efficiency of the system. This is an additional level of induced resistance, that the fans must overcome, and supplementary input power may be required to reach expected performance. By studying the different Operating Points in more detail, it becomes clear that the flow from the interaction area tends to not reach the outlet of the duct, but rather curve back towards Fan 1. Additionally, one could observe the formation of a backflow behind the fans, with a lot of swirling eddy motions. Another problematic aspect can be noticed by closely analysing Fan 1 for Operating Point 1, as there appears to be a rotating motion within the fan’s outlet that is created, which is shown more clearly in *Figure 43*. This is not optimal and shows that the fan does not function as intended for that given condition.

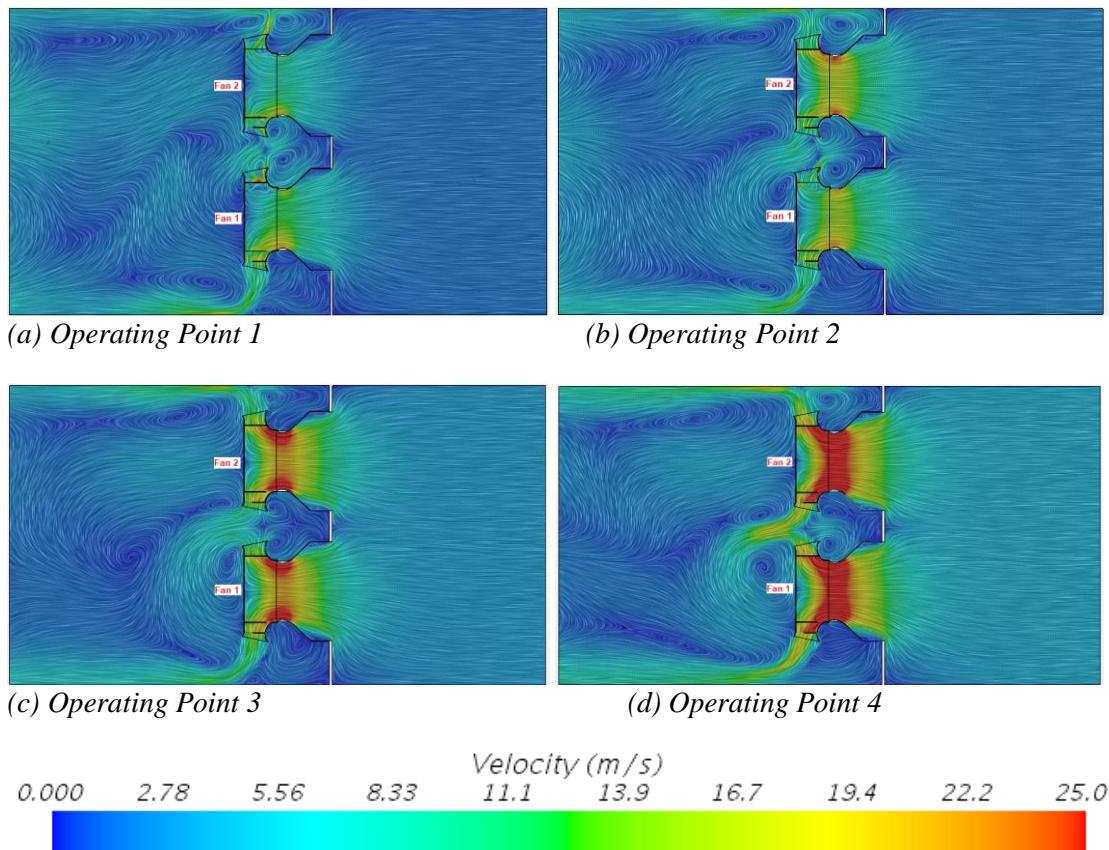


Figure 42: Vector flow for the different regions shown in a plane section cutting through the AHU, valid for Operating Points 1-4.

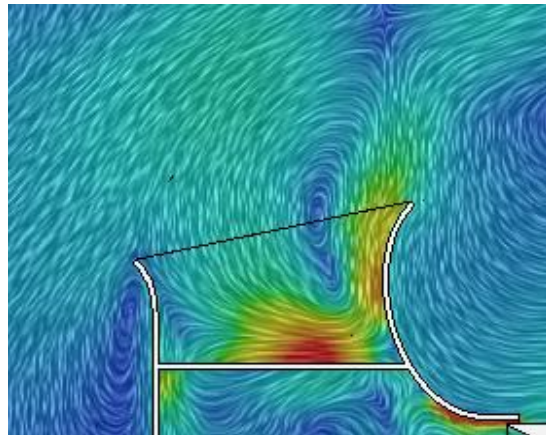


Figure 43: Swirl within fan 1, Operating Point 1.

4.1.4 Notation about Operating Point 1 and its stability

Judging by the performance data given in *Table 6* and seen in *Figure 37* for Operating Point 1, there is a clear imbalance between the two operating fans in terms of efficiency. This discrepancy indicates a highly unstable state and is further supported by the unfavourable conditions that have been pointed out for the plots of velocity magnitude and vector flow. As Operating Point 1 is too unpredictable and potentially less accurate, no direct conclusions can be made based on this condition. Potential ways of dealing with this unstable point would be to use a transient solver instead of a steady state one. This is elaborated and discussed more in Chapter 5 (see Section 5.3).

4.2 Comparison between Reference and Modifications

4.2.1 Average Fan Efficiency

A comparison of the average fan efficiency for the reference and the tested modifications is given in *Table 7* and *Figure 44*. There are four different modifications that outperform the reference model across all Operating Points, and those are presented in decreasing order based on their performance: “Half Distance Wall”, “Full Distance Wall”, “1 Guiding Vane” and “1 Guiding Vane with Wall”, the latter being the least effective, positive modification. A common aspect of these modifications, based on the shapes of their curves, is that the peak efficiency can be found between the second and third Operating Points (see *Figure 44*). The modifications named “Offset Fan 2” and “3 Guiding Vanes” show mixed results with slightly better average efficiency in Operating Point 2, significantly worse efficiencies in Operating Point 3 and on par or worse in Operating Point 4.

Table 7: Average fan efficiency for reference and modifications in tabular form.

Average fan efficiency	Reference	Full Distance Wall	Half Distance Wall	Offset Fan 2	3 Guiding Vanes	1 Guiding Vane	1 Guiding Vane with Wall
Representation	--- x ---	--- ▲ ---	--- ■ ---	--- ● ---	--- + ---	--- ◇ ---	--- ◇ ---
Average efficiency	η_{Avg} [%]	η_{Avg} [%]	η_{Avg} [%]	η_{Avg} [%]	η_{Avg} [%]	η_{Avg} [%]	η_{Avg} [%]
Operating point 1	49,6	49,0	54,4	48,8	51,2	51,9	51,4
Operating point 2	62,3	69,2	69,7	64,5	64,1	65,1	64,0
Operating point 3	61,7	66,1	67,0	58,2	57,5	63,4	62,7
Operating point 4	38,8	42,2	42,6	35,6	39,9	39,7	38,9

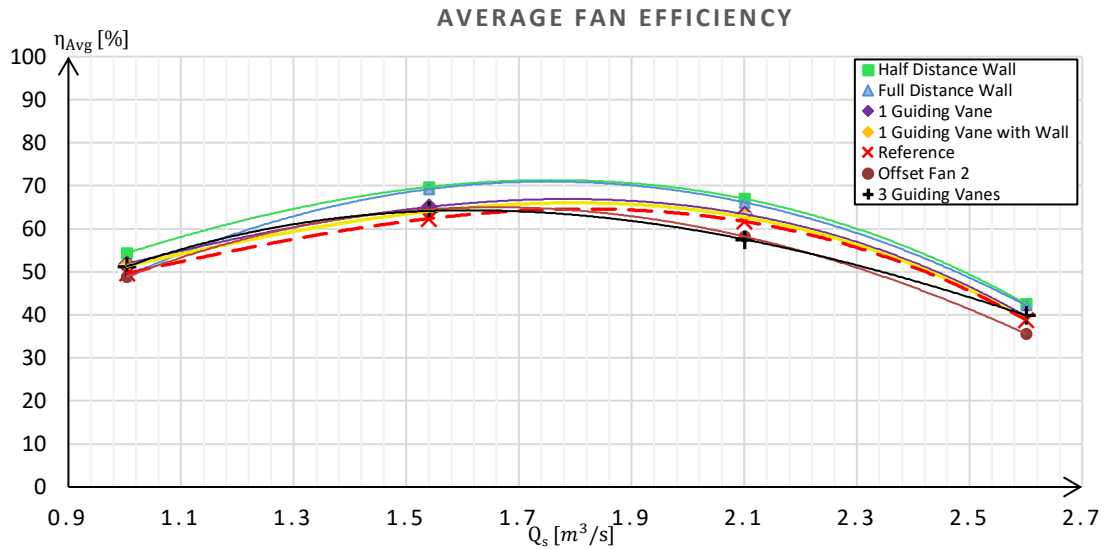


Figure 44: Graphic representation of the average fan efficiency for the reference model and its modifications.

4.2.2 AHU Efficiency

Similar results are present in Table 8 and Figure 45 for the AHU efficiencies. As there is a high conformity between the average fan efficiency and the AHU efficiency, the values of the Operating Points and the shapes of the curves are almost identical to those presented in Table 6 and Figure 44. Operating Point 3, with a volumetric flow of 2.1 m³/s, introduces the largest difference between simulated designs in terms of efficiency span. As such, this point was chosen for graphical depiction.

Table 8: AHU efficiency for reference and modifications in tabular form.

AHU efficiency points	Reference	Full Distance Wall	Half Distance Wall	Offset Fan 2	3 Guiding Vanes	1 Guiding Vane	1 Guiding Vane with Wall
Representation	-- x --	-- ▲ --	-- ■ --	-- ● --	-- + --	-- ◇ --	-- ◇ --
AHU efficiency	η_{AHU} [%]	η_{AHU} [%]	η_{AHU} [%]	η_{AHU} [%]	η_{AHU} [%]	η_{AHU} [%]	η_{AHU} [%]
Operating point 1	50,0	53,5	54,6	50,9	51,6	52,1	51,3
Operating point 2	62,9	69,8	70,3	65,1	64,8	65,7	64,7
Operating point 3	61,8	66,2	67,0	58,2	57,5	63,5	62,8
Operating point 4	38,8	42,2	42,6	35,5	39,9	39,7	38,9

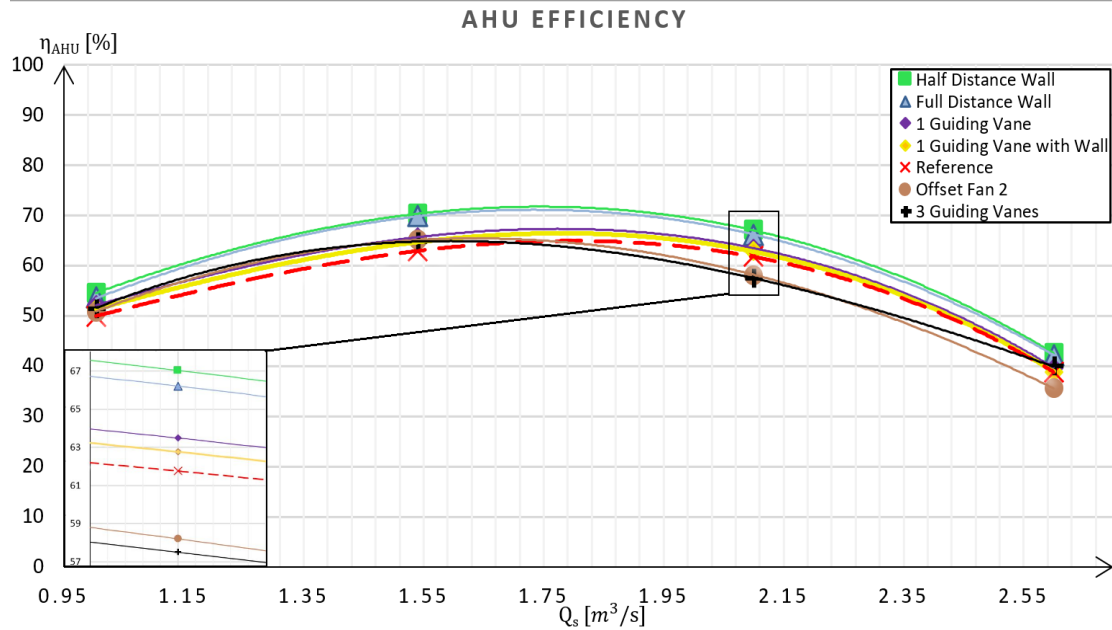


Figure 45: Graphic representation of the AHU efficiency for the reference model and its modifications with an emphasis on the third Operating Point.

4.2.3 Range of Efficiency Improvement

The ranges of efficiency improvements (in percentage points) for the different modifications, compared to the reference, are given in terms of the average fan efficiencies in Table 9. Cells marked in green indicate an increase in average fan efficiency, while red cells are linked to a decrease of the quantity. Since the results indicate that Operating Point 1 is located in an unstable region on the fan curve, the acquired data for this condition was neglected. As such, the improvement ranges are given, based on Operating Points 2, 3 and 4. The graphical illustrations of the efficiency ranges are presented in Figure 46. The four best modifications that can be seen based on this combined data are as follows:

- “Half Distance Wall” with an improvement ranging from 3.8 to 7.3 %;
- “Full Distance Wall” with an improvement ranging from 3.4 to 6.4 %;
- “1 Guiding Vane” with an improvement ranging from 0.9 to 2.8 %;
- “1 Guiding Vane with Wall” with an improvement ranging from 0.1 to 1.7 %.

Table 9: Improvement ranges of modifications for the average fan efficiency based on Operating Points 2-4.

PERCENTAGE COMPARISON	Reference	Full Distance Wall	Half Distance Wall	Offset Fan 2	3 Guiding Vanes	1 Guiding Vane	1 Guiding Vane with Wall
Average efficiency	$\eta_{Avg} [\%]$	$\Delta\eta_{Avg} [\%]$					
Operating point 2	62,3	6,4	7,3	2,2	1,8	2,8	1,7
Operating point 3	61,7	4,4	5,3	-3,5	-4,2	1,7	1,0
Operating point 4	38,8	3,4	3,8	-3,3	1,1	0,9	0,1
Improvement range	-	3,4 to 6,4	3,8 to 7,3	-3,5 to 2,2	-4,2 to 1,8	0,9 to 2,8	0,1 to 1,7

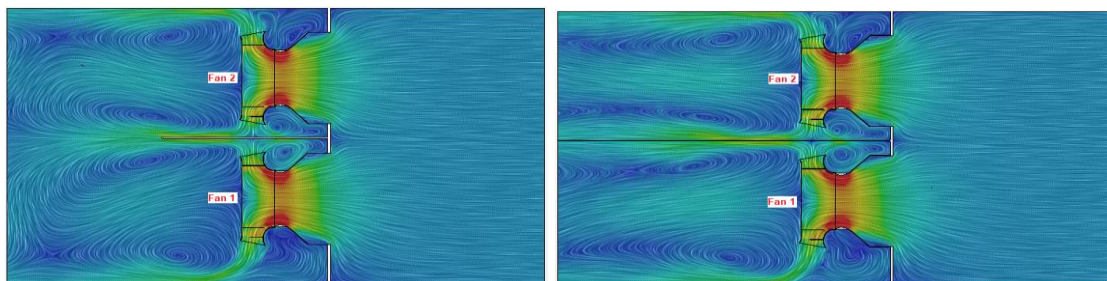


Figure 46: Graphic representation of the average fan efficiency improvement range for each of the modifications.

4.2.4 Vector Flows of the Modifications

A visualization of the vector flow based on velocity for the different modifications is shown in Figure 47. The results are given for a airflow rate of $2.1 \text{ m}^3/\text{s}$ (Operating Point 3) and has been used here as Figures 44 and 45 show that this Operating Point provides the biggest difference in terms of efficiency between the solutions. Therefore, it is a suitable condition for pointing out some of the main differences between these modifications and their relation to the reference.

By comparing the vector flows of the modifications that show improvements (a, b, c and d) with the reference for the same Operating Point (see Figure 42c) one of the most apparent differences is shown in the flow located between the fans which is directed more efficiently towards the outlet of the system for these modifications compared to the reference case. In other words, it seems that it is possible to have a bigger part of the flow move in the desired direction instead of flowing backwards or ending up in a swirling motion within the outlet region. This is something that is achieved simply by adding a wall or guiding vanes in between the fans.



(a) Half distance wall, Operating Point 3

(b) Full distance wall, Operating Point 3

Results

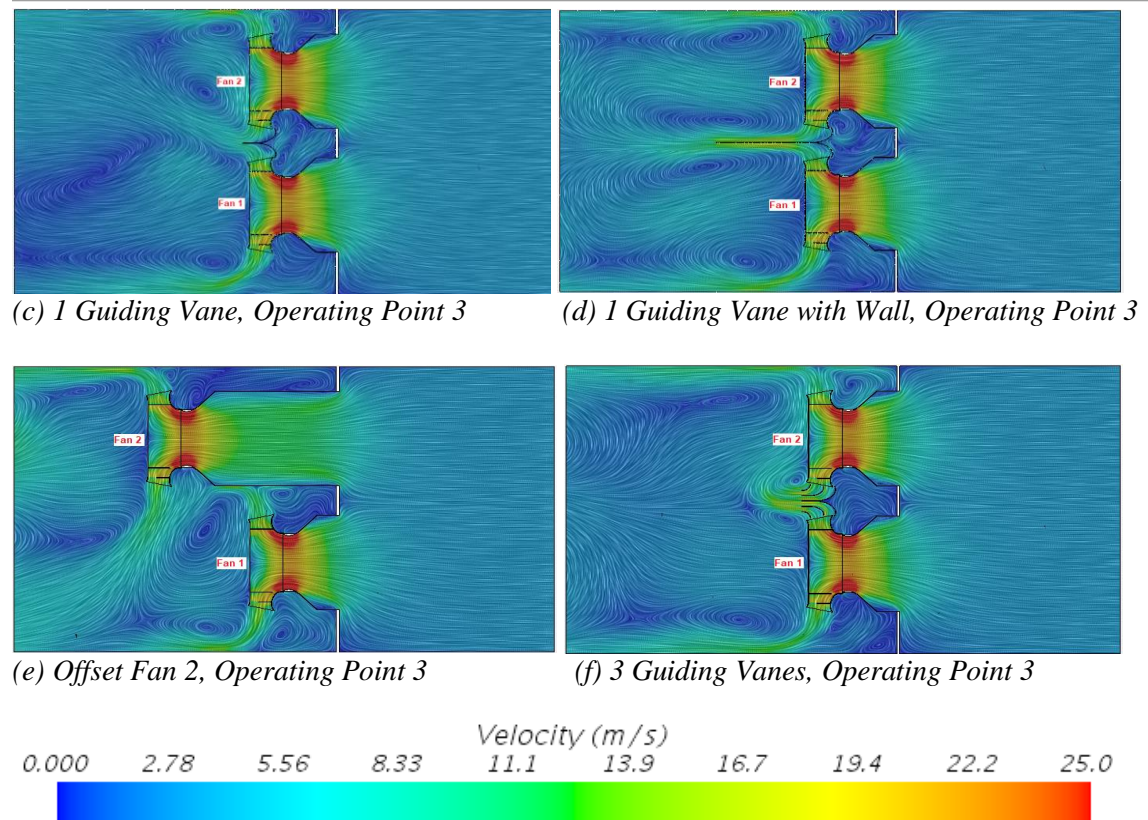


Figure 47: Vector flow for the different modifications at Operating Point 3.

For the modifications that show mixed results (*e* and *f*), there are some inherent issues in the flow field that may explain the degradation of the fan performance. Through the offset of Fan 2, an obstacle is introduced downstream for Fan 1. As a result, the stream that is exhausted from Fan 1 will directly collide with the exhausted air coming from the outlet of Fan 2. This type of crossflow is detrimental when it comes to the efficiency of the operation since it leads to a part of the exhausted flow from the first fan to be trapped in a small region of the chamber. In addition, the extended inlet of the second fan adds another layer of resistance to the system. This happens due to its close proximity to the outlet of Fan 1, and a big part of the outgoing airflow from this fan will then hit this obstacle and would have to curve around it. When it comes to the modification with multiple guiding vanes, it can be established that adding more vanes does not seem to help too much with the overall direction and or guiding of the flow. In fact, more vanes would have a negative effect due to the addition of friction resistances applied to the airflow, as well as inducing a larger velocity to the flow in the given region, leading to stronger backflows that affect the performance of the fans.

5 Discussion

In the fifth chapter a more in depth discussion is brought up of the obtained results for the reference and modifications, where some of the underlying reasons of the observed outcomes are explained. The chapter ties to the qualitative and quantitative questions that were defined in the goal formulation and, in addition, the methods and their validity are used as an important basis for a discussion regarding potential sources of errors.

5.1 Reference

By observing the results obtained from the reference case, where two centrifugal fans are operating in parallel and where no modifications have been applied, the first question of the goal formulation can be discussed in more detail. The question refers to why the individual fan efficiency decreases in this state relative to a case where only one fan is used and what kind of flow phenomena that is linked to this deficiency in performance.

As mentioned before, the main problems arise from the interaction area directly in between the fans, where the air streams coming from the two fans (in opposite directions) collide and interfere with each other. The generation of dynamic pressure from the increased air velocity, at the outlets of the fans, will quickly be converted to a high static pressure zone, when these two fronts meet and as the air accumulates. This is highly undesirable from a performance point of view, as less of the overall flow is lead towards the outlet of the casing. This effect is illustrated more clearly in the plots for the vector flow that were based on the velocity for the reference (*see Figure 42*). The flow from the interaction area tends to curve backwards, affecting the fans in their operation, instead of being transported further downstream in the outlet region of the casing. One could intuitively imagine that the input power to the individual fans has to be increased in order to overcome this resistance that is present in the system, especially in cases where the fans do not manage to deliver the air flow rates established beforehand due to low efficiency operation. Comparing this to a setup where only one fan is used, these problems will not be as apparent as there is no interaction area where the air is trapped and prevented from being moved further downstream. However, as mentioned before, it is not always possible to use a single, larger fan in these types of applications. Space constraints, such as those present in this type of industrial problem, dictate the use of a parallel fan setup as the most viable option to implement.

When it comes to the fans and their stability, the collected data shows some interesting trends that can be compared to the theory of fans in parallel operation (see Section 2.1.7). As stated before, there is a risk of induced fan instability, a “*hunting*” effect, when the operating point of the fans is located to the left of the peak pressure on the combined fan curve. This would explain the instability and the difference in fan load presented by Operating Point 1, which is believed to be located in this *Region of Instability*. This effect appears to be present not only for the reference, but also for the modifications, hence no other conclusions could be drawn for this unstable condition.

As presented in the theory chapter (see section 2.1.1), centrifugal fans increase the pressure of the circulated air that is exhausted through the outlet of each fan. Due to their close proximity and the constantly changing surrounding conditions (such as pressure or flow direction) in which the two fans operate, each fan encounters different flow resistances leading to uneven operation. These unbalanced conditions cause the air flows through each fan to vary, even when the system supplies a constant air flow. The study was performed for fans that operate with the same rotational speed of 2800 [rpm] throughout all simulations, thus removing its impact in the

Discussion

efficiency analysis. As a result, according to the formula provided by Swegon (see Section 3.1.7), the fan efficiency depends on the circulated flow and momentum, since the formula assumes the same pressure difference across both fans at each given moment. As the fan momentum depends on the power generated by the motor, which in terms is related to the flow demand and the system resistances, a single most relevant variable that affects fan efficiency has been determined to be the circulated air flow.

Low air flow demands from the system are especially interesting to consider. The air that passes through each of the fans varies leading to one of the fans to operate overloaded, while the other circulates the remaining flow (underloaded). This discrepancy is also a cause for the reduced fan efficiency. An analysis was performed on the Reference Model, in which the efficiency of a single running fan was determined through a set of simulations. The results were subsequently compared with the the ones obtained for both fans operating in parallel and plotted together with the specific air flows for each case (the flow that passes through each fan). This comparison can be observed in *Figure 51*.

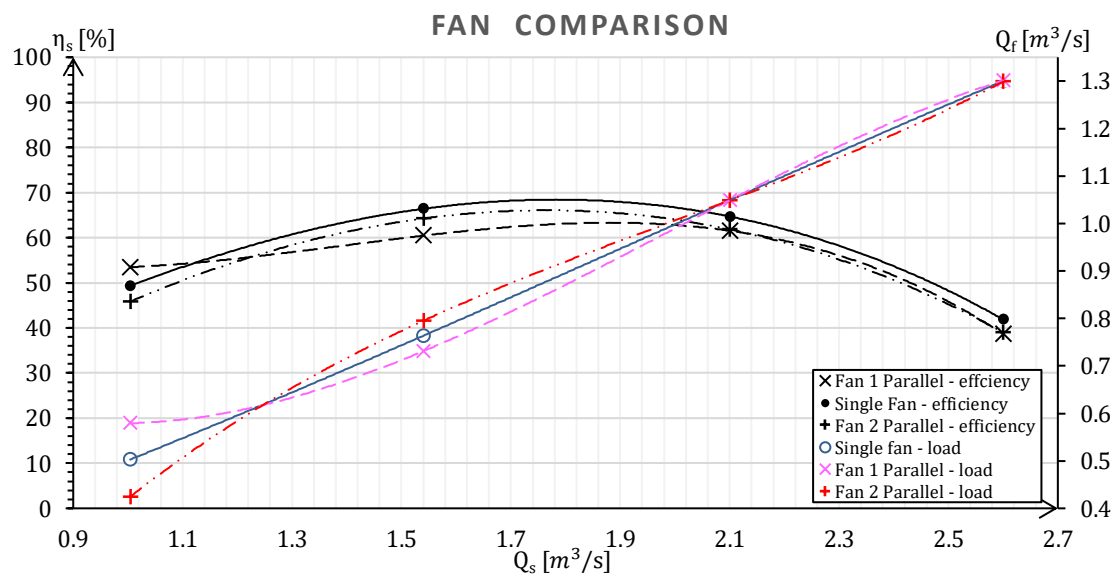


Figure 51: Comparison between a single operating fan and parallel operating fans, in terms of static efficiency and circulated flow.

Based on the figure seen above, a validation regarding the uneven operation of the two fans can be observed. For the first two Operating Points, where a reduced supplied flow (Q_s) is circulated, the two fans behave in disequilibrium. This effect can be seen in the uneven distribution of the air flows through each fan (Q_f) when compared to the case in which a single fan is operated. This does further support the belief that the first Operating Point is located in an unstable region on the combined fan curve described in the theory (see Section 2.1.7). As the flows tends to get closer to each other for Operating Point 2 this indicates a more stable operation, although it cannot be completely ruled out that this condition is outside of the unstable region, as a difference in flow between the fans still can be observed. Some concluding comments for the figure above is that it has been observed and confirmed that the individual efficiency of the fans in parallel operation is reduced compared to the case in which a single fan is used to supply the flow. Upon closer inspection of the first point, it can be observed that the amount of flow that passes through a fan, plays a large role in the static fan efficiency. This effect can be observed clearly for the case of Fan 1.

Among the observed effects was the amount of backflow generated by the vortices generated by the exhausted air. By increasing the fan load, larger flows are exhausted and thus, more energy is sent towards the Outlet. This energy is partially lost in the formation of eddies and vortices which are the source of the various forms of backflows present in the studied cases.

This backflow can sometimes affect the direction of the exhausted air, leading to a decrease of the system performance, as well as inducing an additional level of resistance to the fans.

5.2 Modifications

The second question in the goal formulation was about how much the fan efficiency could be improved through alternative designs and what that would mean for energy saving purposes. According to results, the most promising designs are those in which the two fans are separated by a vertical, continuous wall. Out of two such designs, the one titled “*Half Distance Wall*” obtained the best results, with an improvement of averaged fan efficiency ranging between 3.8-7.3 %. For the “*Full Distance Wall*”, “*1 Guiding Vane*” and “*1 Guiding Vane with Wall*” efficiency improvements across all Operating Points could also be observed, although not with the same magnitude as for the “*Half Distance Wall*” (see Section 4.2.1). A common aspect of these modifications is the principle of separating and guiding the flow in the interaction area.

The indication of a potential increase in efficiency due to the implementation of the studied designs would enable important energy savings, as running the fans can be power intensive in large industrial and/or commercial applications. For each percentage point that is improved in fan efficiency, less amount of power is required, leading to a decrease of the operational costs and a reduced environmental impact.

When comparing the “*Full Distance Wall*” with the “*Half Distance Wall*”, one of the potential reasons as to why the latter performs slightly better is the lowered amount of backflow that is produced. By letting the air streams on each side of the wall mix and align at the halfway point of the outlet region, an improvement of the flow field situation appears to be achieved, leading to less overall flow resistance. The motivation behind the modification “*1 Guiding Vane with Wall*” was to take the “*Half Distance Wall*” and “*1 Guiding Vane*”, the two different types of modifications that showed the best results in their own categories, and try to combine them into a superior modification. Unfortunately, as can be seen by the simulation results, that would not give an overall better solution.

The third and last question of the goal formulation refers to difficulties that could be encountered for the viable designs and how could they be overcome, also needs to be considered. From an implementation point of view, it is actually beneficial that the wall modifications show better results compared to the ones where guiding vanes have been used. The reason why the wall modifications present a benefit is due to a lower investment cost and a simpler implementation through the use of a straight wall compared to curved walls that would be used for the guiding vanes. However, the “*Full Distance Wall*” would most likely introduce some problems as it separates the whole outlet region in two separate parts. This makes it harder to perform maintenance operations, as one of the fans would be completely blocked behind this wall. Since the unit is opened through a side panel, visualisation and access to the fan located behind the wall would be a challenge as the current designs for the AHU’s do not provide support for the implementation or removal of such a wall in case of maintenance. Potential solutions could be found through the use of a sliding, transparent wall that would allow visual and physical access, while satisfying mechanical requirements for resistance, vibrations and structural integrity without impairing the current design. As previously mentioned, since the most promising design is “*Half Distance Wall*”, these impediments could be easier to overcome.

5.3 Methods

Even though some of the presented results may be promising and show improvement potential, one should keep in mind that some of the settings that have been used here are based on assumptions and simplifications, which were necessary given the limited time and resources allocated to perform a project of this scope. Some of these factors are brought up here and discussed in more detail. To begin with, it is important to mention that modelling in itself is based on ideal conditions that are highly controllable, contradictory to the complexity of real life conditions, where the smallest disturbances may induce and give a completely different outcome compared to expected modelling results.

One of the major simplifications that needs to be considered and pointed out is the fact that steady state was used for all the performed simulations. In a case such as this, where close to 30 simulations have been run in total across all the different models, and where each simulation took approximately 1-2 days to run until convergence, it would not have been possible to use a transient solver for all these computational points. Transient simulations require more computational power and much longer simulation time to perform. In comparison, a single simulation in a transient state could take weeks or even months to run, depending on the amount of cells that are accounted for. Fortunately, the physics behind the simulations work in the same principal way, whether they are applied in a steady state or transient solver. The drawbacks with only using steady state simulations would be the inability to observe how the solutions change with time, and the potential risks of getting more inaccurate solutions, due to some time dependent variables in the equations being assumed to zero (which is not the case for the transient solver).

Linked to the topic of using either a steady state or transient solver, Operating Point 1 would have most likely benefited from being run in a transient state instead of a steady state, to combat the instability that occurs for that condition. A brief analysis of the plot for the velocity magnitude across the fans for Operating Point 1, with an example presented in *Figure 41a*, shows a lack of guarantee that the areas of spiked velocity magnitude are constantly positioned as shown in the plane. By having a transient solver, it would have been possible for the fans to actually rotate with each time step, and see how these zones fluctuate with time.

As mentioned before, some geometry parts had been omitted from the outlet region of the casing when performing the different simulations. This could have had an impact on the results since a real system contains devices such as motors, control equipment and additional fan frameworks that would influence the flow field around and downstream of the fans. However, this simplified geometry had to be used in order to decrease the level of complexity and time requirements of the study, and as the primary aim was to study the interaction area in between the fans, these simplified models would suffice to meet this objective. Given the fact that the interaction of the fans is based on their position next to each other, with a small clearing distance in between, and the fact that the simplified reference geometry manages to replicate this condition is what is of most importance. At the same time, the modifications can also be deemed as valid simplifications, as they are built on the principle of adding additional surfaces where it is known that free space is available within the casing, to prevent any type of physical conflict. However, it would still have been interesting to see how much this additional equipment, that exists in reality, would have affected the overall flow field and simulation results. Presumably, it would be reflected in more accurate results.

Naturally, obtained simulation results must be validated and compared with real life results. This would be done by testing in a laboratory facility, more specifically a wind tunnel, where a prototype of the exact unit (with all its constituting parts) could be placed and evaluated for different flow conditions. One of the benefits with this kind of physical testing is that a variable flow rate can be provided to the inlet of the AHU, hence there is no restriction to only test the

Discussion

four Operating Points used in this investigation. For example, it would have been of interest to see what happens in actuality between Operating Points 2 and 3, and see if the modified prototype unit provides optimal performance for this air flow rate, in accordance with the simulation results presented in this study. Unfortunately, there were limitations in time for Swegon to perform wind tunnel tests alongside this project. The prototype of the AHU together with the modifying details needs to be manufactured beforehand, and this process on its own can take week or even months to do. A decision needs to be made from Swegon's side which of the modifications that should be tested, as each of the potential modifications would take time to prepare. Most likely, it would be a good idea to test those modifications that show the most promising potential, like when adding a wall or guiding vanes in between the fans.

6 Conclusion

The primary objective of this thesis was to investigate the factors which lead to efficiency losses of parallel operating fans in modern AHU's and to find and propose potential solutions for improving fan efficiency by reducing the analysed negative effects. In order to save computational time and resources, the study was realized on a simplified model of the AHU, with the initial conditions required for the simulations and the turbulence model (k- ϵ) being provided by Swegon.

The study was performed with the program Star-CCM+, where steady-state simulations were applied in order to utilise the allocated time as efficiently as possible and to facilitate the process of analysing multiple models. In the given timeframe, the reference model and six concepts were designed and investigated to understand the phenomena and the effects to which the fans were subjected. The concluding notes are compiled below:

- Fan efficiency is decreased in parallel operation systems such as the one analysed in this case due to their mutual influence. On one hand, the released air streams from the two fans collide in a small region and form an increased static pressure zone through the conversion of the exhausted dynamic pressure. This pressurised region presents a resistance for both fans during operation. On the other hand, a result of this interaction between the two streams is that a fraction of the released air tends to curve backwards, opposite to the intended direction of the flow. As a consequence, a part of the exerted energy of the fans is lost in an unproductive manner by pressurising the wrong end of the outlet chamber.
- Throughout all simulated models, the first Operating Point, with the lowest airflow rate, showed inconsistencies in the results, such as large differences in fan load, indicating unstable operation. The effect upon the study was that this Operating Point could not be used in the investigation to draw any conclusions.
- Among the tested models, two modifications of the same type stood out as being the best performing. The principle of this type was to add a wall in between the two fans. Results have shown that the model titled "*Half Distance Wall*" would provide an average fan efficiency improvement ranging from 3.8% to 7.3%, closely followed by another model named "*Full Distance Wall*" with an efficiency increase of 3.4% to 6.4%. However, one must also consider that the simulations were performed on virtual, simplified models. This aspect together with the fact that none of the presented results have been backed up by experimental tests renders the values to be taken as indicators rather than facts. Consequently, the results show the potential of a realistic efficiency improvement somewhere between 1% to 3% according to estimations from Swegon.

7 Future Work

Based on the acquired data and gained insight, a follow up to this project would be to create one or several physical prototypes of the best performing modifications, in order to test the results in a wind tunnel and, if approved, proceed with a detailed analysis and further development of said prototypes.

This study was one of the first steps in the development of a new and more efficient design for the small scale AHUs. However, more work is required in order to finalize the project. A few questions related to and potentially answered by future work are:

- How would the results change if transient simulations were to be performed for the different models? It would be interesting to conduct transient simulations in order to study the dynamic fan interaction. Unfortunately this could not be done in this study due to limitations in computational power and time.
- If the implementation of a wall is a suitable solution, what other potential unintended effects, besides the ones found by this study, could be created? How would one remedy this at the same time as respecting the mechanical constraints of the AHU?
- How would the obtained results compare to the results for an AHU with three fans in parallel operation? Would the suggestions found in this paper still be valid as solutions to implement, or would the additional fan bring forward new issues that would require totally different ways of solving the problem?

References

- [1] ASHRAE. HVAC Systems and Equipment Handbook (SI). *Fans*. Chapter 18, 2000.
- [2] U.S. Department of Energy and AMCA. *Improving Fan System Performance: A Sourcebook for Industry*. Washington, DC, 2003.
- [3] F. M. White. *Fluid mechanics*. 7th ed. McGraw-Hill Education. New York, N.Y 10121, 2011.
- [4] AMCA International. *Introducing the Fan Energy Index: An AMCA International White Paper*. 30 West University Dr. Arlington Heights, IL 60004 USA, 2016.
- [5] Twin City Fan Fan Companies, Ltd. Engineering data 2400: *Fan Performance Characteristics of Centrifugal Fans*, 5959 Trenton Lane, Minneapolis.
- [6] Chalmers University of Technology. *ENM045 – Heating, Ventilation and Air Conditioning Systems Engineering, VIN032 – Indoor climate and HVAC*. Building Services Engineering, S-412 96 Göteborg, Sweden, 2016.
- [7] Kruger. *Fan Inlet System Effects*. Technical Bulletin - TBN010.0/1998.
- [8] ASHRAE *GreenGuide - The Design, Construction, and Operation of Sustainable Buildings (3rd Edition)*. American Society of Heating, Refrigerating and Air-Conditioning Engineers, Inc., 2010.
- [9] AMCA International. *Fan Performance and System Effect*. PowerPoint presentation.
- [10] AMCA International. *Fan Performance*. PowerPoint presentation prepared by Mark Stevens, 30 W. University Drive Arlington Heights, IL 60004 USA, 2011.
- [11] M. Ekh. *Mechanics of solids & fluids. Part I: Fundamentals*. Tech. rep. Div. of Material and Computational Mechanics, Chalmers University of Technology, Göteborg, Sweden, 2016.
- [12] B. Andersson, R. Andersson et. al. *Computational Fluid Dynamics for Engineers*. Cambridge University Press, New York, 2012.
- [13] J. D. Anderson, Jr. *Chapter 2: Governing Equations of Fluid Dynamics*. Springer-Verlag Berlin Heidelberg, 2009.
- [14] L. Davidson. *Fluid mechanics, turbulent flow and turbulence modeling*. Department of Mechanics and Maritime Sciences, Chalmers University of Technology, Göteborg, Sweden, 2019.
- [15] Y. A. Cengel, J. M. Cimbala et. al. *Fundamentals of Thermal Fluid Sciences*. 4th ed. in SI-units. McGraw-Hill. New York, NY 10020, 2012.
- [16] W. P. Jones and B. E. Launder. *The prediction of laminarization with a two-equation model of turbulence*. International Journal of Heat and Mass Transfer, 15(2):301–314, 1972.

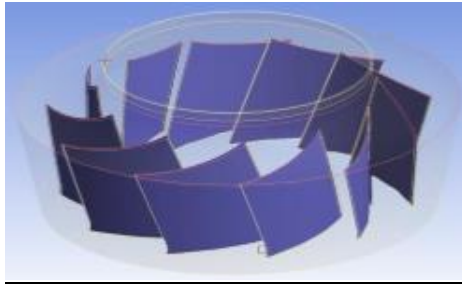
References

- [17] E.Sjösvärd. *Numerical Estimation of the Aerodynamic Tones Radiated From a Centrifugal Fan*. Master thesis. Chalmers University of Technology, 2016.
- [18] Siemens. STAR CCM+ User Manual. *Simcenter-STAR-CCM+: K-Epsilon Turbulence*. Accessible with a license of STAR-CCM+.
- [19] Siemens. STAR CCM+ User Manual. *Simcenter-STAR-CCM+: Mesh Quality*. Accessible with a license of STAR-CCM+.

Appendix

A.1 Mesh Settings

Blades



<input type="checkbox"/> ● Target Surface Size	
Size Type	Absolute
Percentage of Base	0.2
Absolute Size	2.0 mm
<input type="checkbox"/> Custom Prism Values	
<input type="checkbox"/> ● Number of Prism Layers	
Number of Prism Layers	5
<input type="checkbox"/> ● Prism Layer Near Wall Thickness	
Value	0.2 mm
<input type="checkbox"/> ● Prism Layer Total Thickness	
Size Type	Absolute
Percentage of Base	0.122
Absolute Size	1.22 mm
<input type="checkbox"/> ● Surface Growth Rate	
Surface Growth Rate	1.25

Appendix

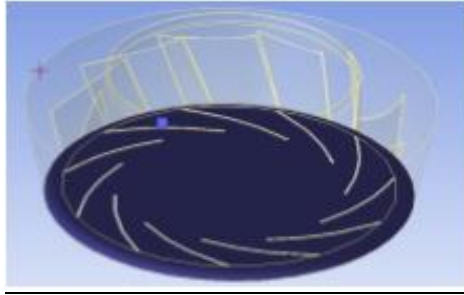
Shroud



<input type="checkbox"/> ● Target Surface Size	
Size Type	Absolute
Percentage of Base	0.5
Absolute Size	5.0 mm
<input type="checkbox"/> Custom Prism Values	
<input type="checkbox"/> ● Number of Prism Layers	
Number of Prism Layers	5
<input type="checkbox"/> ● Prism Layer Near Wall Thickness	
Value	0.2 mm
<input type="checkbox"/> ● Prism Layer Total Thickness	
Size Type	Absolute
Percentage of Base	0.122
Absolute Size	1.22 mm
<input type="checkbox"/> ● Minimum Surface Size	
Size Type	Absolute
Percentage of Base	0.499000000000000005
Absolute Size	4.99 mm

Appendix

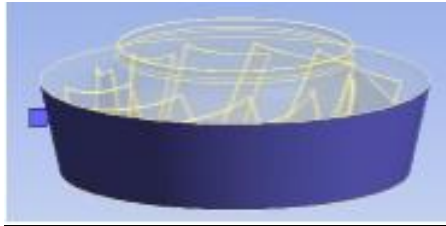
Backplate



<input type="checkbox"/> ● Target Surface Size	
Size Type	Absolute
Percentage of Base	1.0
Absolute Size	1.0 cm
<input type="checkbox"/> Custom Prism Values	
<input type="checkbox"/> ● Number of Prism Layers	
Number of Prism Layers	5
<input type="checkbox"/> ● Prism Layer Near Wall Thickness	
Value	0.2 mm
<input type="checkbox"/> ● Prism Layer Total Thickness	
Size Type	Absolute
Percentage of Base	0.122
Absolute Size	1.22 mm
<input type="checkbox"/> ● Minimum Surface Size	
Size Type	Absolute
Percentage of Base	0.9900000000000001
Absolute Size	0.99 cm

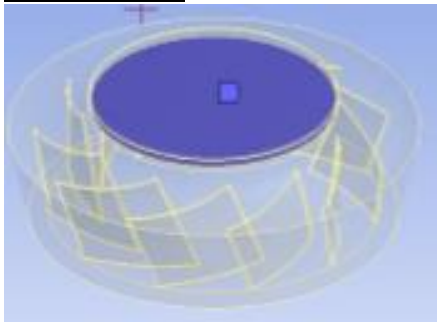
Appendix

Outlet Interface



<input checked="" type="checkbox"/> ● Target Surface Size	
Size Type	Absolute
Percentage of Base	0.5
Absolute Size	5.0 mm
<input checked="" type="checkbox"/> ● Minimum Surface Size	
Size Type	Absolute
Percentage of Base	0.499000000000000005
Absolute Size	4.99 mm

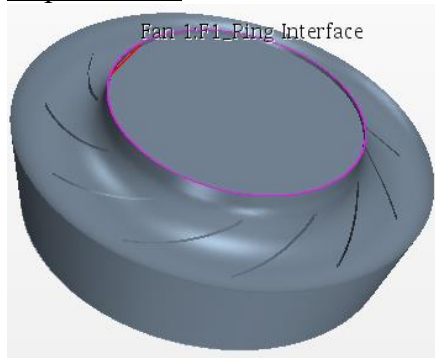
Inlet Interface



<input checked="" type="checkbox"/> ● Target Surface Size	
Size Type	Absolute
Percentage of Base	0.5
Absolute Size	5.0 mm
<input checked="" type="checkbox"/> Custom Prism Values	
<input checked="" type="checkbox"/> ● Number of Prism Layers	
Number of Prism Layers	2
<input checked="" type="checkbox"/> ● Prism Layer Near Wall Thickness	
Value	0.08 mm
<input checked="" type="checkbox"/> ● Prism Layer Total Thickness	
Size Type	Absolute
Percentage of Base	0.1
Absolute Size	1.0 mm
<input checked="" type="checkbox"/> ● Minimum Surface Size	
Size Type	Absolute
Percentage of Base	0.499000000000000005
Absolute Size	4.99 mm

Appendix

Gap Interface



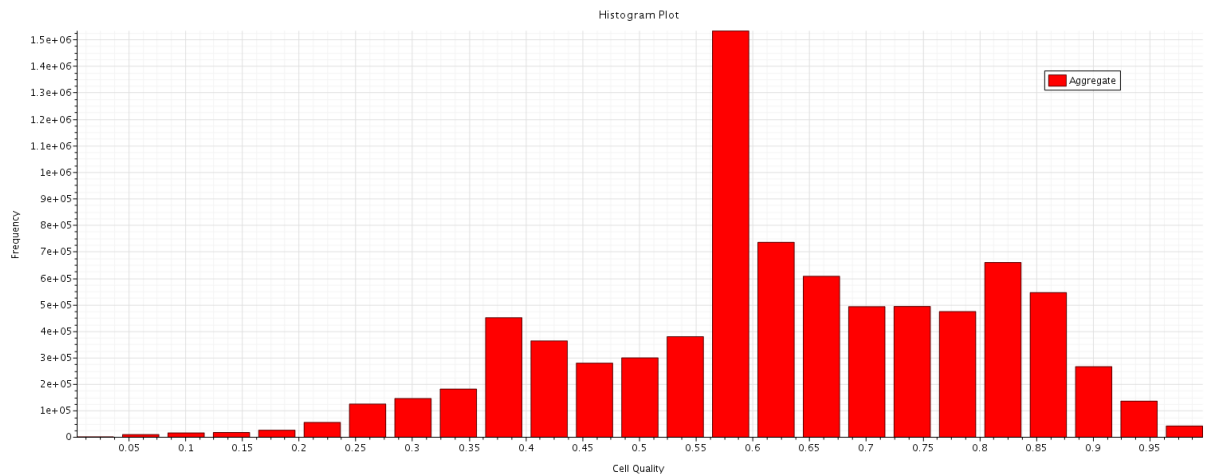
☒ ● Target Surface Size	
Size Type	Absolute
Percentage of Base	0.05
Absolute Size	0.5 mm
☒ ● Minimum Surface Size	
Size Type	Absolute
Percentage of Base	0.0499
Absolute Size	0.499 mm

A.2 Mesh Quality

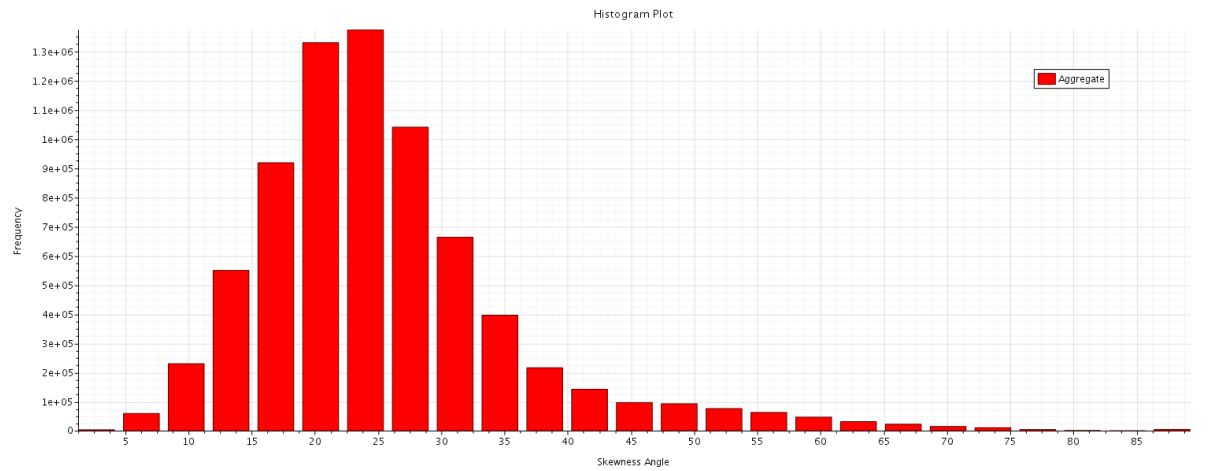
Reference

Fan 2 Offset

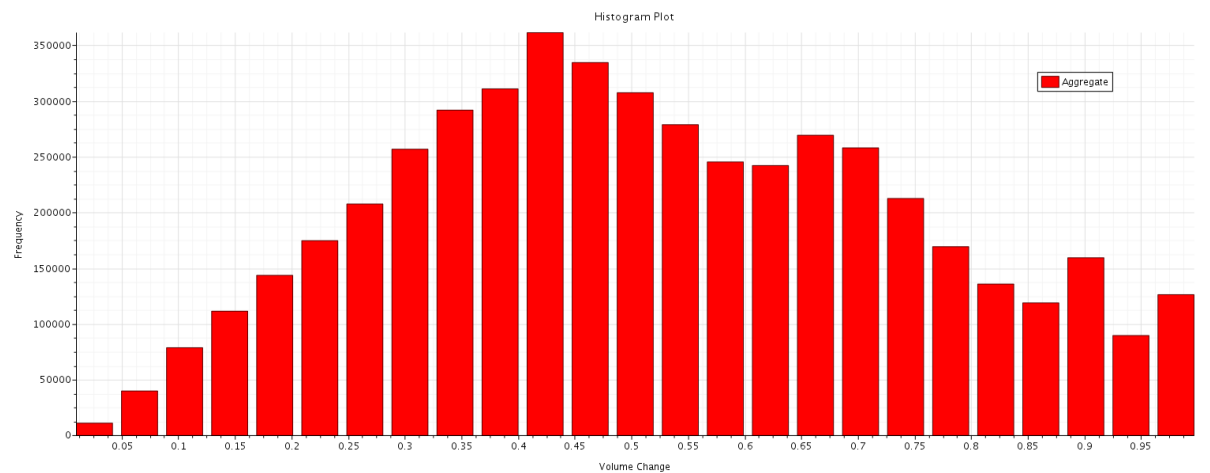
Cell Quality



Skewness Angle

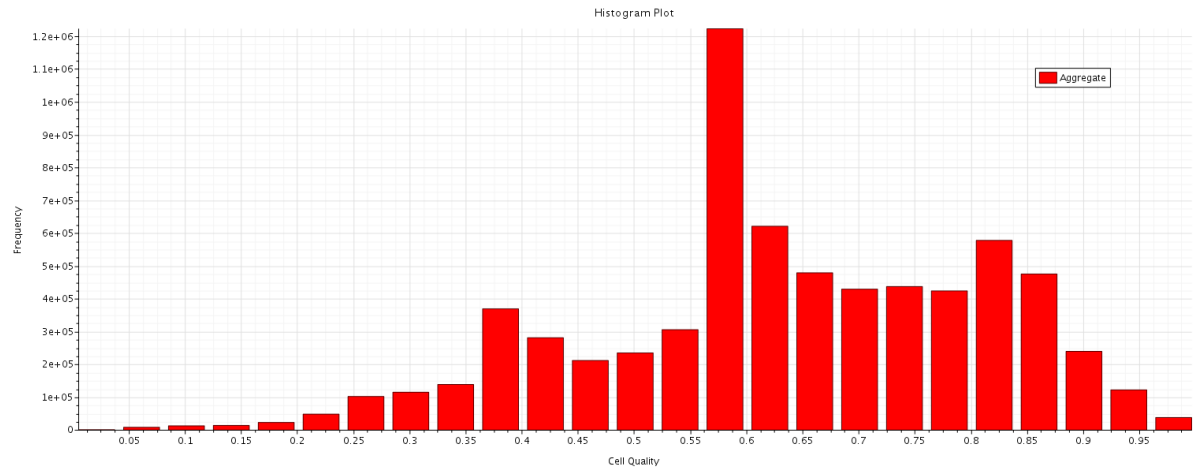


Volume Change

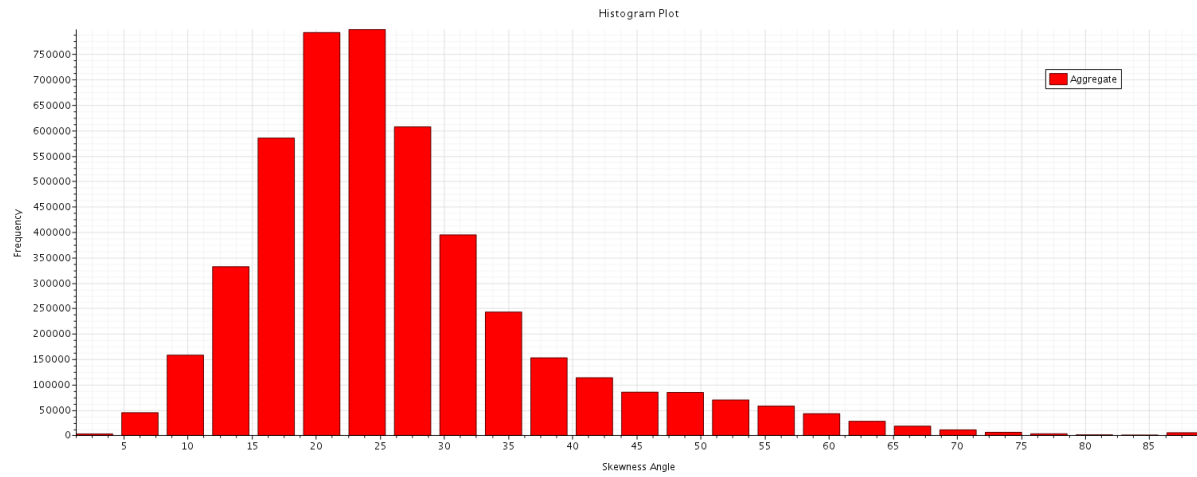


Full Distance Wall

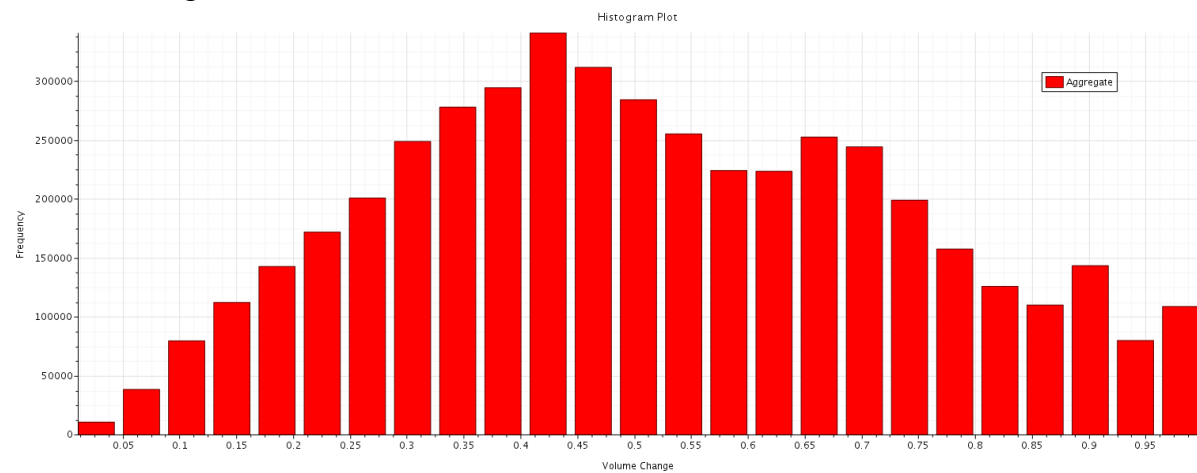
Cell Quality



Skewness Angle

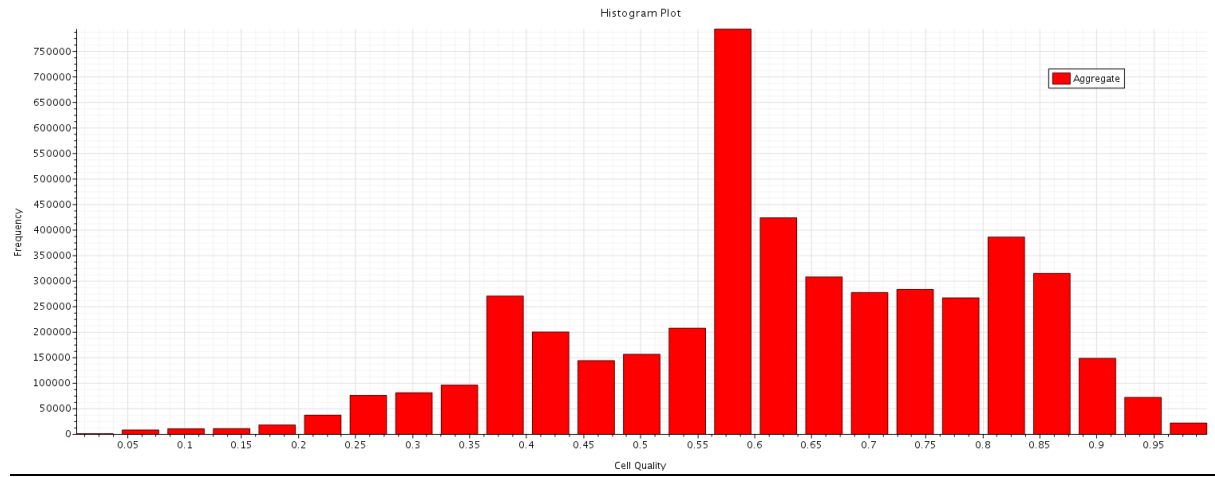


Volume Change

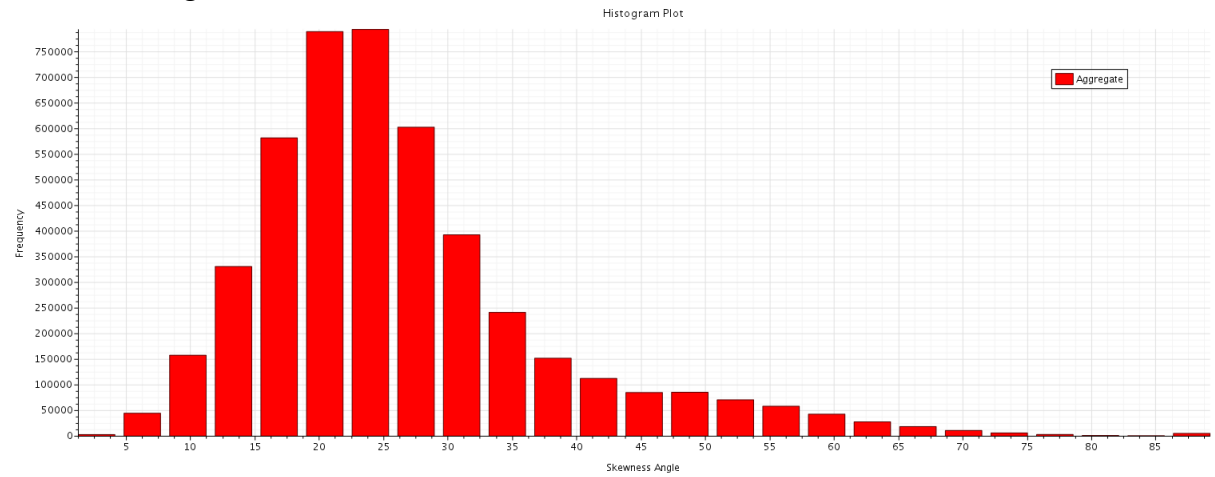


Half Distance Wall

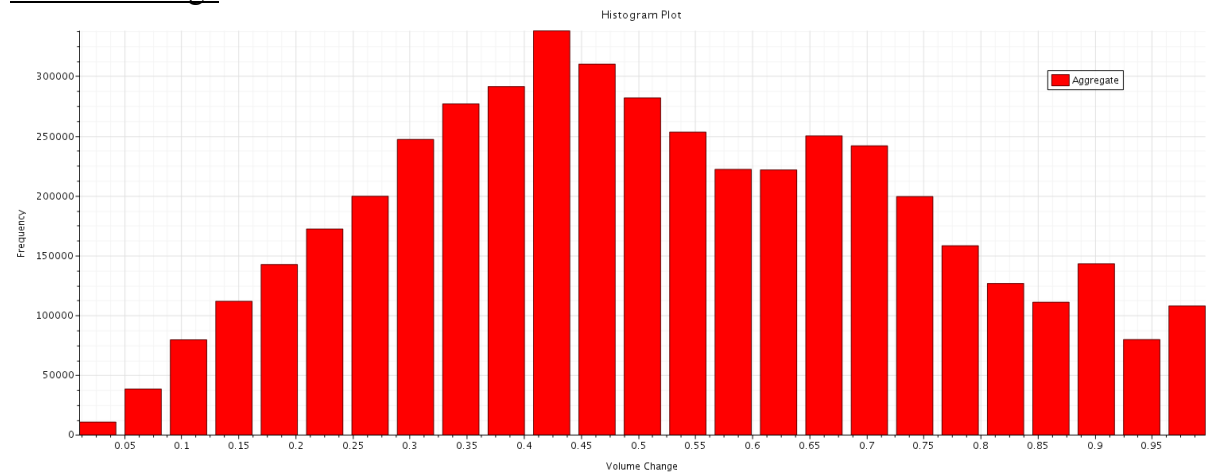
Cell Quality



Skewness Angle

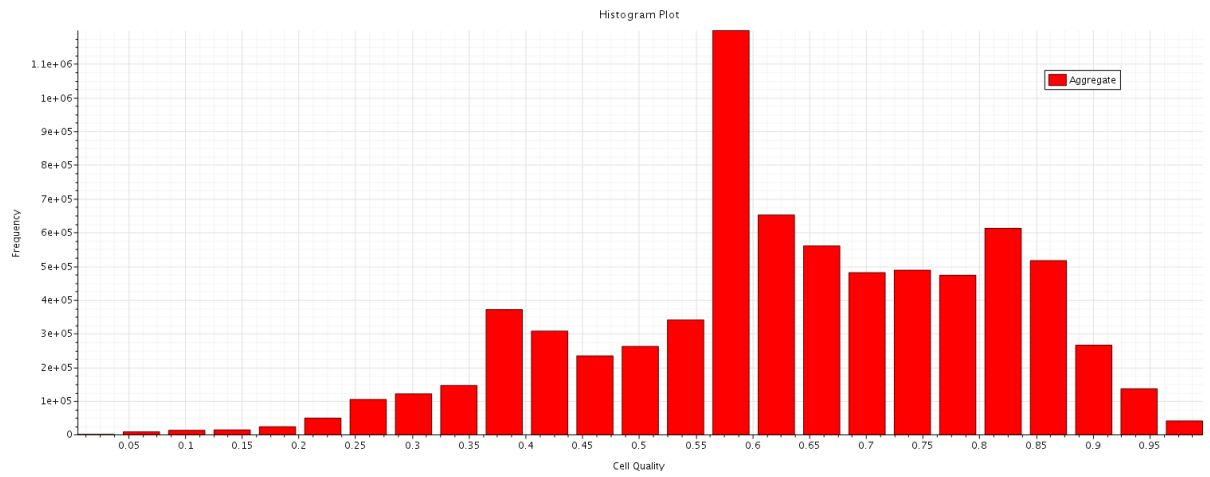


Volume Change

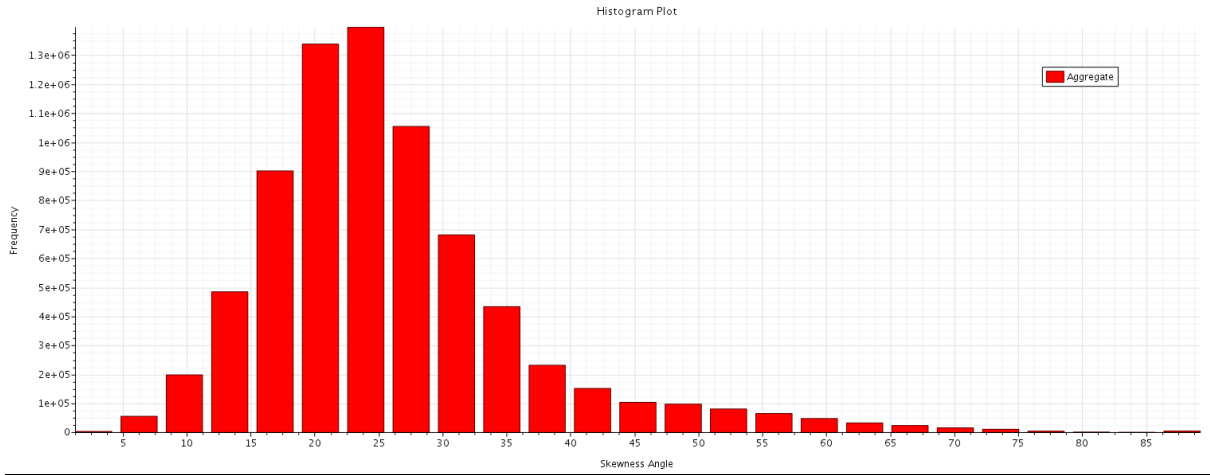


1 Guiding Vane

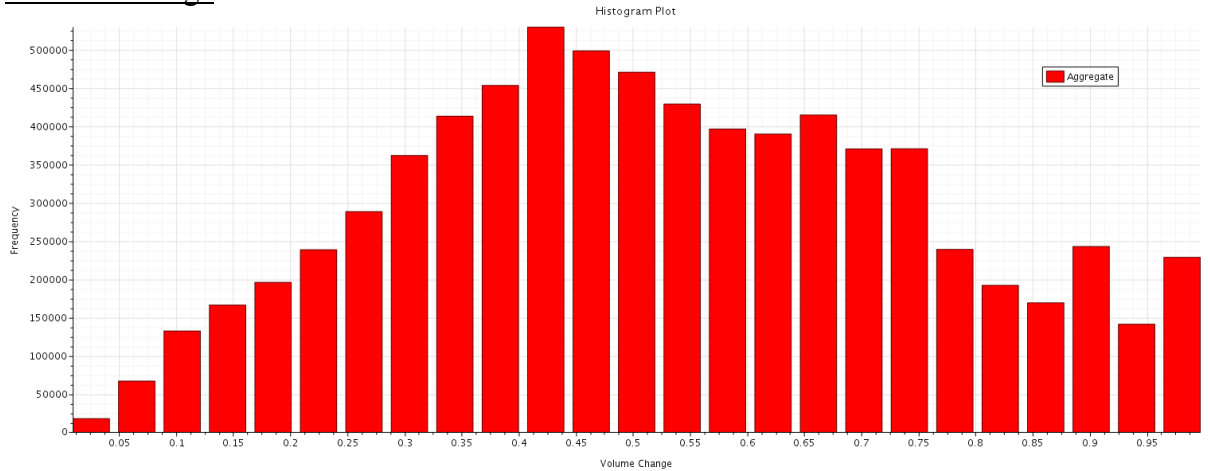
Cell Quality



Skewness Angle

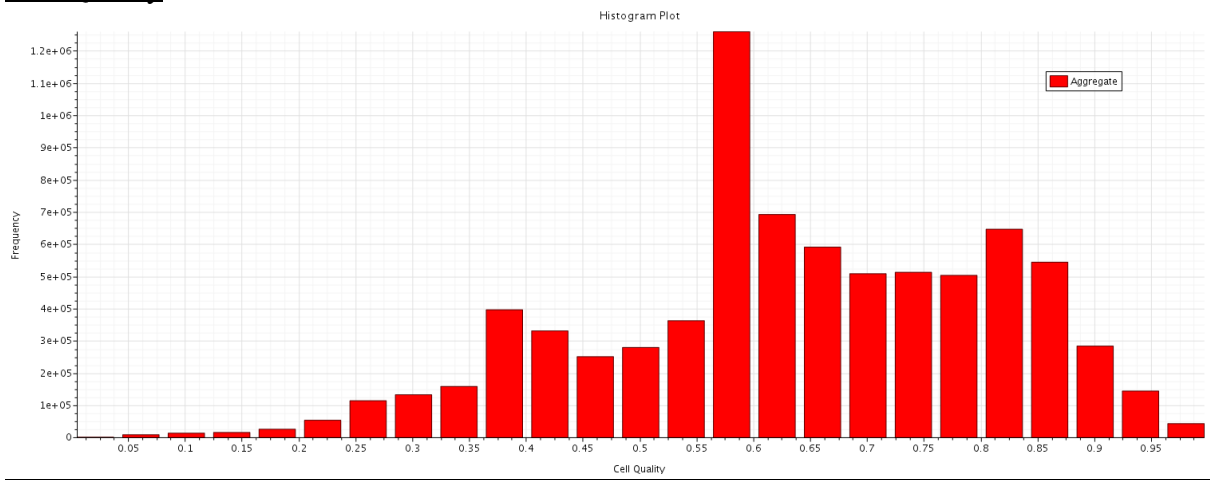


Volume Change

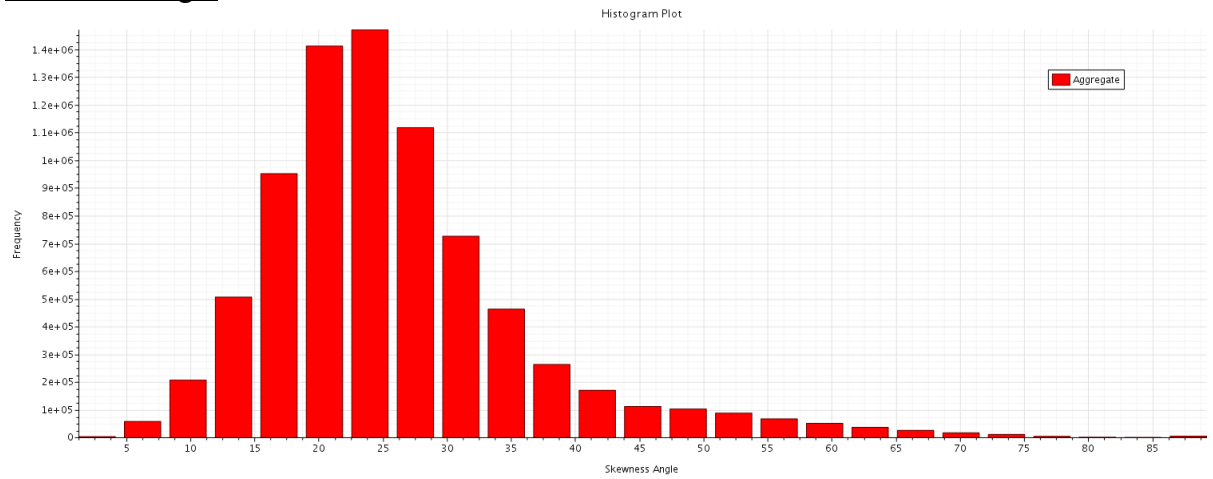


3 Guiding Vanes

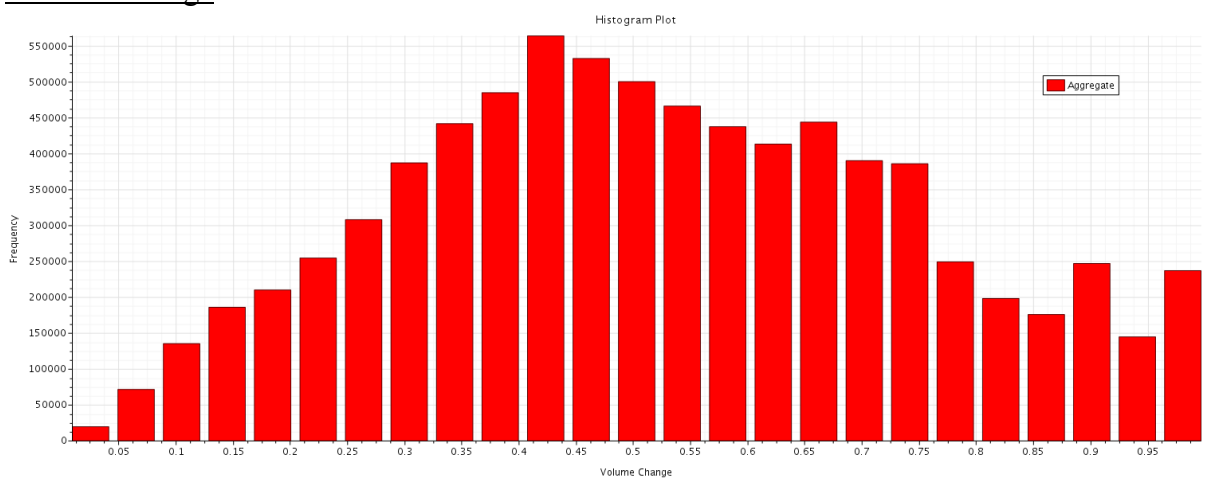
Cell Quality



Skewness Angle

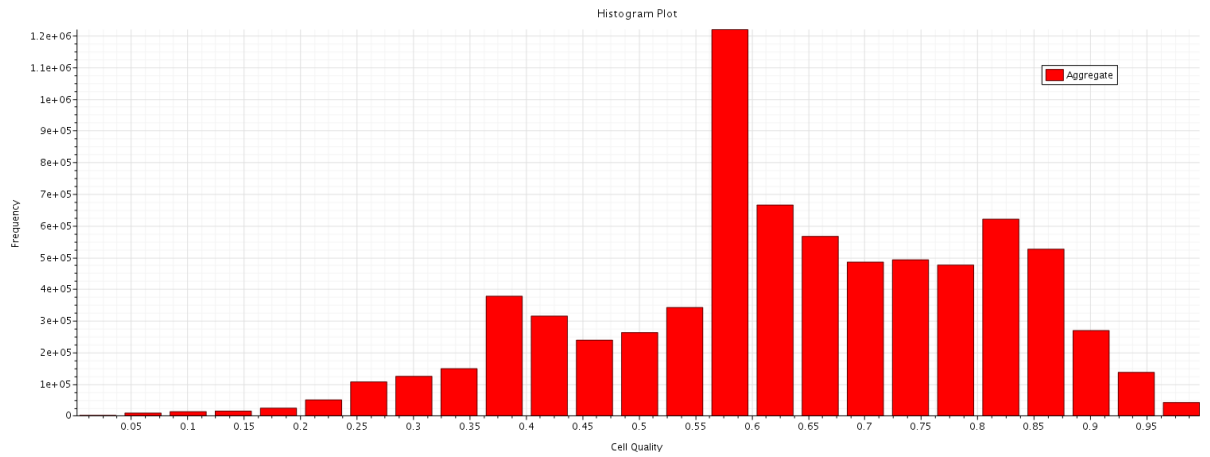


Volume Change

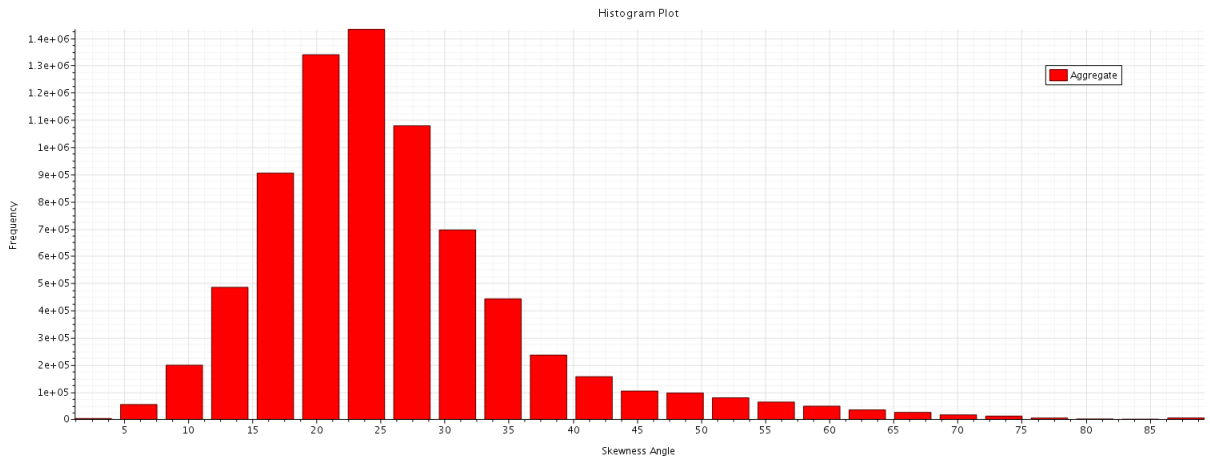


1 Guiding Vane with Wall

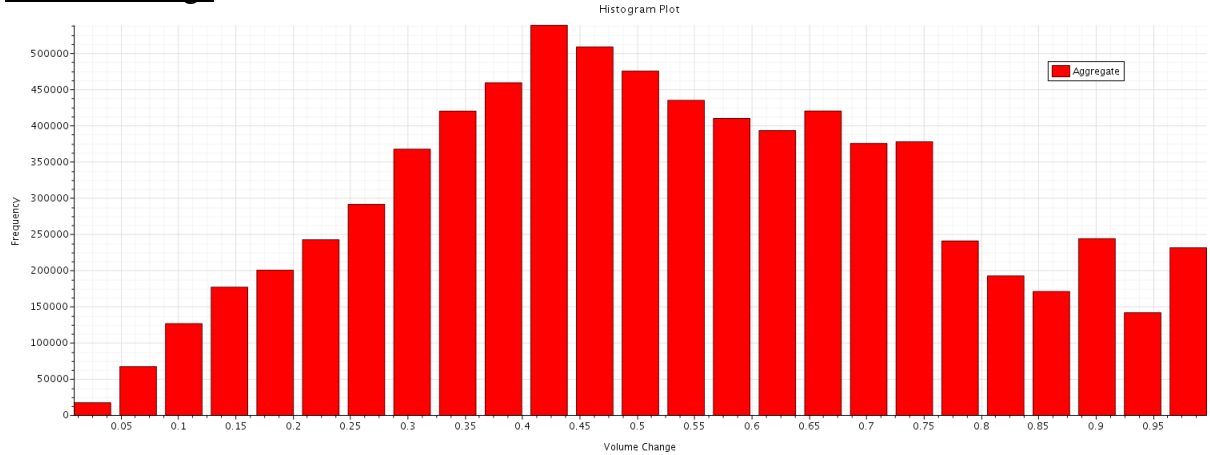
Cell Quality



Skewness Angle



Volume Change



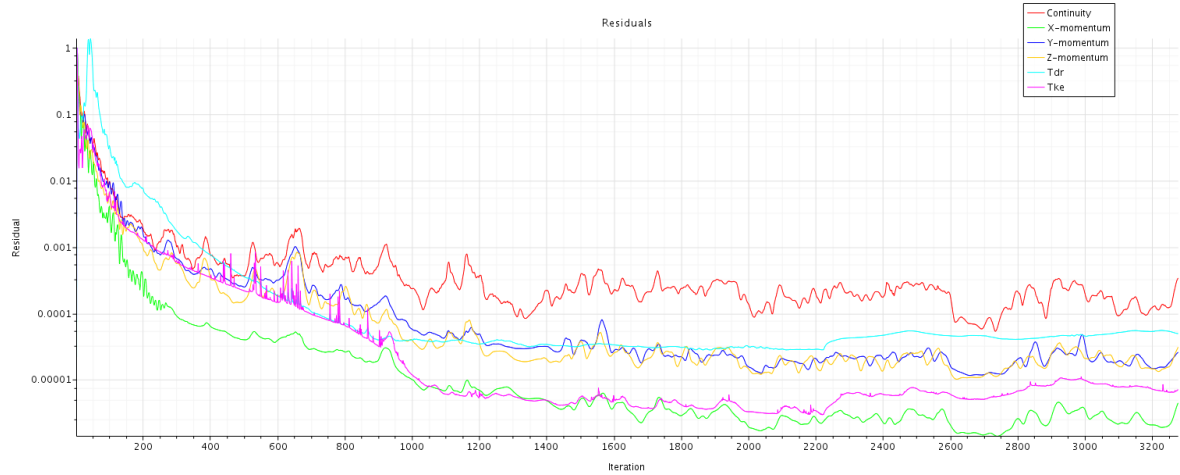
A.3 Cell Count and Iterations

Case	Number of Cells	Iterations
Reference	Fan 1: 2 266 055 Fan 2: 2 254 869 Inlet: 111 556 Outlet: 2 155 261 Total: 6 787 741	Operating Point 1: 3275 Operating Point 2: 1617 Operating Point 3: 1273 Operating Point 4: 1205
Fan 2 Offset	Fan 1: 2 375 113 Fan 2: 2 389 036 Inlet: 172 392 Outlet: 2 463 025 Total: 7 399 566	Operating Point 2: 1764 Operating Point 3: 1268 Operating Point 4: 1547
Full Distance Wall	Fan 1: 2 254 393 Fan 2: 2 272 192 Inlet: 111 557 Outlet: 2 301 411 Total: 6 939 553	Operating Point 2: 1125 Operating Point 3: 3250 Operating Point 4: 1159
Half Distance Wall	Fan 1: 2 255 377 Fan 2: 2 247 017 Inlet: 111 557 Outlet: 2 289 691 Total: 6 903 642	Operating Point 2: 1559 Operating Point 3: 3190 Operating Point 4: 1664
1 Guiding Vane	Fan 1: 2 373 321 Fan 2: 2 371 475 Inlet: 111 556 Outlet: 2 569 691 Total: 7 426 043	Operating Point 2: 1634 Operating Point 3: 1014 Operating Point 4: 1082
3 Guiding Vanes	Fan 1: 2 388 901 Fan 2: 2 355 823 Inlet: 111 556 Outlet: 3 023 560 Total: 7 879 840	Operating Point 2: 1384 Operating Point 3: 1433 Operating Point 4: 956
1 Guiding Vane with Wall	Fan 1: 2 382 902 Fan 2: 2 382 855 Inlet: 111 556 Outlet: 2 647 415 Total: 7 524 728	Operating Point 2: 1776 Operating Point 3: 1251 Operating Point 4: 1581

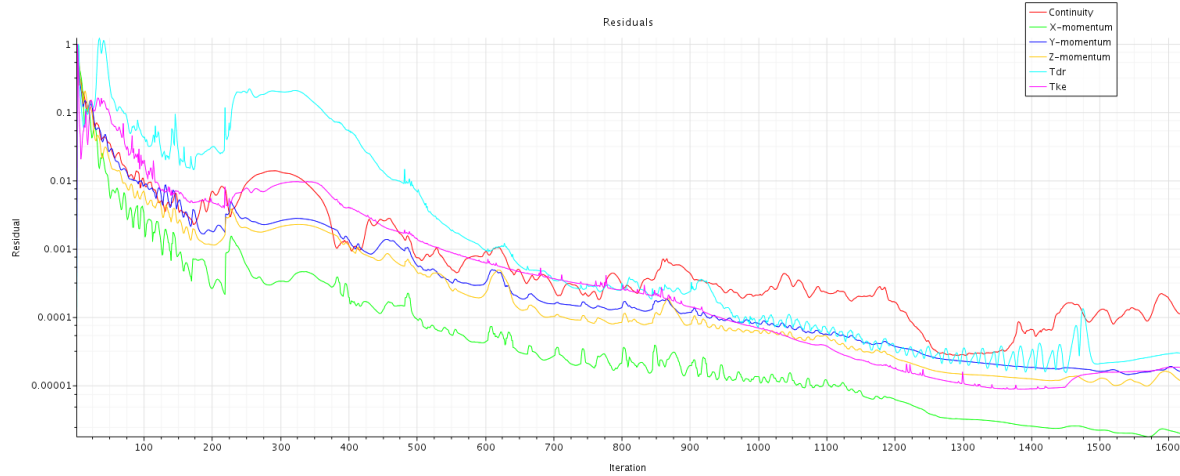
A.4 Residuals

Reference

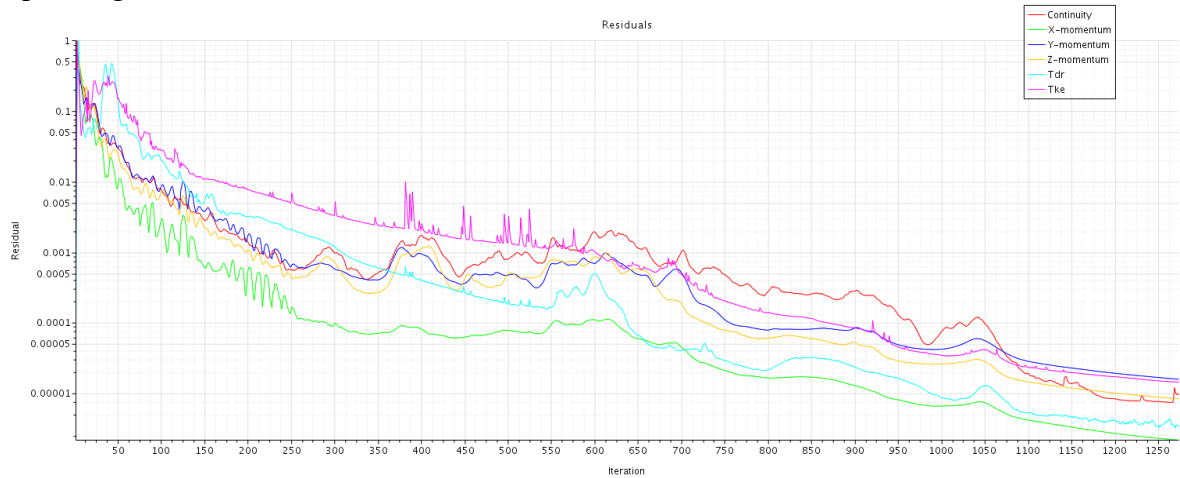
Operating Point 1



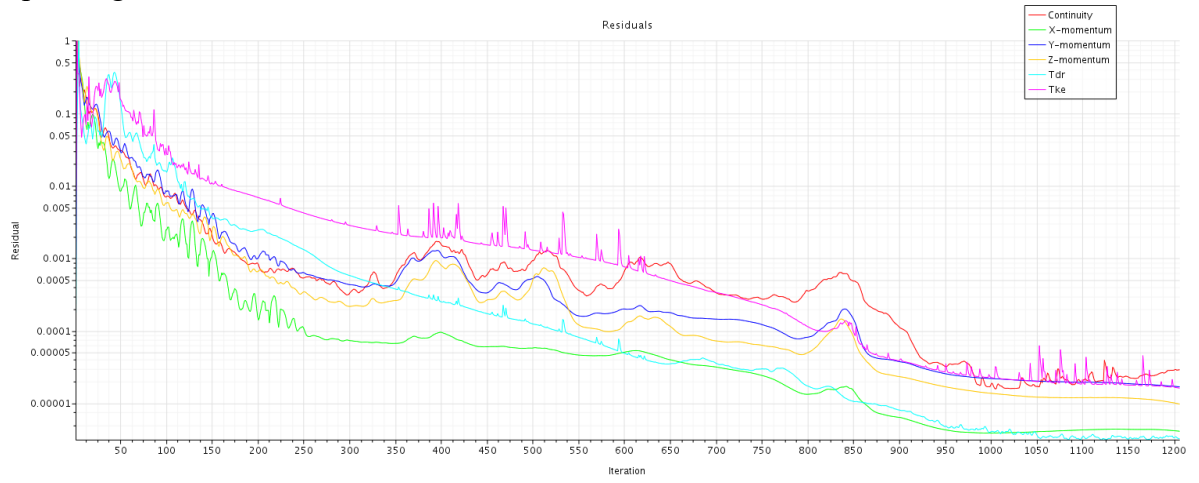
Operating Point 2



Operating Point 3

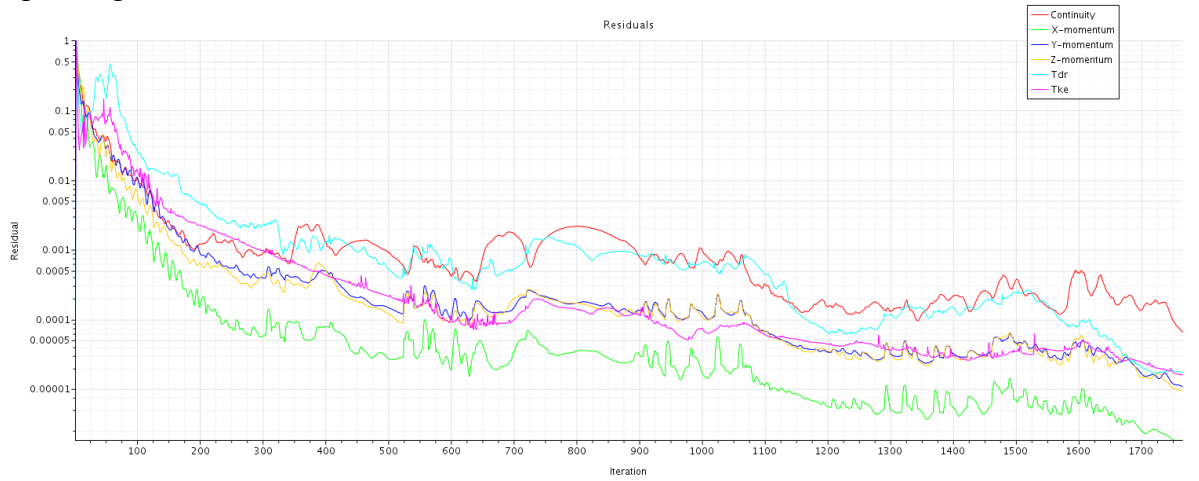


Operating Point 4

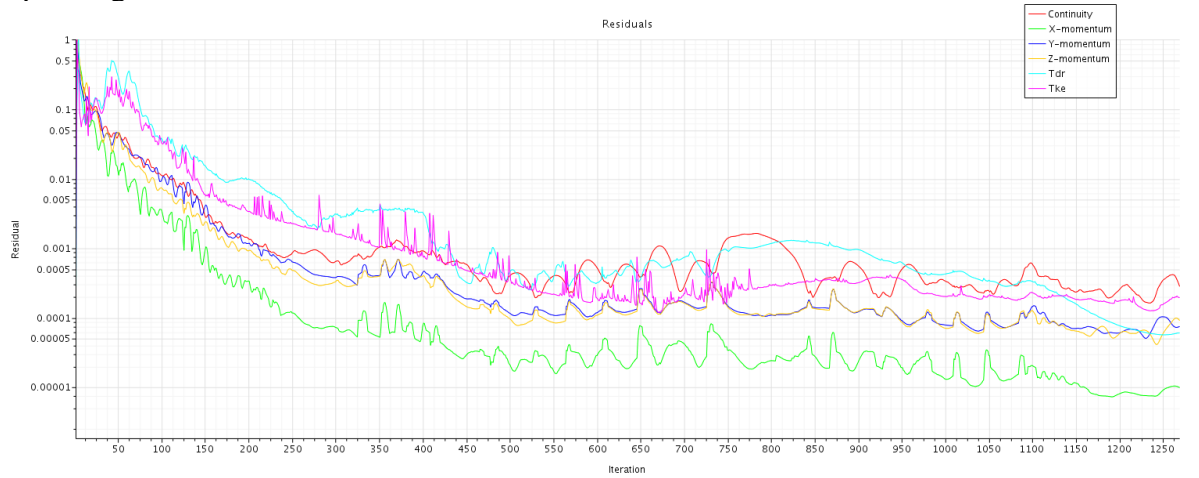


Fan 2 Offset

Operating Point 2

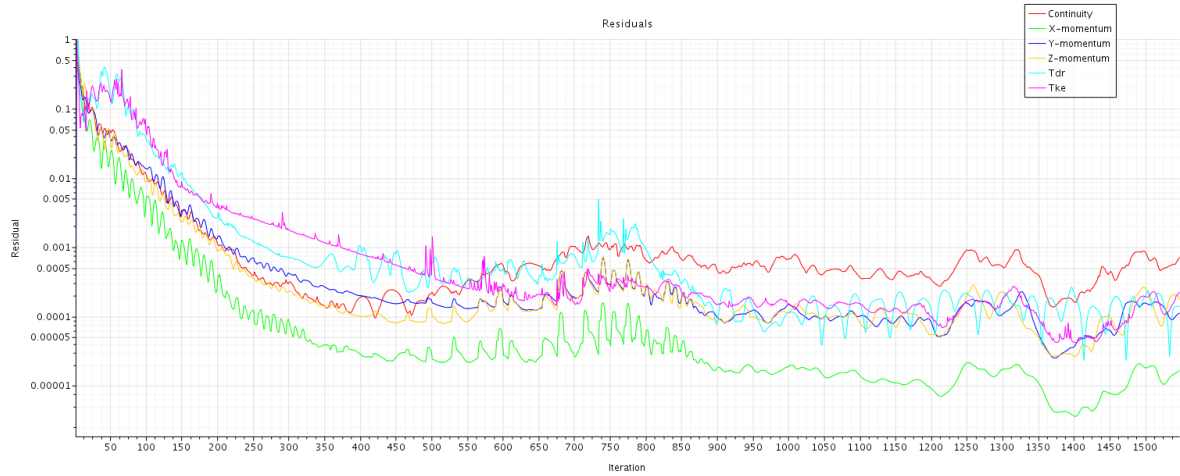


Operating Point 3



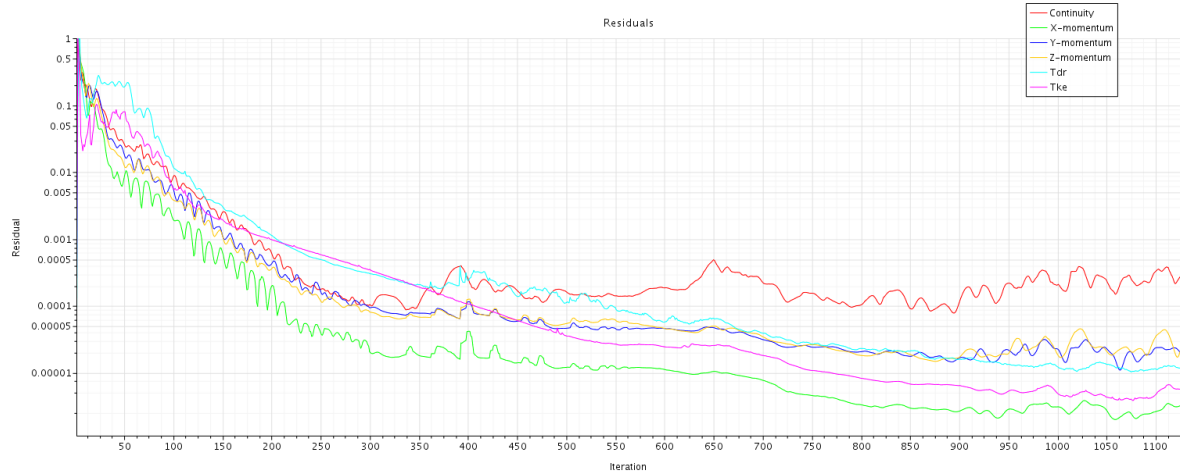
Appendix

Operating Point 4

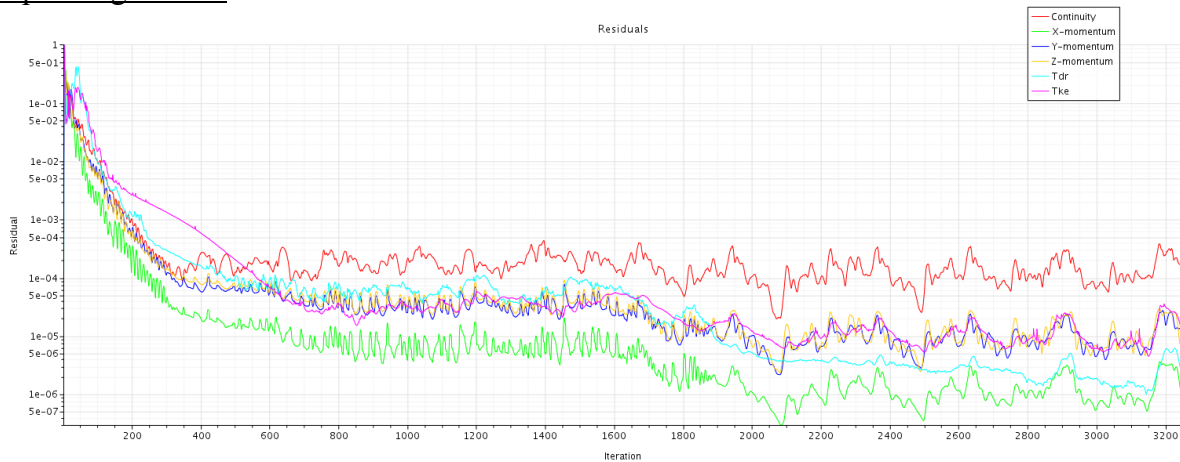


Full Distance Wall

Operating Point 2

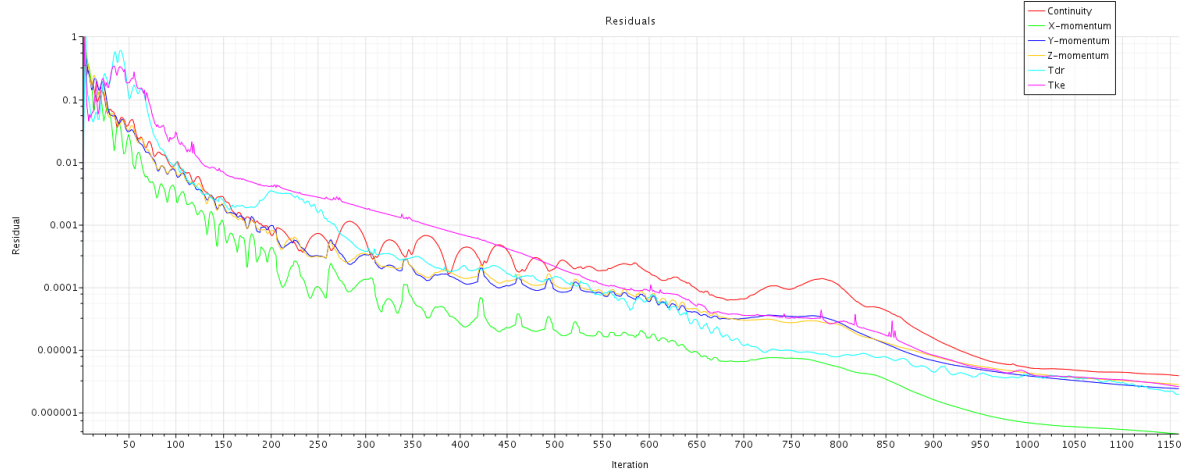


Operating Point 3



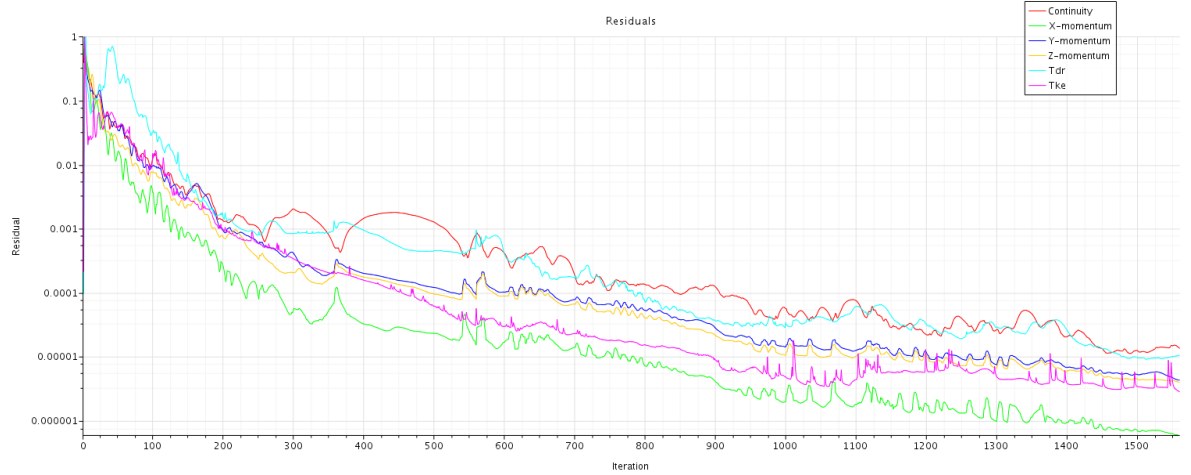
Appendix

Operating Point 4

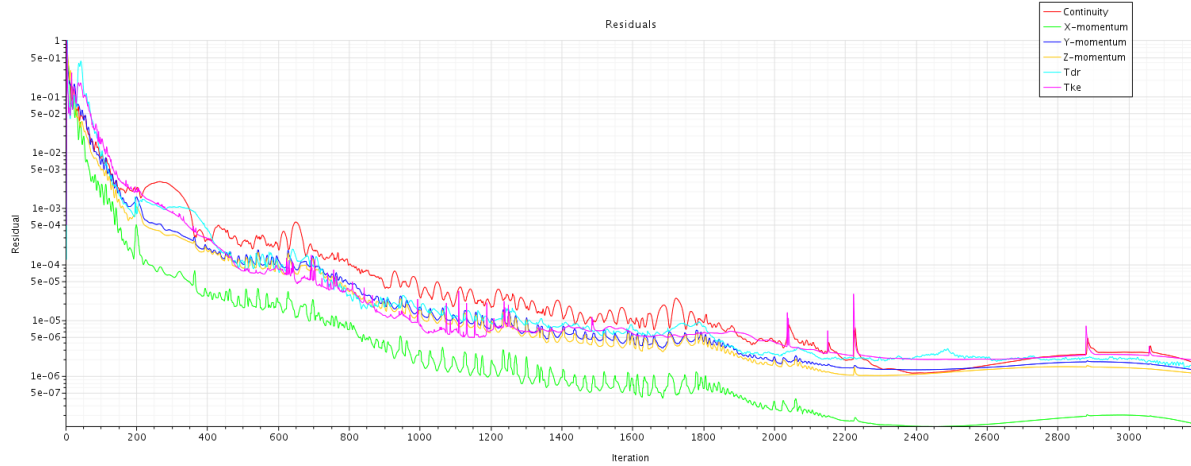


Half Distance Wall

Operating Point 2

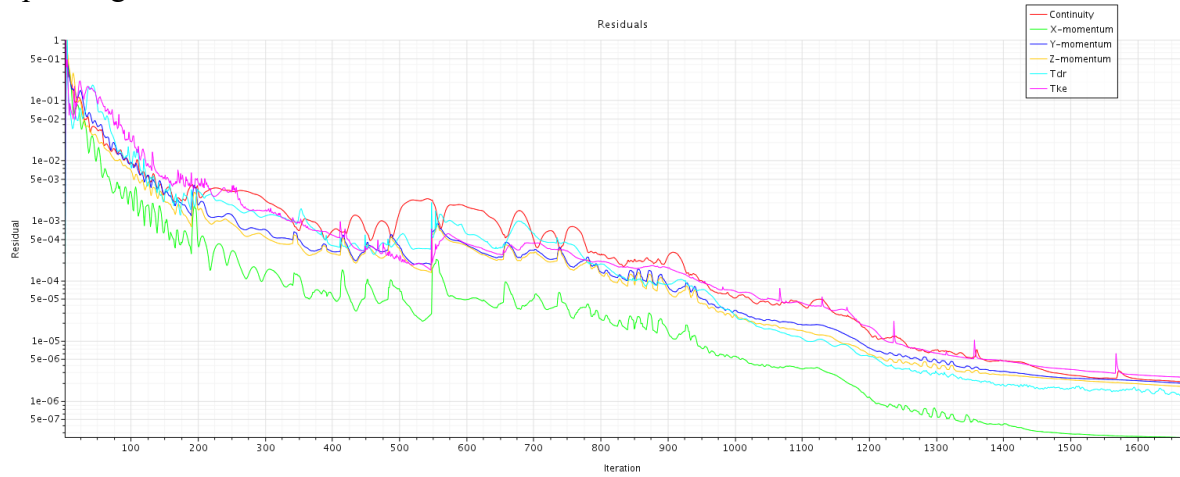


Operating Point 3



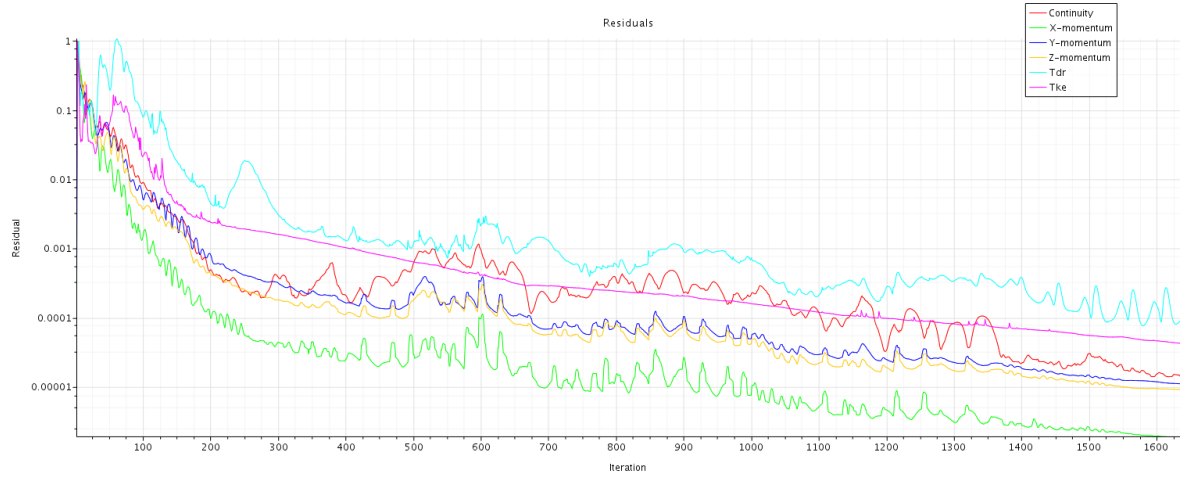
Appendix

Operating Point 4

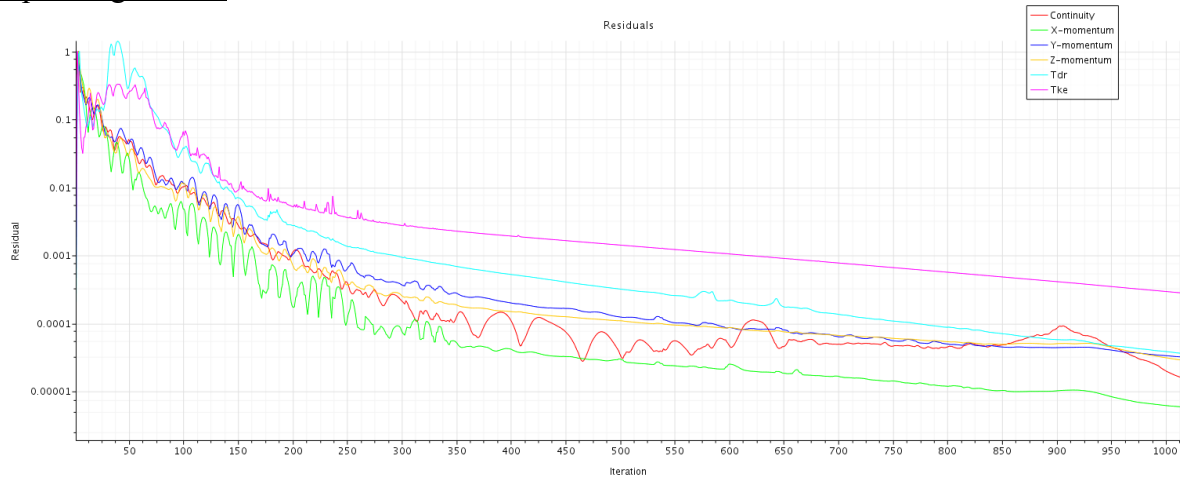


1 Guiding Vane

Operating Point 2

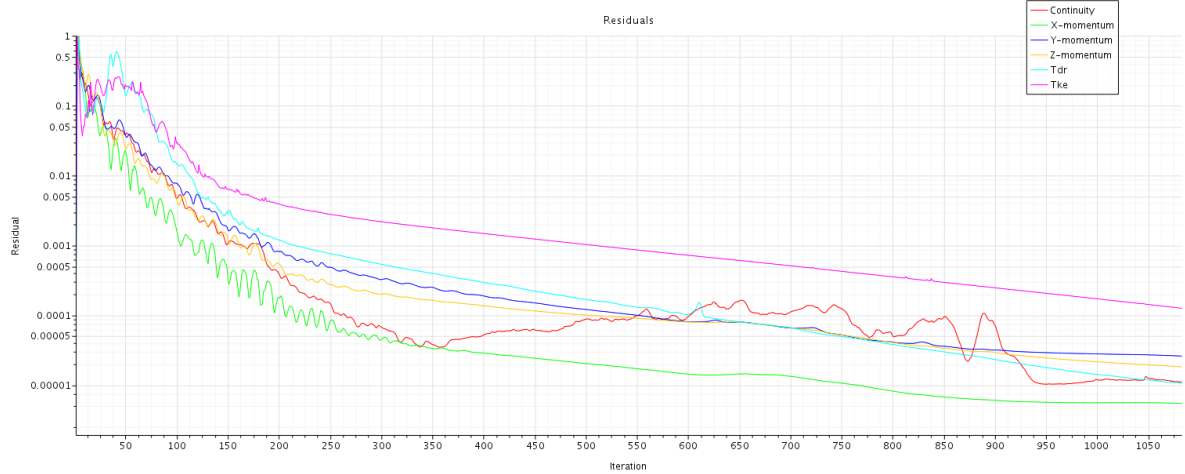


Operating Point 3



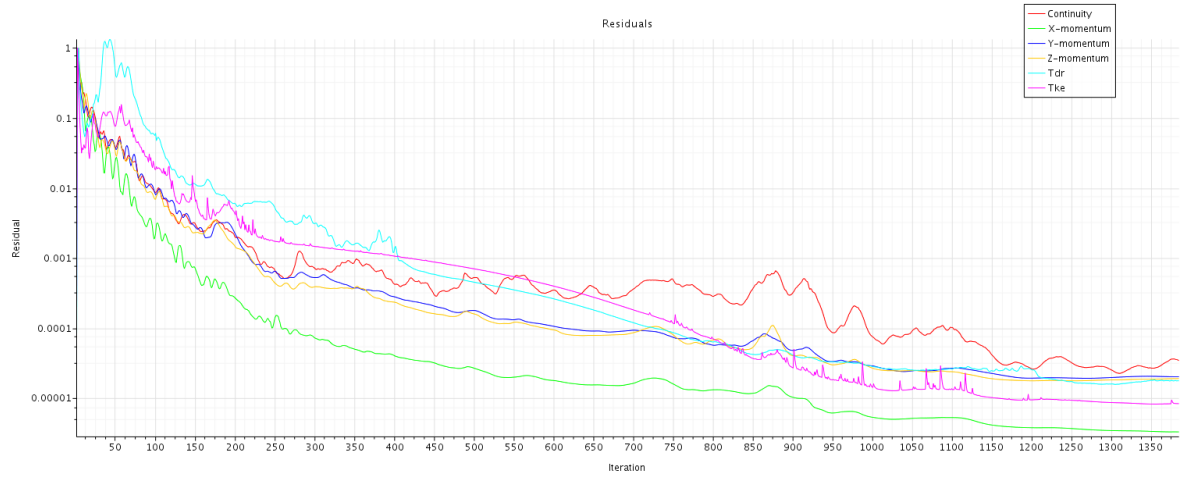
Appendix

Operating Point 4

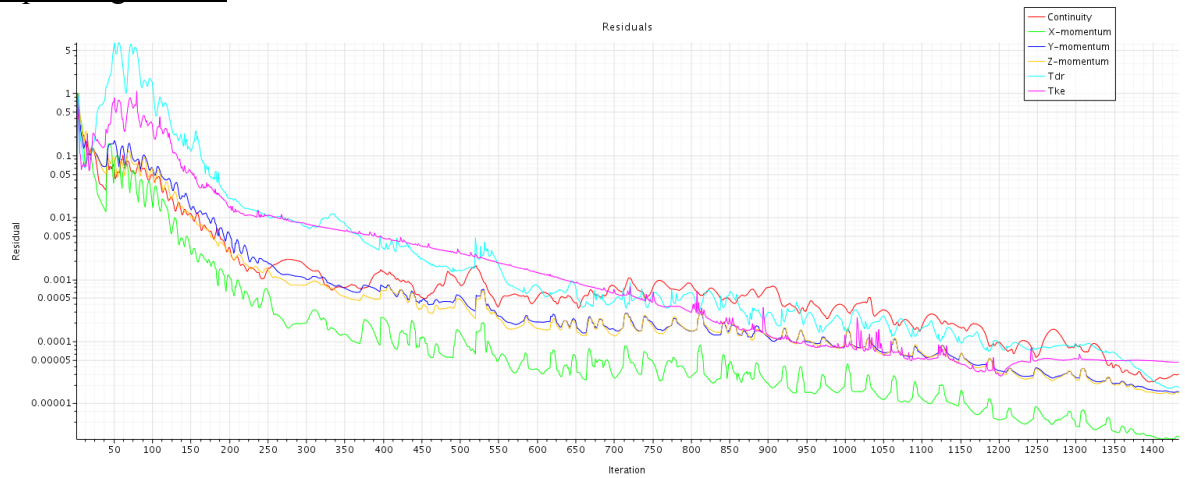


3 Guiding Vane

Operating Point 2

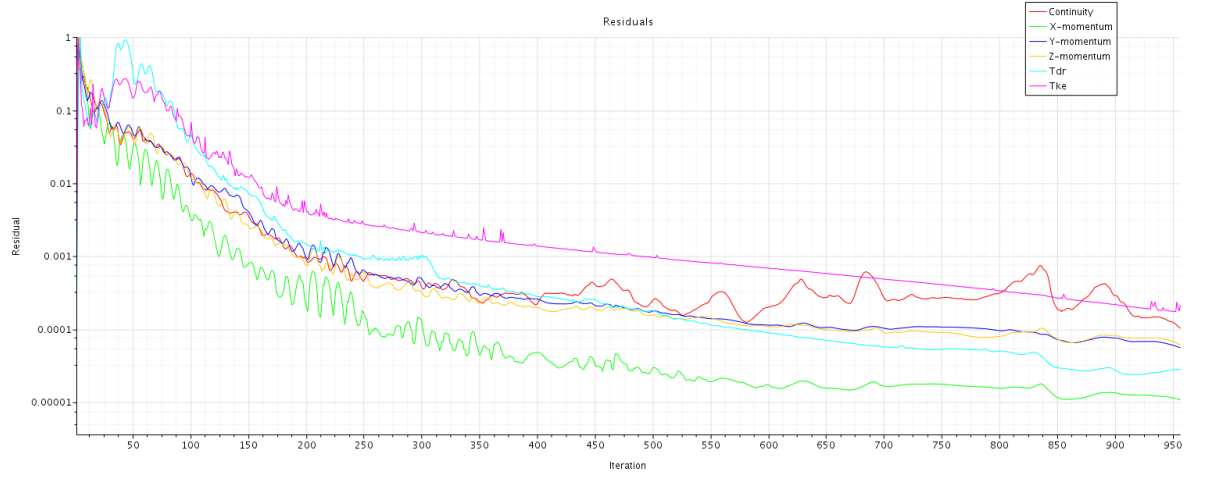


Operating Point 3



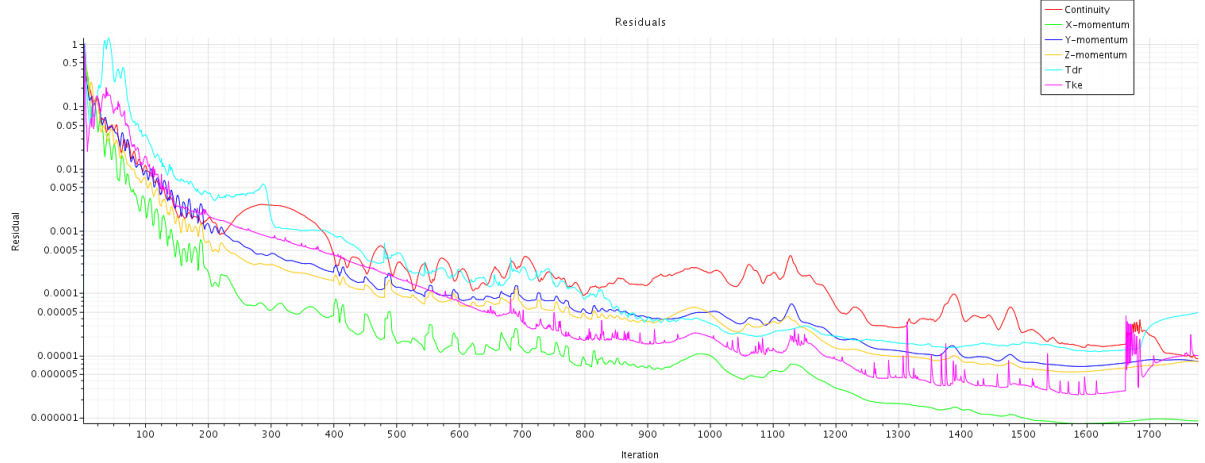
Appendix

Operating Point 4

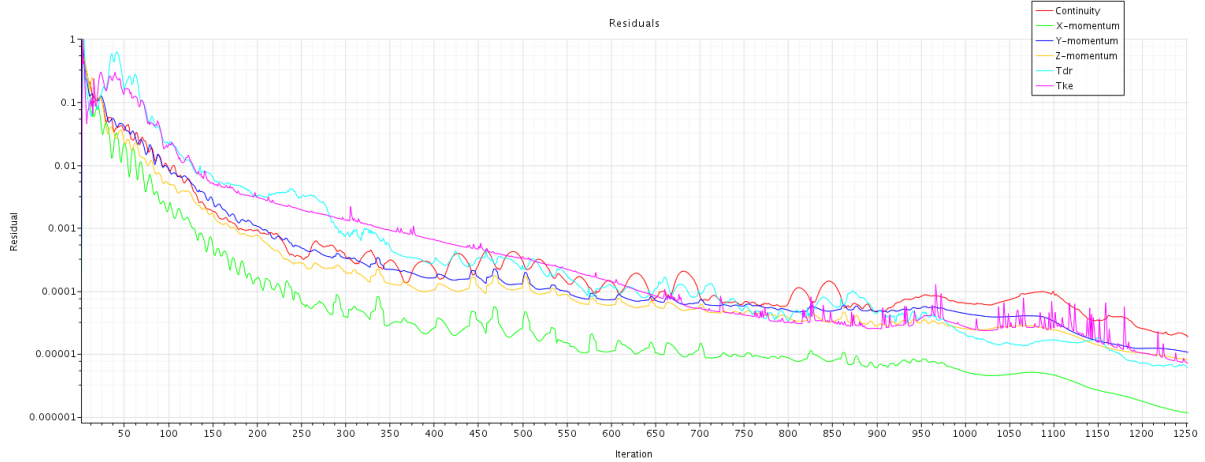


1 Guiding Vane with Wall

Operating Point 2



Operating Point 3



Appendix

Operating Point 4

